LIBRARY Michigan State University

PLACE IN RETURN BOX to remove this checkout from your record. TO AVOID FINES return on or before date due.

DATE DUE	DATE DUE	DATE DUE

1/98 c:/CIRC/DateDue.p65-p.14

VISCOUS FINGERING DURING REACTIVE FILLING: A THEORETICAL STUDY OF THE PHENOMENON IN LIQUID MOLDING

Ву

Chilukuri Nageshwara Satyadev

A DISSERTATION

Submitted to
Michigan State University
in partial fulfillment of the requirements
for the degree of

DOCTOR OF PHILOSOPHY

Department of Chemical Engineering

1998

ABSTRACT

VISCOUS FINGERING DURING REACTIVE FILLING: A THEORETICAL STUDY OF THE PHENOMENON IN LIQUID MOLDING

By

Chilukuri Nageshwara Satyadev

During the mold filling stage in liquid molding operations, the resin flowing through fiber "preforms" is continuously polymerizing, leading to a changing, adverse viscosity gradient in the filled region. The effects of resin age distribution and the polymerization kinetics on the stability of mold filling flows are investigated here. When the extent of reaction is significant, the driving force for resin penetration into the fiber bundles has been found to increase as the viscosity increases, thus improving the wetting of fibers. But the adverse viscosity gradient generated has an inherent tendency to generate fingers. A linear stability analysis of the equations describing the mold filling operation has been performed to derive criteria for growth/decay of fingers. When the derivative, S, of the reaction rate with respect to conversion is negative, fingers of large widths are damped; conversely, when this factor S is positive, disturbances of all sizes grow without attenuation. Small fingers are not stabilized by the reactive coupling. This is attributed to the relatively long time scale of chemical reaction, in comparison to the time scale of finger growth: fingers grow faster than reactive coupling can act to damp them out. Marginal stability plots have been computed to illustrate the effects of several resin parameters like gel time, activation energy and fill time/reaction time on the fingering phenomenon. It has also been found that the combined effect of chemical reaction and mass dispersion is to stabilize disturbances of both large and small wavelengths; this is in

contrast to the cases where dispersion alone damps out narrow fingers and reaction alone helps damp out large fingers.

ACKNOWLEDGMENTS

It has been a great experience working with my advisor, Dr. K. Jayaraman of the Chemical Engineering Department, Michigan State University. I thank him for his help in every stage of my graduate studies at MSU; his contribution to my doctorate degree is immeasurable and his immense patience and readiness to assist me and advise me is gratefully acknowledged.

I thank Dr. Charles Petty of the Chemical Engineering Department at the Michigan State University for his valuable inputs and insights and for his help whenever approached. The helpful comments of the other members on the advisory committee are also acknowledged with thanks: Dr. Lawrence Drzal, CMSC/MSU and Dr. C.Y. Wang, Department of Mathematics, MSU.

I was fortunate to have been taught by several excellent teachers at MSU and am grateful to them all for the knowledge they imparted during my interaction with them.

Thanks are due to my colleagues from our research group over the last few years, for their company and cooperation and helpful comments at the group meetings and otherwise.

I acknowledge with great respect and gratitude the role played by my parents, C. Shyamalamba and C. Ramachandra Murty, both before and during this endeavour. They are two of the greatest human beings I have ever known. My thanks to my brother, C.K. Mohan, and sister-in-law, Sudha Kailar, for their moral support and guidance throughout.

My wife, Sarada Chilukuri, deserves all praise for her patience and care in dealing with me during these graduate student years. Thank you, Sarada, for believing in me! And special thanks to my son, Sriram Mukunda Chilukuri, for brightening up my environs during the home stretch.

TABLE OF CONTENTS

LIST OF TABLES	iii
LIST OF FIGURES	ix
NOTATION	ii
CHAPTER 1 INTRODUCTION	
1.1 Introduction And Motivation	
1.2 Background	
1.2.1 Liquid Molding Operations	
1.2.2 Effects Of Fluid Rheology In RTM	
1.2.3 Viscous Fingering	
1.3 Liquid Molding And Viscous Fingering	
1.4 Summary	17
CHAPTER 2 POLYMER SYSTEMS IN LIQUID MOLDING: A REACTION	
KINETICS POINT OF VIEW	18
2.1 Introduction	18
2.2 Polyurethanes	
2.3 Polyamides	25
2.4 Epoxies	27
CHAPTER 3 VISCOSITY VARIATIONS DURING REACTIVE FILLING OF	
FIBER PREFORMS	
3.1 Introduction	
3.2 Role Of Resin Rheology In Liquid Molding	
3.2.1 Resin Rheology And Apparent Permeability	
3.2.2 The Mathematical Model	
3.2.3 Discussion Of Computed Results	
3.2.4 Summary	50

CHAPTER 4 VISCOUS FINGERING DURING REACTIVE FILLING OF FIBER

PREFORMS: EFFECT OF CHEMICAL REACTION	52
4.1 Introduction	52
4.2 Problem Formulation	55
4.2.1 The Governing Equations	55
4.2.2 Scaling	60
4.2.3 The base state equations	62
4.2.4 The base state solution	64
4.2.5 Stability analysis	73
4.3 Numerical Approach	
4.4 Results and Discussion	
4.4.1 Isothermal Reaction	84
4.4.2 Adiabatic Reaction	91
4.5 Mechanism of stabilization	107
4.5.1 Effect of S on the growth rate	
4.5.2 Stabilization of large fingers	
4.6. Summary	
CHAPTER 5 VISCOUS FINGERING DURING REACTIVE FILLING OF	FIRER
PREFORMS: EFFECTS OF DISPERSION AND REACTIO	
5.1 Introduction	
5.2 Model Problem And Equations	
5.3 Scaling And Dimensionless Form Of The Equations	
5.4 Stability Analysis	
5.5 Initial Growth Rate	
5.5.4 Results	
5.6 Summary	
CHAPTER 6 CONCLUSIONS	143
6.1 Summary And Conclusions	143
6.2 Recommendations for future work	146
APPENDIX A: Exchange of stabilities analysis for mold filling with chemic reaction, without dispersion	
APPENDIX B: Derivation of component mass balance equations	151
DIDI IOCD ADUV	154

LIST OF TABLES

Table 4.1 Thermal, kinetic and rheological data for the resin and glass fibers 5
Table 4.2 Scaling factors for different variables
Table 4.3 Computational results for isothermal reaction
Table 4.4 Computational results for adiabatic reaction
Table 4.5 Cutoff wavenumber data for adiabatic reaction
Table 5.1 Computational results from eq. (5-36)
Table 5.2 Cutoff wavenumber data at several values of θ

LIST OF FIGURES

Figure 1.1	Mechanism of finger growth due to viscosity gradients 7
Figure 1.2	Typical molded plaque: to illustrate the generation of fingers. White - older resin; Shaded: fresh resin [after Losure, 1994]
Figure 1.3	Filling with no reaction or dispersion [after Hickernell and Yortsos, 1987]
Figure 1.4	Filling with dispersion, no reaction [after Tan and Homsy, 1986] \dots 15
Figure 2.1	Schematic of a RIM Machine [after Macosko, 1989]
Figure 2.2	Types of chemical reactions classified by S behavior
Figure 2.3	Viscosity changes during a RIM cycle
Figure 2.4	Reaction scheme for an Epoxy system
Figure 3.1	One-dimensional flow of resin, transverse to fibers, in an end-gated mold
Figure 3.2	Rheology of Devcon epoxy resin
Figure 3.3	Rheology of Derakane resin
Figure 3.4	Apparent transverse permeability Vs viscoelasticity-Hexagonal array 36
Figure 3.5	Resin penetration into fiber bundles
Figure 3.6	Dimensionless superficial velocity at various flow front positions 43
Figure 3.7	Location of y_I at various positions of the flow front
Figure 3.8	Location of y_{II} at various positions of the flow front
Figure 3.9	Velocity reduction factor Vs LMMDR [f,I]
Figure 3.10	LMMDR [f,I] at various positions of the flow front - regime II 48

Figure 3.11	Pressure profiles at various locations of the flow front
Figure 4.1	Schematic of reactive filling, frozen at time "t", in an end-gated mold 56
Figure 4.2	Non-dimensional reaction rate for polyurethane resin: isothermal and adiabatic cases, $T_0 = 325^{\circ}K$
Figure 4.3	Non-dimensional viscosity for polyurethane resin: isothermal and adiabatic cases, $T_0 = 325^{\circ}K$
Figure 4.4	Base state conversion profiles: isothermal and adiabatic cases, $T_0 = 325^{\circ}K$
Figure 4.5	Base state dimensionless pressure profiles: adiabatic case, $E_R = 53$, $E_{\mu} = 41$, $\alpha_{gel} = 0.65$, $T_o = 325^{o}K$
Figure 4.6	S, V profiles for isothermal filling: $E_R = 53$, $E_{\mu} = 41$, $\alpha_{gel} = 0.65$, $T_o = 325^{\circ}K$
Figure 4.7	S, V profiles for adiabatic filling: $E_R = 5$, $E_{\mu} = 41$, $\alpha_{gel} = 0.65$, $T_o = 325^{\circ}K$
Figure 4.8	Schematic of the numerical scheme - orthogonal collocation on finite elements with Legendre polynomials
Figure 4.9	Growth rate curves for isothermal filling of polyurethane resin: $z_f = 0.8$, 1.0, 1.2, 1.5; $E_R = 53$, $E_{\mu} = 41$, $\alpha_{gel} = 0.65$, $T_o = 325^{\circ}K$
Figure 4.10	Marginal stability curve for isothermal filling, data from figure 9: Damkohler number (Da = flow time / reaction time)
Figure 4.11	Growth rate curves for S = 0 for isothermal filling for identical base state viscosity profiles as for fig. 9
Figure 4.12	Upper limit of growth rate Vs Damkohler number for isothermal filling, $T_0 = 325^{\circ}K$
Figure 4.13	Growth rate curves for varying activation energy during adiabatic fill 97
Figure 4.14	Marginal stability curve for adiabatic filling: activation energy 101
Figure 4.15	Marginal stability curve for adiabatic filling: fill time and varying

	temperature; $E_R = 169$, $E_{\mu} = 131$, $\alpha_{gel} = 0.80$, $\Delta T_{ad} = 38^{\circ} K \dots 104$
Figure 4.16	Marginal stability for adiabatic filling: gel conversion 105
Figure 4.17	Schematic representation of the effect of S on growth rate 108
Figure 4.18	Effect of S on growth rates for identical conversion and viscosity profiles in the base state
Figure 5.1a	Flow of reacting liquid through a porous medium (moving frame) . 118
Figure 5.1b	Profiles of conversion, viscosity and S at t=0
Figure 5.2	Initial growth rate curves - varying θ
Figure 5.3	Marginal stability: θ
Figure 5.4	Initial growth rate curves - positive values of S
Figure A.1	Schematic for shell balance - one dimensional flow

NOTATION

All variables with an overbar () indicate base case quantities.

All variables with a hat (^) indicate dimensioned quantities.

All primed (') variables indicate the perturbations.

- a length scale used for Deborah number calculation
- A amplitude of conversion disturbance

 A_R , A_μ Arrhenius constants

- b defined in eq. (4-22)
- $b_1 K_x/K_1$
- $b_2 K_v/K_1$
- c concentration of reactant (mol/m³)
- c_o inlet concentration of reactant (mol/m³)
- C_o , R_o concentration and reaction rate at reference conditions
- C_p volume fraction averaged specific heat capacity (J/kg K)
- C_1 , C_2 constants in the viscosity expression
- D isotropic dispersion coefficient (m²/s)
- Da Damkohler number, tp/tR
- De Deborah number
- E_μ activation energy for viscosity
- E_a activation energy for the reaction (J/mol)

 E_{R} dimensionless activation energy for reaction, $E_a/(R_g \Delta T_{ad})$ G' shear storage modulus H,W transverse dimensions of the shell in shell balance İз unit vector in the flow direction I initiator concentration k wavenumber K permeability tensor $\mathbf{K}_{\mathbf{D}}$ dimensionless permeability tensor $\mathbf{k}_{\mathbf{I}}$ initiator rate constant $\mathbf{K_1}$ longitudinal permeability $k_{\mathbf{R}}$ rate constant for simple n-th order kinetics K_{t} transverse permeability K_{to} Newtonian transverse permeability (constant) k_x , k_y disturbance wavenumbers in the transverse directions k₁, k₂ rate constants for non-simple kinetics (e.g. eq. 2-2) LMMDR[f,I] logarithmic mean mobility difference ratio order of reaction m, n apparent mobility m_a m_f, m_I apparent mobility for regime I and at the front, respectively M the initial mobility ratio

xiii

inlet pressure for constant injection process

amplitude of pressure perturbation

p

Po

- P pressure
- Pe Peclet number, t_D/t_F
- q velocity in the moving reference frame
- q_{ξ} $\;\;$ amplitude of the $\xi\mbox{-component}$ of the velocity disturbance
- R rate of reaction (mol/m^3-s)
- R_g gas constant (J/mol ^oK)
- R reaction rate with no explicit temperature dependence
- $S \partial \overline{R}/\partial \overline{\alpha}$
- t time (s)
- T temperature
- t_D, z_D dispersive scales for time and length
- t_F , z_F flow scales for time and length
- to, vo, zogeneral scaling factors for time, velocity, length respectively
- T_o inlet temperature
- t_R reactive scale for time
- T_{ref} reference temperature
- t_{I} , t_{II} , t_{III} time bounds for flow regimes I, II, III respectively
- <u>u</u> velocity in the fixed frame of reference
- U_b interstitial velocity (m/s)
- U_o uniform injection (superficial) velocity
- $V d(\ln \overline{\lambda})/d\xi \equiv -\rho \times (d\overline{\alpha}/d\xi)$
- x, y coordinate directions transverse to the flow

- y_A location of the front at time t_I
- z length, in the fixed reference frame
- z_f position of the flow front

Greek Symbols

- α conversion
- α_g gel conversion
- β defined in eqn.6
- $-\Delta H_R$ heat of reaction (J/mol)
- ΔT_{ad} adiabatic temperature rise (${}^{o}C$)
- Δz shell thickness
- $\Delta \alpha = \alpha_1 \alpha_2$, the initial jump in conversion across the interface
- ε porosity
- θ (Da) x (Pe) = t_D/t_R
- λ 1/
- μ viscosity = 1/mobility
- $\mu_i \qquad initial \ viscosity$
- $\mu_o(T)$ Arrhenius' term in the viscosity expression
- ξ length coordinate along the flow direction in the moving reference frame
- ρ d(ln)/ $d\overline{\alpha}$
- ρ_f volume fraction averaged density (kg/m³)
- σ exponential growth rate

- τ relaxation time
- ψ stream function form of the velocity perturbation, defined in eqn.35
- ω frequency (rad/s)

CHAPTER 1 INTRODUCTION

1.1 INTRODUCTION AND MOTIVATION

This work investigates the flow of reactive, polymeric liquids through fiber bundles with specific reference to viscous fingering during the mold filling stage in liquid molding operations. The effect of the polymerization reaction along with the various thermochemical properties of the resin, and the effect of dispersion during the filling process, on the growth of fingers, are studied.

The motivation for this study comes from a necessity to understand the flow processes involved in the manufacture of fiber reinforced polymer composite materials. The relevant composite manufacturing process is Liquid Molding, of which Resin Transfer Molding (RTM) and Structural Reaction Injection Molding (S-RIM) are specific techniques. Flaw-free parts are the major requirement of any composite manufacturing process. Microstructural defects in the final part may arise from a number of causes -- uneven distribution of the resin, voids embedded within the fiber bed and viscous fingering of fresh resin with a lower viscosity into aged resin of higher viscosity within the mold. The scale of the defects is important to determine whether they affect the mechanical performance of the molded part significantly. Inhomogeneities, caused either by voids or by an uneven distribution of the resin across the fiber bed, may lead to weak spots in the final parts. The possible role of viscous fingering during mold filling, in the generation of these inhomogeneities, is studied.

Mold filling processes involve the flow of polymeric matrix material past

anisotropic arrays of fibers. Since the dimensions of the fiber tows are extremely small in comparison to those of the mold itself, the impregnation of the bed of fibers is treated as a flow through porous media. As a result of the polymerization reaction occurring during mold filling, a continuous variation of viscosity of the resin develops across the filled portion of the mold, at any time. Such a viscosity gradient is found to result in the phenomenon called fingering of more mobile fluid.

This phenomenon of viscous fingering has been observed in solvent-flushing of packed beds and filters [Hill, 1952], as also in the secondary extraction of crude oil from rock formations under the surface of the earth, and has been reviewed by Homsy (1985). During mold filling, one possible mechanism for the formation of inhomogeneities could be the rejoining of the fingers downstream, as they grow, thus enclosing a region containing resin with properties drastically different from those of the resin in its neighborhood. The structure and behavior of the fingers is expected to depend on the fibrous nature of the medium, due to its effect on the degree of mixing by dispersion, and also on the thermochemical properties of the resin being injected.

An introduction to liquid molding processes and the effects of fluid rheology thereon are also discussed briefly in this chapter. The current state of the art and the background to studies in viscous fingering are presented in the subsequent chapters in this section. The mechanism of the effect of adverse viscosity gradients on the growth or attenuation of fingers, is also reviewed.

The focus of this dissertation is on the effect of the polymerization reaction on the stability of the mold filling process. Chapter 2 discusses the types of polymer resins used in liquid molding operations, with emphasis on their reaction kinetics. This chapter offers

an insight into the factors one needs to look at, to have an *a priori* inkling of what to expect would happen to any incipient disturbances during the mold filing process.

The rheological data for an epoxy resin and a vinyl ester resin were taken and a mathematical model presented for the adiabatic, one-dimensional filling of fiber bundles with these reacting resins in an end-gated mold. The prediction of the moving front and the evolving pressure distribution inside the filed portion of the mold at any time are presented in chapter 3. This analysis and results were presented at the VII Annual Advanced Composites Conference and Expo, at Detroit in October, 1991 (Jayaraman and Satyadev, 1991).

The stability analysis on the mold filling process and the results on its application to a polyurethane resin, along with the base state results, are presented and discussed in Chapter 4. The effects of dispersion were not included in this analysis and so this chapter discusses the influence of polymerization reaction on the finger growth in the absence of any other stabilizing/destabilizing mechanism. These results were presented at the Annual AIChE Meeting at Miami in November, 1992. The combined effects of mass dispersion and chemical reaction are presented in Chapter 5. A model problem is discussed, that depicts this combined effect on the initial growth rates by means of a simple, analytical method. This analysis was presented at the V International Conference in Numerical Methods in Industrial Forming Processes - NUMIFORM '95 at Ithaca in June, 1995 (Satyadev and Jayaraman, 1995).

The last chapter in this dissertation presents the conclusions from this work on the effects of chemical reaction on the stability of mold filling in liquid molding operations.

1.2 BACKGROUND

1.2.1 LIQUID MOLDING OPERATIONS

Resin transfer molding (RTM) and Structural - Reaction Injection Molding (S-RIM) are techniques that are commonly treated under the category of liquid molding operations in the polymer composites manufacturing industry. In both these techniques, the method consists of injection of a low viscosity, unreacted polymer resin inside a closed mold with a fiber preform in place. The mold must be filled well before the viscosity of the resin rises to gelation. The main difference between the two techniques lies in the desired production rate of finished parts; S-RIM is a high speed process, while RTM involves relatively larger fill times. These differences eventually translate to difference in operational costs, too.

1.2.2 EFFECTS OF FLUID RHEOLOGY IN RTM

Analysis of the filling process in resin transfer molding is usually done with the assumption that liquid advancing through the fiber preform maintains a constant viscosity and remains inelastic (Coulter and Guceri, 1988; Kim et al, 1991; Parnas and Phelan, 1991; Bruschke and Advani, 1990). This assumption is frequently questionable, in practice for the following reasons.

a) Often a thermoplastic binder holds the fiber tows or fabric together and allows it to be shaped before impregnation with resin; this binder usually dissolves in the resin and is removed from the fiber surface by miscible displacement (Owen et al, 1989). Dissolution of binder raises the viscosity by a factor of two or more, as observed by Chen et al (1995). b) High speed versions of resin transfer molding that are now under development employ resins that cure very fast (Babbington et al, 1987). In filling large preforms with these

resins the extent of reaction at various time steps of filling is significant, producing changes in both shear viscosity and extensional viscosity.

c) In contrast to filling of empty mold cavities where fluid memory effects are not significant (Wang and Hieber, 1988), viscoelastic effects may be significant in filling of molds with fiber preforms. Permeation rates transverse to the fiber axis have been observed to be significantly lower for viscoelastic fluids, compared to that for inelastic resins with the same shear viscosity (Chmielewski and Jayaraman, 1992). The reduction in permeation rate depends on the extensional viscosity displayed by the fluid as it is subjected to varying stretch rates in the fiber array.

Hence the changing resin rheology (both inelastic and elastic components) during the miscible displacement of binder or during the reactive filling process affects the resin pressure distribution in the mold in a complex way.

1.2.3 VISCOUS FINGERING

Hill (1952) published the first paper on viscous fingering while studying the displacement of sugar liquors by water (lesser viscosity) during regeneration of packed beds, where he observed significant channeling of the water through the more viscous sugar solution. Saffman and Taylor (1958) developed a stability criterion to explain viscous fingering in immiscible fluids. They showed that the differences in viscosity between the displacing and displaced fluids, along with the velocity of displacement, governed the growth rates of disturbances. When the viscosity gradient is unfavorable (the displacing fluid is lower in viscosity), the flow system is inherently unstable and leads to growing fingers. This effect of an adverse viscosity gradient on the growth, or otherwise,

of disturbances is discussed briefly below. This discussion is equally valid for both immiscible and miscible fluids.

Effect of adverse viscosity gradient: In Figure 1.1(a) is shown a single finger that has just developed. To the left of its boundary is the displacing fluid I of viscosity μ_1 (unshaded portion); to its right is the displaced fluid II of viscosity μ_2 (shaded portion). Let the pressure at the plane AA' be P_0 and the pressure at the plane BB' be P_1 . Let the distance between the two planes AA' and BB' be ε . We assume, for this discussion, that the permeability K of the porous medium and the velocity U of the fluid are constant throughout the flow domain. The pressure P_1 at BB' is determined by Darcy's law:

$$P_1 = P_o - \left(\frac{U\varepsilon}{K}\right) \cdot \mu \tag{1-1}$$

In the absence of the disturbance, the space between the planes AA' and BB' would be occupied by fluid Π ; so the pressure P_1 is governed by the value of μ_2 - higher the viscosity, lower the pressure P_1 in comparison to P_0 (i.e. $P_{1,ii}$), and vice versa (i.e. $P_{1,i}$). Once the disturbance has been initiated, however, the fluid inside the finger, at M^- has a viscosity μ_1 ; consequently the pressure just inside the boundary, at M^- , would be P_x , as seen in Figure 1.1(b).

Figure 1.1(b) shows the pressure profiles for the cases of (i) $\mu_1>\mu_2$, (ii) $\mu_1<\mu_2$, and (iii) $\mu_1=\mu_2$ (dashed line). If $\mu_1>\mu_2$, then the pressure just outside the finger, at M⁺, would be $P_{1,i}$ which is greater than P_x ; thus there would be a tendency for flow from the fluid II into fluid I, reducing the finger size; this signifies stable behavior. If $\mu_1<\mu_2$, however, the pressure just outside the finger,

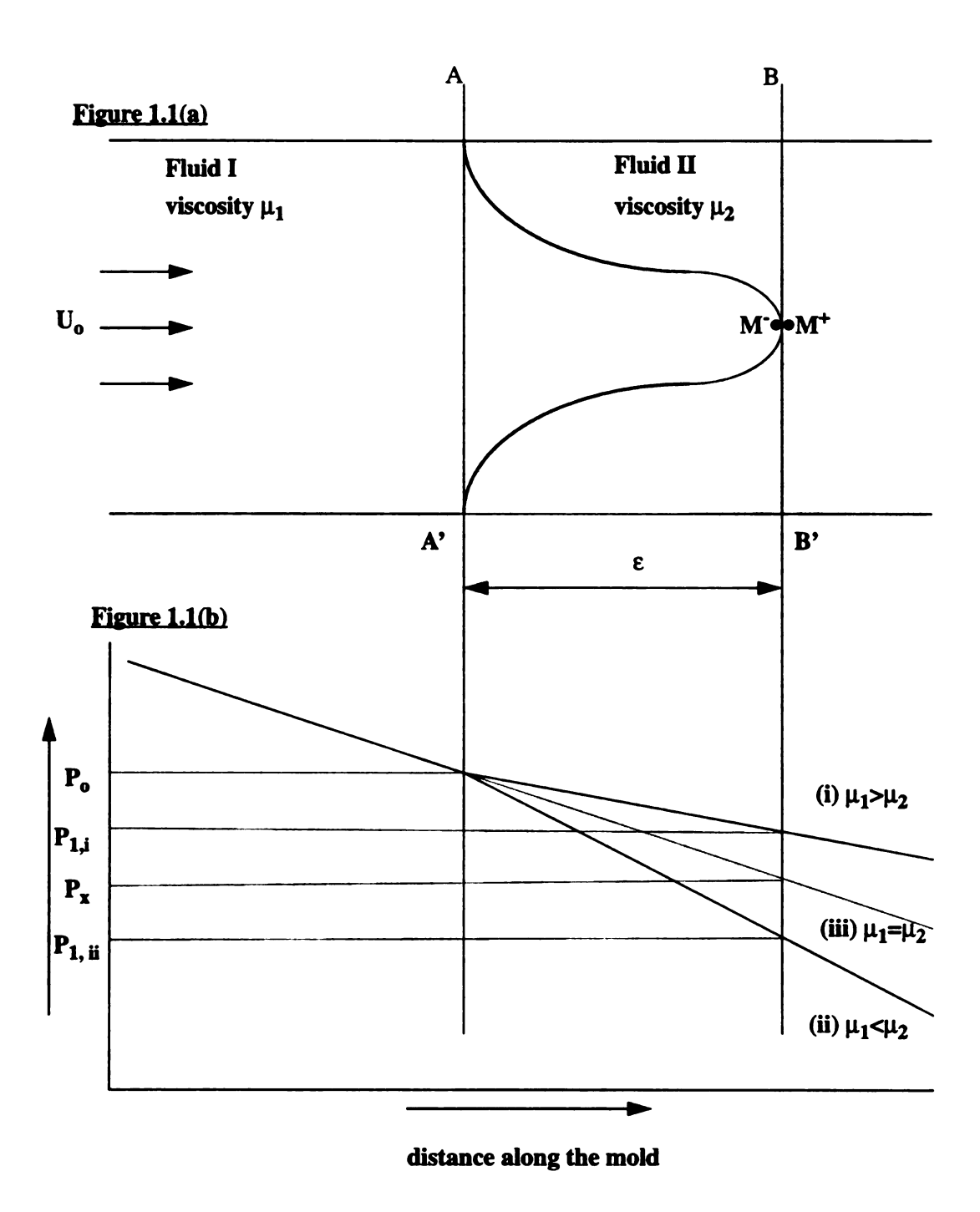


Figure 1.1 Mechanism of finger growth due to viscosity gradients

at M^+ , is $P_{1,ii}$ which is lower than the pressure P_x at M^+ ; this pressure gradient across the finger boundary would cause fluid I to flow outward into fluid II, indicating finger growth - instability.

Thus it may be concluded that incipient fingers would grow if the displacing fluid is of lower viscosity than the displaced fluid, while the fingers would be damped if a higher viscosity fluid displaces a fluid of lower viscosity. The driving force for finger growth is the pressure gradient across the finger boundary, which is determined by the viscosity difference across the two fluids. When a fluid displaces another fluid of higher viscosity, the unfavorable viscosity difference in the flow direction leads to flow instability, causing the low-viscosity fluid to channel through the second fluid, yielding 'fingers'.

Viscous fingering has been studied by researchers in petroleum engineering in the context of secondary oil recovery, using external fluids to push oil from the reservoirs up into the wells. Water has been used, with considerable success, for this purpose. Water, being lower in viscosity than the subterranean oil, pushes the latter through the porous rock formations. But it was observed that this scheme did not always extract all the oil in the formation, with water coming out of the wells after a certain period. This has been seen in laboratories, too, and has been attributed to the phenomenon of viscous fingering. Fingering in both immiscible and miscible displacement has been studied by various workers and has been reviewed by Homsy (1987).

Chuoke et al (1959) developed the first mathematical linear stability analysis for the displacement of two immiscible fluids. They included interfacial tension effects in their analysis, to obtain the necessary and sufficient conditions for instability of slow liquid-liquid displacement in porous media.

In liquid molding operations, however, the displacing and displaced fluids are both completely miscible, both comprising the same reactive resin, albeit of different degrees of polymerization. There is, thus, no interface between the two fluids, and the analyses done will correspond to those for miscible displacement problems. As will be seen below, the miscible nature of the two fluids in question provides an opportunity for dispersive mixing at the edges of fingers, thus smoothing out the viscosity profile. In addition the fresh resin, that pushes the older resin in the mold, is at a lower degree of polymerization than the latter, hence of lower viscosity. An adverse viscosity gradient is, thus inevitable in the liquid molding scenario. Fingers were observed in RTM experiments performed by Losure (1994). To illustrate the generation of fingers, the mold was first fed with the resin and left to react for a certain period. A fresh batch of the resin was then injected; this batch was dyed, to aid visualization of the generated fingers. Figure 1.2 shows a typical liquid molded part, as an illustration.

Miscible displacement does not involve any interfacial tension. Slobod and Thomas (1963) performed experiments to show the development of fingers by a fluid displacing another miscible fluid at different flow velocities. They found that a single, large finger was generated at small velocities and also saw that the edge of the finger was quite blurred and attributed this behavior to dispersive mixing of the two fluids across the edge. Larger flow velocities yielded a number of small fingers that merged, over time, into fewer fingers, though of considerably smaller widths than those seen in the low velocity experiments. No rigorous mathematical analysis was, however, presented in this paper. The type of finger that is produced, i.e. whether it is a single, large finger or comprises several fingers of smaller widths (finger splitting) is discussed by Park and Homsy (1985),

Figure 1.2 Typical molded plaque: to illustrate the generation of fingers. White - older resin; Shaded: fresh resin [after Losure, 1994]

MULTIPLE FINGER TIPS

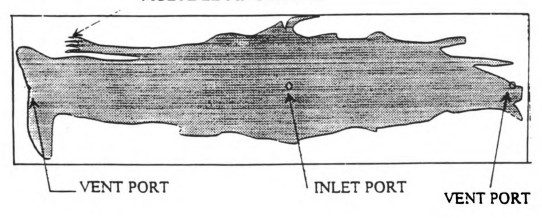


Figure 1.2

where a dimensionless group (Capillary number) is used as a criterion to describe a finger splitting regime in immiscible flows.

Perkins and Johnston (1963) published a review of the effects of diffusion and dispersion in miscible displacement processes in flows through porous media. A summary of the different empirical equations for longitudinal and transverse dispersion coefficients is also given. In a later paper, the same authors (Perkins and Johnston, 1965) suggest a useful way of denoting the size of a finger, as the ratio between the finger width to the spacing between successive fingers.

Schowalter (1965) formulated stability criteria for steady, constant velocity, miscible displacement of fluids in an infinite porous medium and discovered that the criteria for marginal stability are affected by variations in density, viscosity, the displacement velocity and also the effect of diffusion. Paterson (1985) used the analogy between flow through porous media and a Hele-Shaw cell and used viscous dissipation of energy in the displaced fluid as a stabilizing mechanism, to obtain bounds on the disturbance wavelengths for undamped growth for miscible fluids.

A linear stability analysis on miscible displacement, in the absence of any mitigating factors such as dispersive mixing, was performed by Hickernell and Yortsos (1986). The inherent instability of the miscible displacement process, in the presence of an adverse viscosity gradient, is observed and appropriate stability criteria are derived in this theoretical paper. Their results are presented schematically in Figure 1.3. Disturbances of all widths (wavenumbers) are seen to be unstable.

Tan and Homsy (1986) found that, in the presence of an adverse viscosity gradient between two miscible fluids in a porous medium, the flow is inherently unstable and that dispersion tends to stabilize the process by spreading out the mobility profile, more so for

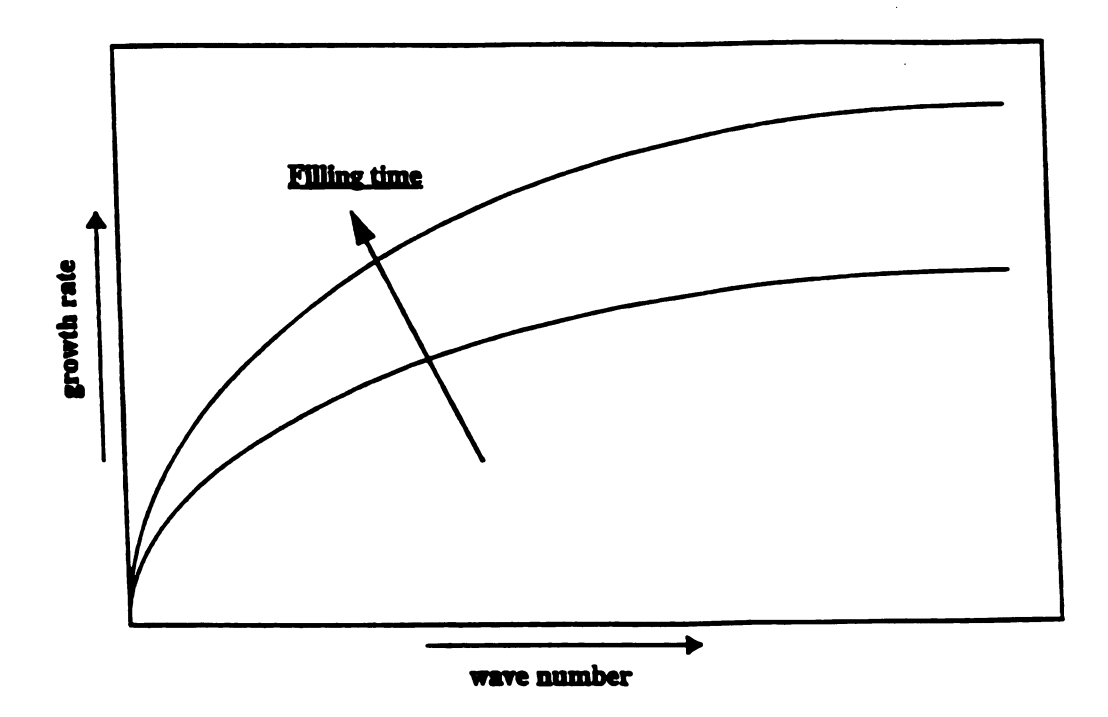


Figure 1.3 Filling with no reaction or dispersion [after Hickernell and Yortsos, 1987]

the higher wave number disturbances. They also studied the effect of anisotropic dispersion on the growth rate; they found that a small transverse dispersion increases the growth rate drastically in comparison to an isotropic case, resulting in a shift to smaller finger widths, while a large transverse dispersion tends to stabilize the system at all length scales. Their results are shown schematically in Figure 1.4, where the growth rates are plotted against wavenumbers at several times. Fingers of large wavenumbers are seen to be stabilized by the dispersion process.

Yortsos and Zeybek (1988) emphasized the dependence of dispersion coefficient on flow rate and concluded that the velocity dependence causes instability at large wavenumbers through a kind of a feedback mechanism. Nonlinear interactions of viscous fingers are discussed in later work by Homsy and co-workers (Tan and Homsy (1988), Zimmerman and Homsy (1991, 1992)). The effect of nonmonotonic viscosity profiles, as opposed to those considered in earlier literature, is presented by Manickam and Homsy (1993). In another paper, Tan and Homsy (1992) include permeability heterogeneities in the porous medium, described by a statistical model, and find a coupling between these heterogeneities and viscous fingering. Bacri et al (1992) experimentally confirm the theoretically predicted trends of the effects of various parameters, e.g. viscosity, flow rate and permeability heterogeneity, on fingering, after including effects of gravity and nonlinear dispersion in their analysis. Gorell and Homsy (1985) made predictions of the most dangerous wavenumber, i.e. the wavenumber at which growth rate is the largest, which would be the fastest growing

Porosity variations can occur in certain situations, e.g. during injection of acid into the formation, to increase crude oil production from a well. Chadam et al (1986) investigate these reaction-induced porosity variations and their effect on fingering

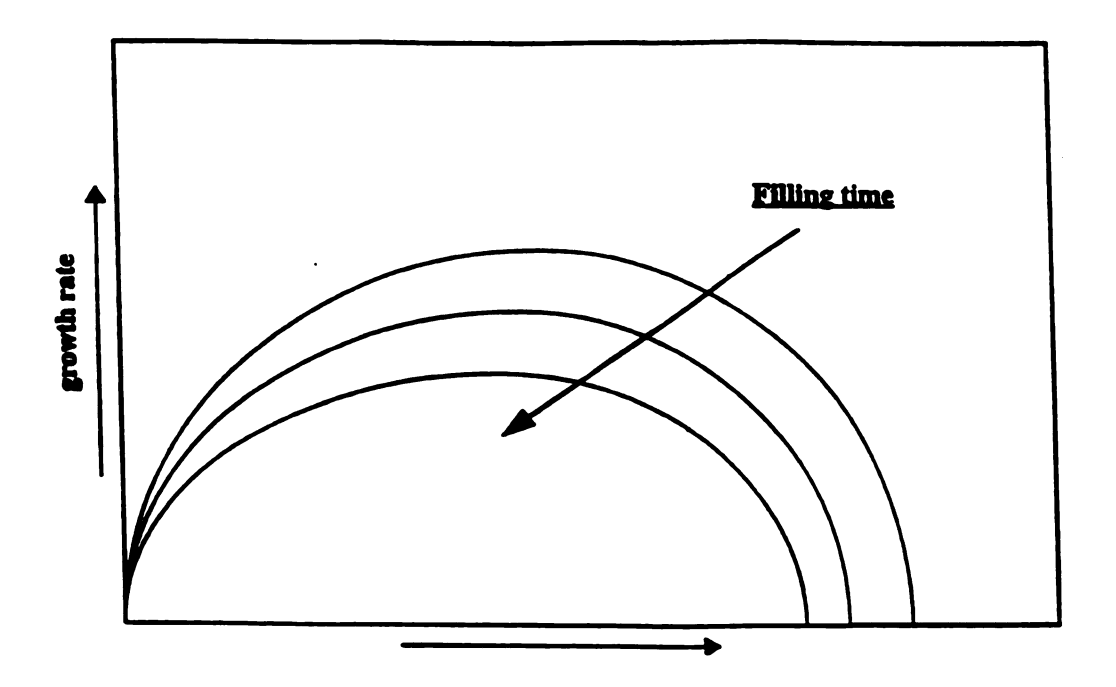


Figure 1.4 Filling with dispersion, no reaction [after Tan and Homsy, 1986]

instabilities. In a later paper, Chadam et al (1991) looked at the coupling of porosity variations with viscosity changes. Schincariol et al (1994) present an analysis of the growth of disturbances in a variable density flow and develop criteria for the growth or decay of disturbances.

1.3 LIQUID MOLDING AND VISCOUS FINGERING

Since the resin being injected in liquid molding operations is continuously polymerizing, the fluid in the filled region of the mold at any time has a constantly changing viscosity; fluid at the flow front has a higher viscosity than the fluid at the inlet to the mold. Though the question of two fluids does not arise, the flow situation may still be visualized as one in which the fresh fluid is pushing the older fluid and, thus, analyses done on miscible displacement of fluids would be applicable. Owing to the adverse viscosity gradient, in the absence of any stabilizing mechanism, the flow would be expected to be inherently unstable. Based on existing literature discussed above, it is easily seen that dispersion across the edge of a finger helps damp out the disturbance. Also, a higher transverse dispersion (transverse to the bulk flow) increases this smearing out effect. A brief discussion of the dispersion coefficients in several types of fiber preforms may be found in Losure (1994).

As seen in Figure 1.4, the fingers that are most likely to grow are the ones with the most dangerous wavenumber, seen in Figure 1.4 as corresponding to the peak.

Disturbances at both ends of the spectrum of wavenumbers have comparatively lower growth rates. The actual dimensions of the liquid molding cell play a major role in determining the size of the fingers. If the most dangerous wavenumber corresponds to a

finger width that is larger than the dimensions of the cell, the instability will not be seen in experiment.

The mechanical properties of a finished part are affected by viscous fingering. The time of generation of a finger, with respect to the injection of fresh resin, governs the strength of the edge of the finger. When the incipient disturbance is closer to the inlet, the degree of polymerization is still fairly low, and there is adequate opportunity for subsequent reaction to create crosslinks across the edge of the finger, thus bringing the finger close enough to the rest of the finished part in mechanical properties. On the other hand, if a disturbance is generated at a later time, when the conversion is fairly high, there is lesser scope for crosslinking across the edge of the finger, which makes the region of the finger behave as an inhomogeneity in the final part, with comparatively poorer mechanical properties.

1.4 SUMMARY

An introduction to the phenomenon of viscous fingering has been presented in the preceding sections of this chapter. The appearance of fingers during mold filling, and their effect on the properties of the final liquid molded parts, was briefly discussed. It was seen that no work has been done on the effects of reactive coupling on the stability of the flow through porous media. The following chapters of this dissertation deal with the role of the polymerization reaction on viscous fingering.

CHAPTER 2 POLYMER SYSTEMS IN LIQUID MOLDING: A REACTION KINETICS POINT OF VIEW

2.1 INTRODUCTION

Reaction Injection Molding (RIM), the precursor to Resin Transfer Molding (RTM) and Structural - Reaction Injection Molding (S-RIM), involves polymerization inside the mold. This is in contrast to conventional thermoplastic injection molding (TIM), where polymer is injected into the mold and allowed to cool to form a solid polymer. Monomer casting and thermoset injection molding processes also use polymerization inside the mold, but they employ heating of the mold walls to activate the reaction. In RIM, monomer and mold temperatures are usually quite close and the reaction is activated by impingement mixing of the reactants just before they enter the mold. A schematic of the RIM machine is shown in Figure 2.1 (Macosko). The two reactants A and B are mixed in appropriate ratios just before they enter the mold, to initialize the polymerization reaction. The resin far from the mold inlet has undergone considerable polymerization reaction compared to resin at the mold inlet.

RIM production began with polyurethanes. Nylon 6, dicyclopentadiene, acrylamate, epoxies, unsaturated polyesters and phenolic materials are several other chemical systems currently in use for RIM operations.

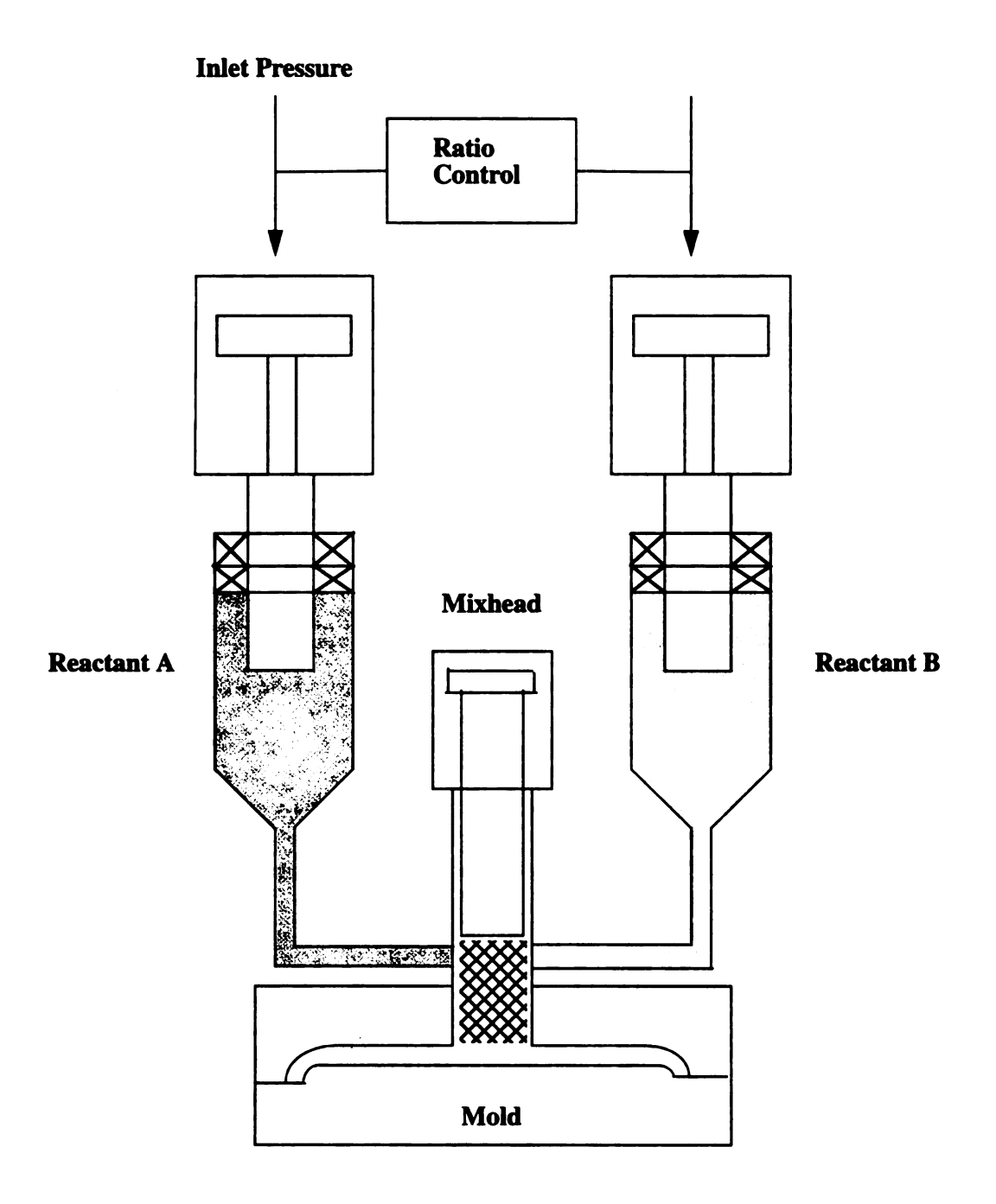


Figure 2.1 Schematic of a RIM Machine [after Macosko, 1989]

As will be seen in chapter 4, the chemical reaction kinetics of the resin used in liquid molding is an important factor in the determination of flow stability of the mold filling step; the stability is dependent on the rate of (polymerization) reaction and its derivatives with respect to conversion and temperature. Thus the form of rate expression that describes the polymerization reaction has a direct effect on subsequent analyses. For example, polyurethanes are usually represented by simple n-th order kinetics:

$$R = k_R (1 - \alpha)^n \tag{2-1}$$

while unsaturated polyesters and epoxies have been known to follow more complex rate expressions of the type:

$$R = (k_1 + k_2 \cdot \alpha^m) \cdot (1 - \alpha)^n \tag{2-2}$$

Several types of chemical reactions are schematically depicted in Figure 2.2, where the reaction rate, R, is plotted against the conversion, α , showing the different classes of reaction systems by the trends in variation of $(\partial R/\partial \alpha) \equiv S$. Reactions with kinetics given by equations of the type eqn. (1) have a negative S for all ranges of conversion, for nonzero orders of reaction, shown in Figure 2.2 as curves (a) and (b), while reactions with kinetics given by eqn. (2) would depend on the values of the kinetic constants and the conversion. When the order of reaction is zero, the reactions follow line (c).

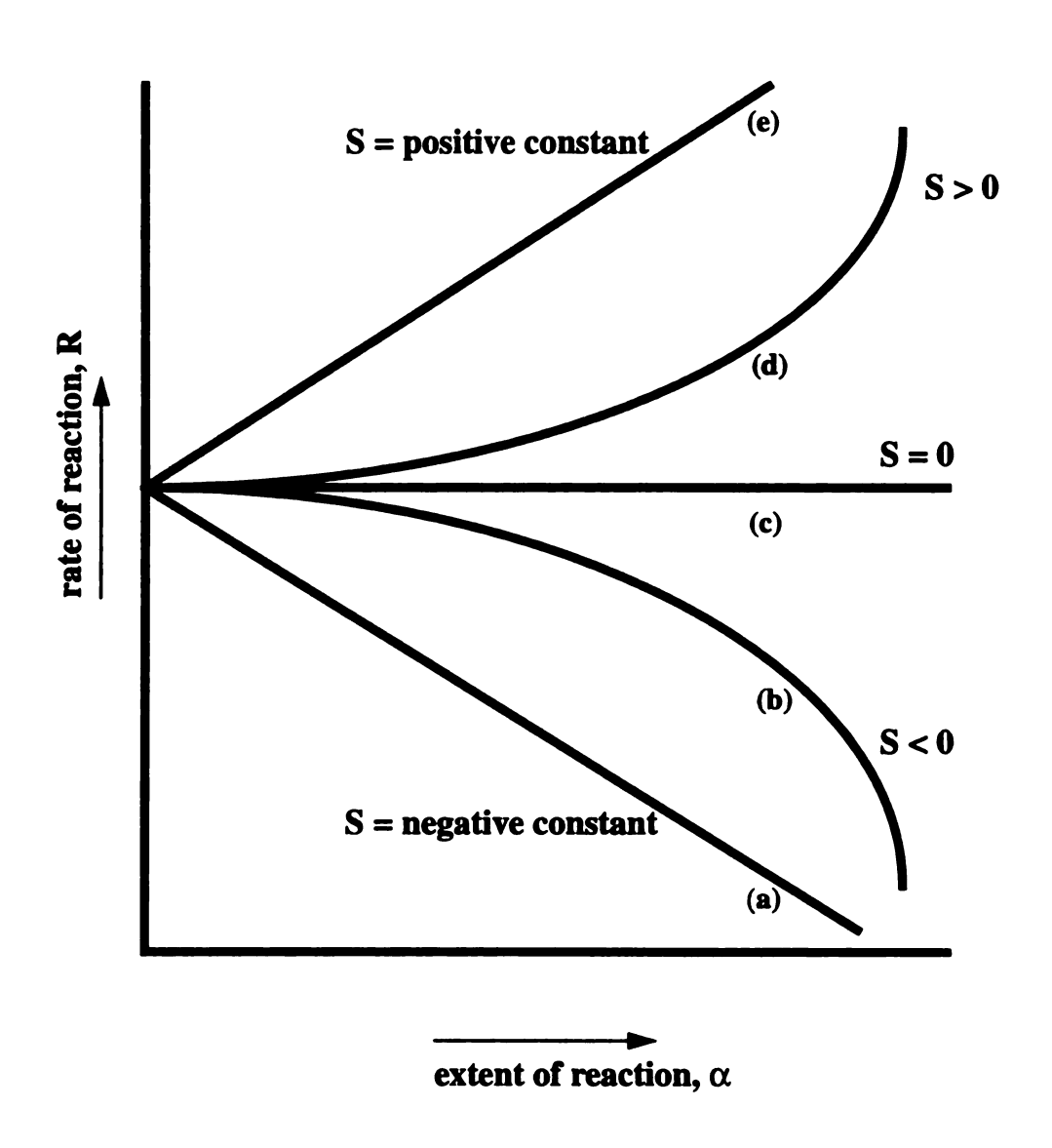


Figure 2.2 Types of chemical reactions classified by S behavior

The solidification process in all liquid molding operations involves crosslinking. The viscosity variations arising from this process are linked to the reaction kinetics of the polymerization process. The rheological changes during a single RIM cycle, up to gelation, are shown in Figure 2.3. The initial viscosity of the reactant mixture is low enough to enable rapid mixing. As the monomers react to form high molecular weight resin, the viscosity rises. This build up must be slow enough for the entire mold to be filled. Once the mold is filled, injection of reactants is stopped and the viscosity allowed to increase rapidly to gelation.

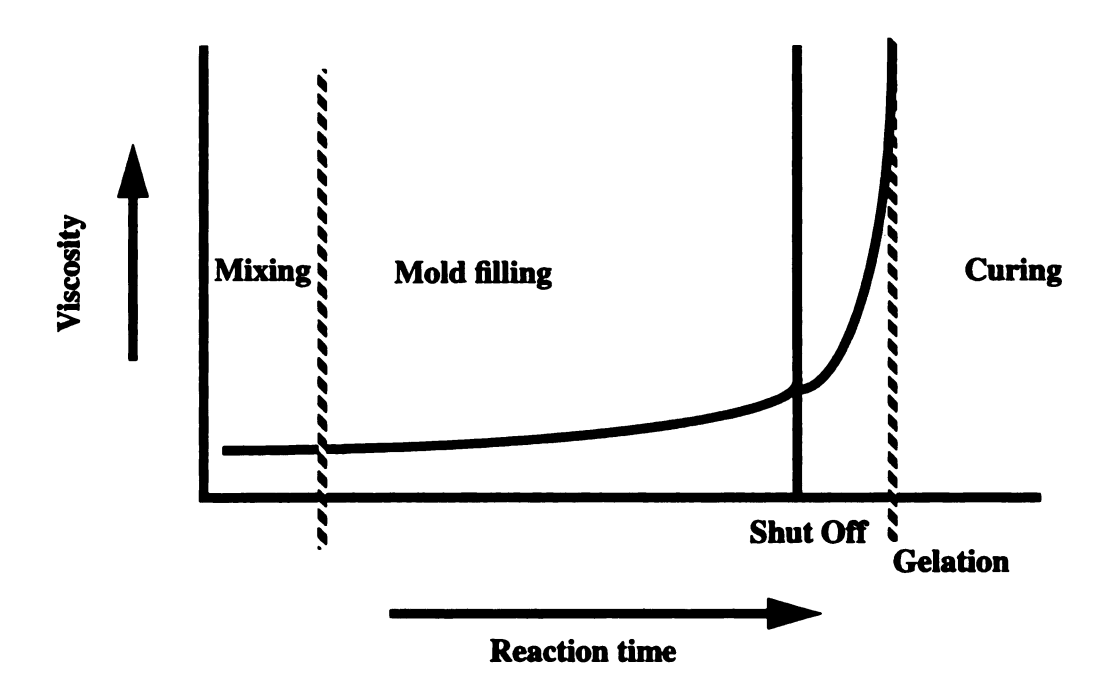


Figure 2.3 Viscosity changes during a RIM cycle

Though fast polymerization reaction is essential for a polymer system to be successfully used in RIM processes, not all such fast polymerizations are suitable.

Polymerizations in solution, emulsion or suspension are not suited for production of a molded part; polyethylene or polypropylene, which are made only in solution or suspension, are ruled out. Polyesters, which need extensive condensation of a small molecule, are poor candidates for liquid molding. Monomers that need to be heated to their melting temperature for polymerization also are unsuitable since this would need preheating the mold to high temperatures for the reaction to occur, followed by cooling to cause crystallization. High initial viscosity of the monomeric liquid makes some polymer systems unsuitable for RIM.

A brief study of some polymer systems that are amenable to liquid molding follows. The focus of the discussion in the rest of this chapter will be on the reaction kinetics of the polymer system under consideration and its effects on the viscosity, since they are the factors essential for the analysis of the stability of mold filling processes in later chapters.

2.2 POLYURETHANES

Formation of polyurethanes involves the reaction of isocyanates with compounds containing an active hydrogen. The active hydrogen compound, e.g. an alcohol, adds across the carbon-nitrogen double bond of the isocyanate group.

$$R - NCO + HO - R' \rightarrow R - NH - CO - O - R'$$
 (2-3)

The {-NH-CO-O-} linkage is called the urethane bond.

Water reacts with isocyanate to form a urea, so careful drying of reactants and catalysts is done; typical water level in RIM materials is < 0.07%. Reaction of amines

with isocyanates also yields ureas. Organometallic compounds can greatly increase the rate of urethane formation. Isocyanates can also undergo addition or auto-condensation reactions. Dimerization of isocyanates is reversible at high temperatures, while the products of trimerization (Isocyanurates) are more stable. The urethane bond is also known to be reversible at high temperatures and care has to be taken during RIM and postcuring operations, where temperatures can go to fairly high levels. Urethane reactions give no byproducts. They go to a high degree of conversion and also can be very fast, depending on the active hydrogen compound. These factors render urethanes well suited to liquid molding operations.

RIM processes require that a polymerization goes to completion in a few minutes, preferably less than one. Reaction kinetic data are necessary for modeling the rheological changes which control mold filling and curing. It has been observed (Macosko 1989) that most urethane reactions proceed according to the following, simple n-th order, kinetic expression:

$$-\frac{d[NCO]}{dt} = k_R [NCO]^m$$
 (2-4)

Here the reactants are assumed to be in stoichiometric ratios, as is normally the case, and the concentration of the catalyst is absorbed into the rate constant. The overall order of the reaction "m" typically has a value of 2. The rate constant, k_R , is described by the usual Arrhenius form:

$$k_R = A_R \exp\left(-\frac{E_a}{RT}\right) \tag{2-5}$$

In terms of the extent of reaction (conversion), α , the rate expression then becomes:

$$R = \frac{d\alpha}{dt} = A_R \exp\left(-\frac{E_a}{RT}\right) (1 - \alpha)^m$$
 (2-6)

From this form of the rate equation, it may be seen that polyurethanes follow chemical reactions of the type (a) or (b) in Figure 2.2, depending on the order of the reaction.

Viscosity is dependent on conversion and temperature, both of which are continuously varying during the molding process. Kinetic results can be combined with structural relations (probability arguments) to derive expressions for the evolution of the molecular weight with time and temperature. From these molecular weight expressions, viscosity is also easily determined. Empirical data on several polyurethane resins suggested the following expression for the viscosity:

$$\mu = \mu_o(T) \left[\frac{\alpha_g}{\alpha_g - \alpha} \right]^{C_1 + C_2 \alpha}$$
 (2-7)

where $\mu_0(T)$ is represented by an Arrhenius type of equation:

$$\mu_o(T) = A_{\mu} \exp\left(\frac{E_{\mu}}{RT}\right) \tag{2-8}$$

 α_g in these equations is the gel conversion for the urethane formulation in question due to formation of a network. Equation 7 suggests that viscosity depends on the reaction kinetics through the extent of reaction, α .

2.3 POLYAMIDES

Polyamides are the basic unit of Nylon 6 and are the most studied nonurethane RIM system. They have the advantage of a high modulus, high impact strength and high temperature stability. They are commonly made by anionic polymerization of ecaprolactum with a suitable initiator and metal catalyst. The mechanism involves a steppropagation. Acyl lactam is an example of initiator used. Sodium caprolactam and Magnesium caprolactam are the most commonly used catalysts.

The reaction kinetics for the formation of polyamides has been well studied (Malkin et al 1982). An autocatalytic model fits a large amount of data for the sodium catalyzed reaction. The rate equation is found to be of the form:

$$\frac{d\alpha}{dt} = k_1 \exp\left(-\frac{E_a}{RT}\right) \left(\frac{I^2}{M_o}\right) (1 - \alpha) \left(1 + \frac{k_I \alpha}{I}\right)$$
 (2-9)

where "I" is the concentration of the initiator and is the same as the catalyst concentration. M_0 is the initial monomer concentration and α is the extent of reaction (conversion), " k_1 " is the rate constant and " k_1 " is an autocatalytic term. It is seen that the reaction kinetics for this polymer follows a more complicated rate expression than for the polyurethane system, due to the presence of the autocatalytic term.

From the above form of rate expression, it is seen that $\partial R/\partial \alpha$ is negative for conversions greater than or equal to 50%; for lower conversions, it depends on the numerical values of the initiation rate constant, "k_I", and the initiator concentration "I".

The reactant viscosity is low and the reaction rate is relatively slow. This ensures that molds are easily filled. Gel times are typically over 20s. However, the low viscosity may lead to bubble problems. One disadvantage for this Nylon 6 system is that of a high operating temperature and require high temperature RIM machines.

2.4 EPOXIES

Suitable catalysts and hot molds are needed to adapt epoxy formulations to liquid molding. Most epoxy formulations are based on bisphenol A and aliphatic diamines. Highly crosslinked networks result from the reaction since both amino hydrogens can react with the epoxy groups. A typical reaction scheme for an epoxy system is shown in Figure 2.4. The reaction is found to follow simple n-th order kinetics, given by a rate equation of the form:

$$\frac{d\alpha}{dt} = A_R \exp\left(-\frac{E_a}{RT}\right) (1 - \alpha)^n \tag{2-10}$$

The order of the reaction, "n", depends on the polymer system being considered. An amino-ethyl-piperazine formulation is found to have an order n = 2.8 (Osinski 1983), while a Diglycidyl ether of bisphenol A (DGEBA) / triethylene tetramine (TETA) system has an order n=1.64 (Kim and Kim 1987). Like the polyurethanes, epoxies also are seen to be represented by curves (a) or (b) in Figure 2.2.

The viscosity in typical epoxy resins is high; so the reactants have to be preheated to enable easy mold filling. The need for hot molds and a typically large exotherm can cause degradation problems. However, the reactions themselves are relatively slow compared to typical injection times. Therefore the problems arising from viscosity buildup and premature gelation are absent.

Kim and Kim (1987) have found that the viscosity rise during reaction, for the DGEBA/TETA system, follows equation 7 that was presented in the discussion of polyurethanes. The gel time for a DGEBA/TETA system at 50°C has been found by

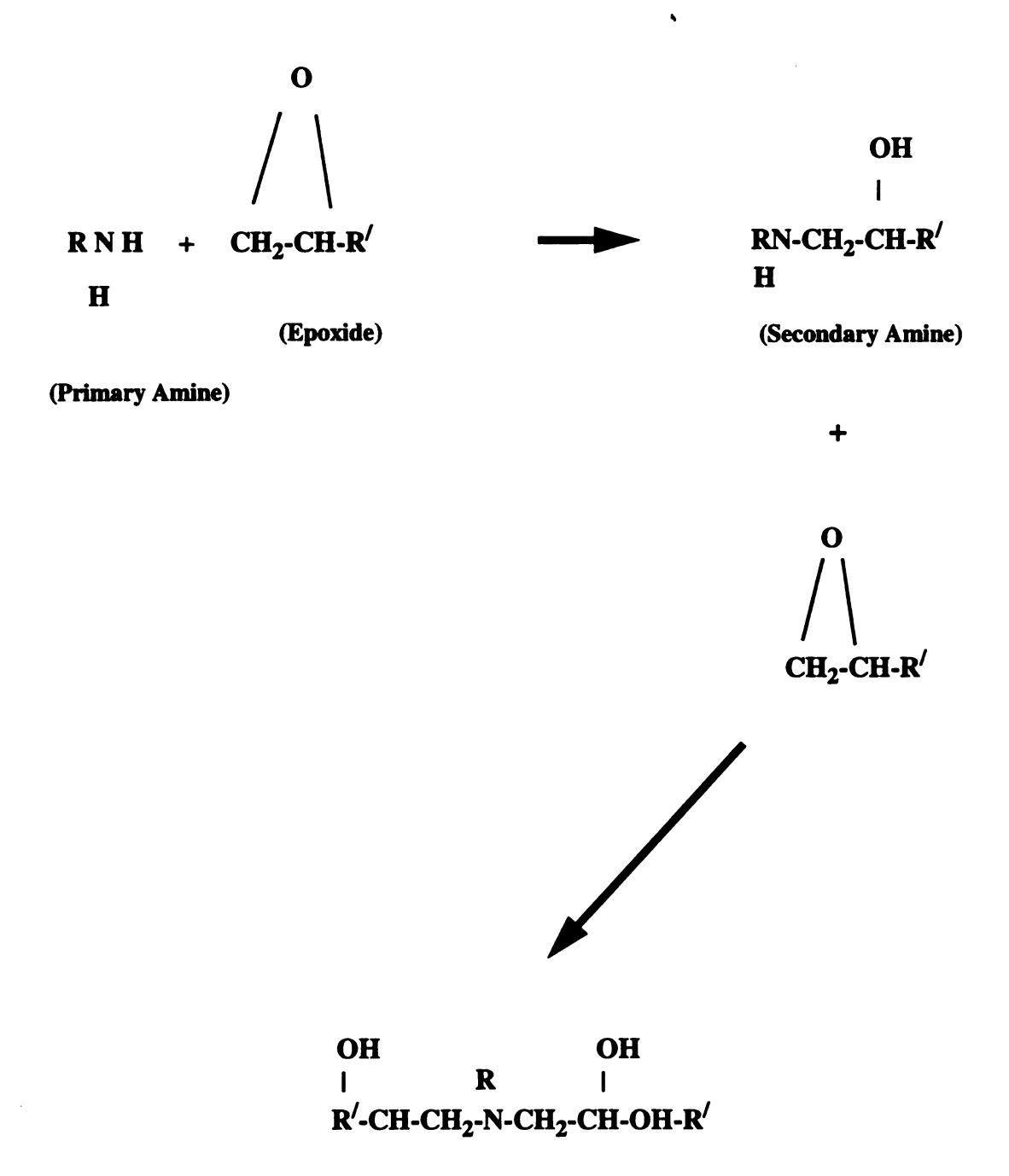


Figure 2.4 Reaction scheme for an Epoxy system

Losure (1994) to be about 30 minutes. Thus, in comparison to both polyurethanes and polyamides, the epoxy resins have a significantly higher gel time.

CHAPTER 3 VISCOSITY VARIATIONS DURING REACTIVE FILLING OF FIBER
PREFORMS

3.1 INTRODUCTION

Analysis of the mold filling process in liquid molding is usually done with the assumption that liquid advancing through the fiber preform maintains a constant viscosity and remains inelastic. This assumption is frequently questionable. During the filling process in resin transfer molding there is a constant variation of the viscosity of the resin, and also a significant rise in the elastic nature of the resin, due to various reasons, which were discussed in chapter 1.

Hence, the changing resin rheology during the miscible displacement of binder or during the reactive filling process affects the resin pressure distribution within the mold in a complex way. The next section presents an analysis to show the effect of resin rheology on several measurable quantities during mold filling in an end-gated mold. Rheological data taken from experiments conducted on an epoxy resin and a polyester are used to investigate these effects of changing rheology.

3.2 ROLE OF RESIN RHEOLOGY IN LIQUID MOLDING

The problem addressed in this section is the adiabatic flow of reacting resin through a fiber preform placed in an end gated rectangular mold. The fibers are aligned transverse to the flow and the model pertains to one dimensional motion of the resin with constant inlet pressure P_0 at the gate (see Figure 3.1). A complete description of reactive

filling would couple the changing rheology to the species mass balance and the energy balance (Garcia et al). The effect of changing rheology is illustrated directly with the help of rheological data obtained on the resin as it cures within the gap of a rheometer.

The rate of change in rheology with increasing extent of cure, varies with resin formulation. With some resin formulations for which the conversion at the gel point is low, this variation is abrupt -- the change is hardly noticeable upto the gel conversion; then gelation occurs very rapidly. With other formulations, the change in rheology occurs smoothly -- both the viscosity and the elastic modulus of the resin change over a range of conversions leading up to the gel point. The effect of such changes in resin rheology upon the front motion, and upon the resin pressure distribution during the filling process in resin transfer molding is examined here with a rectangular, end gated mold at constant inlet pressure.

3.2.1 RESIN RHEOLOGY AND APPARENT PERMEABILITY

The changing rheology of two different resin formulations has been monitored in the gap between parallel plates in an RMS-800 instrument. Both the Devcon epoxy resin and the Derakane vinyl ester resin reach the gel point over a time frame of several minutes in the laboratory. Figures 3.2 and 3.3 show the time evolution of the steady shear viscosity and of the dynamic shear storage modulus G' at a fixed, low frequency ω of 1 rad/s, for these resins. A fluid relaxation time, τ , may be calculated with the expression

$$\tau = \frac{G'}{\omega^2 \mu} \tag{3-1}$$

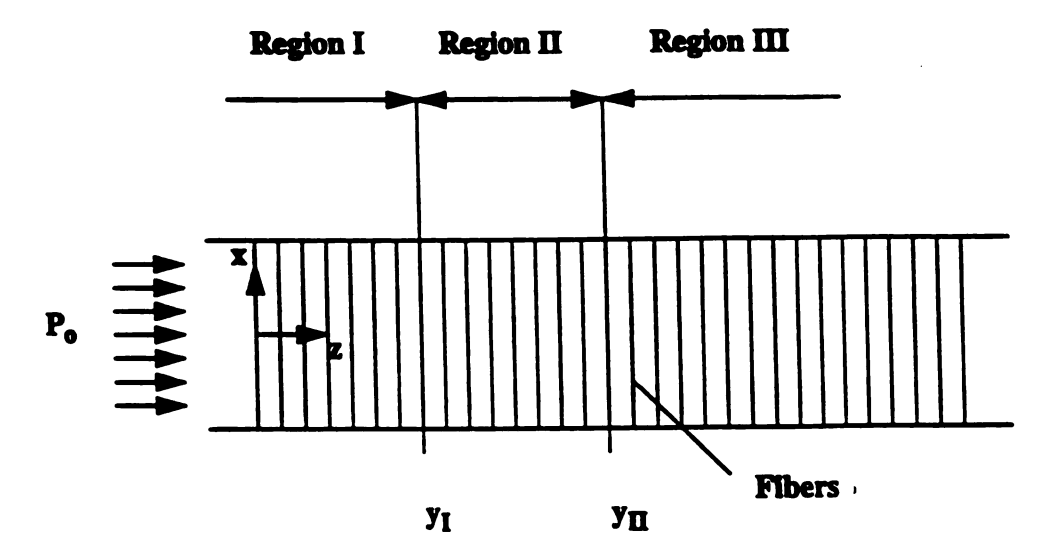


Figure 3.1 One-dimensional flow of resin, transverse to fibers, in an end-gated mold

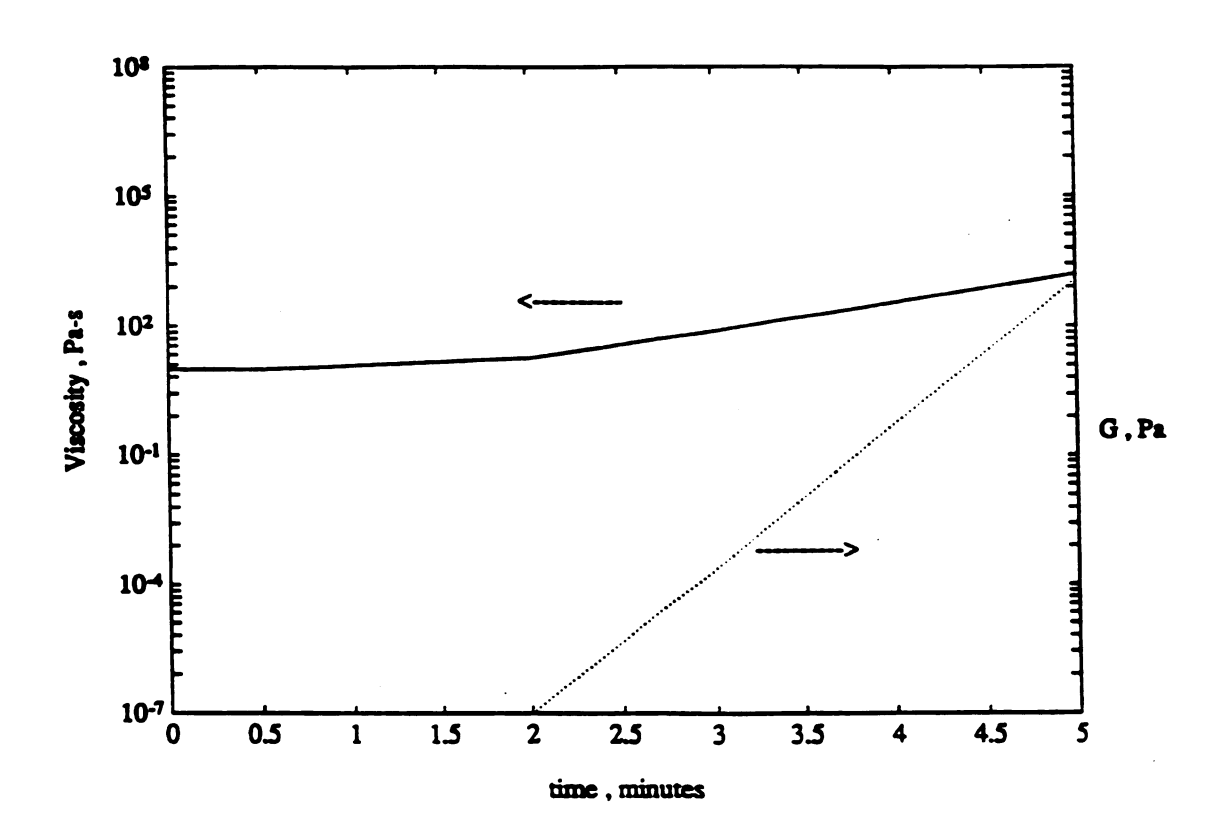


Figure 3.2 Rheology of Devcon epoxy resin

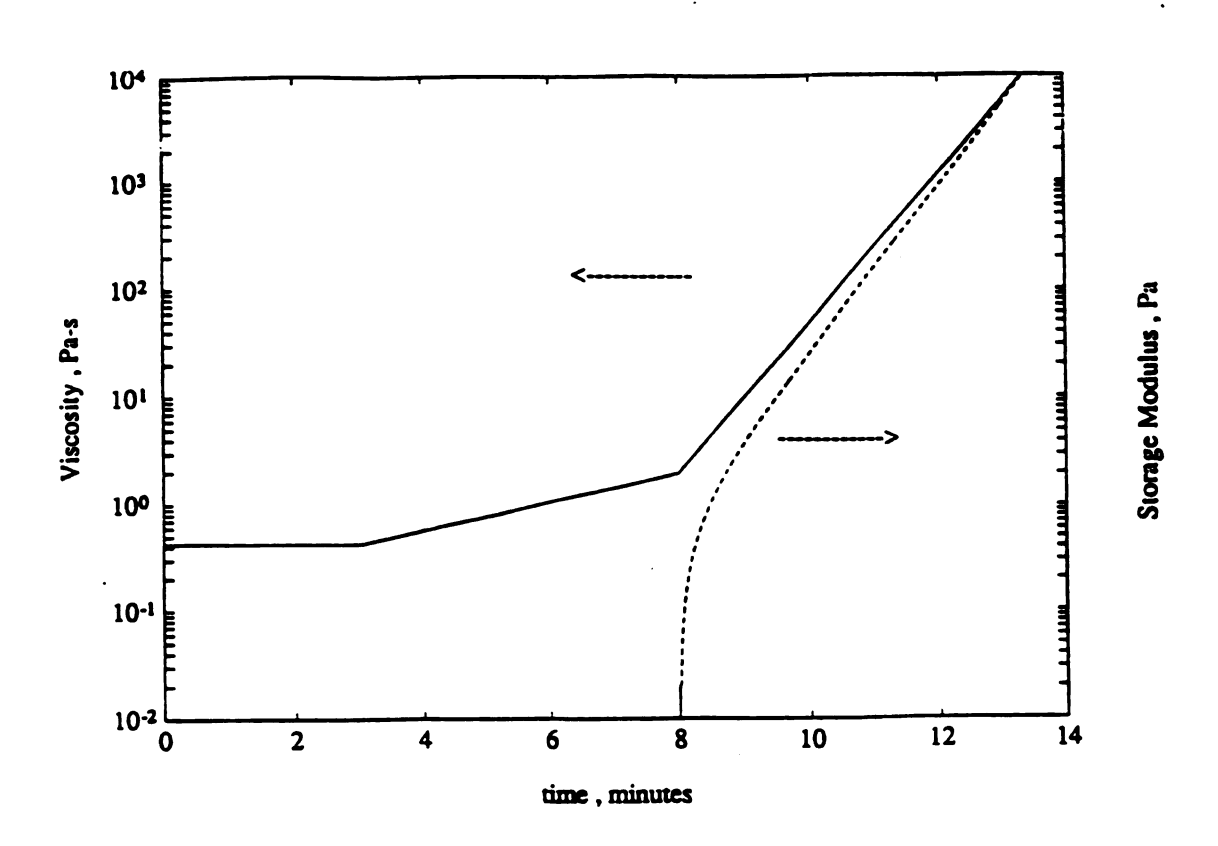


Figure 3.3 Rheology of Derakane resin

Different regimes were identified on the basis of these curves. In the first regime ($t < t_I$), the resin is an inelastic fluid of constant viscosity. In the second regime ($t_I < t < t_{II}$), the fluid remains inelastic but displays an increasing viscosity. In the third regime ($t > t_{II}$), the fluid develops viscoelasticity in addition to an increasing shear viscosity. The fluid viscoelasticity developed at various stages is associated with increasing extensional viscosity of the resin. These figures show that the progression from inelastic resin to gel is more abrupt for the Derakane resin.

The bulk flow of incompressible, Newtonian fluids through porous media at low Reynolds numbers is described by Darcy's law. This macroscale representation of the superficial velocity in anisotropic media requires the specification of two or more directional permeability coefficients defined by the geometry of the preform. The permeability K_t transverse to the fiber axis is typically several times lower than the longitudinal permeability along the fiber axis. The apparent transverse permeability of fiber arrays with hexagonal packing and a fiber volume fraction of 30 percent, to viscoelastic liquids, is plotted against a measure of viscoelasticity on Figure 3.4. Increasing viscoelasticity is represented by increasing values of a dimensionless ratio of fluid time scale to flow time scale -- the Deborah number, De.

$$De = \frac{\tau U_o}{a} \tag{3-2}$$

The permeability K_t (normalized with the constant value for Newtonian liquids, K_{to}) starts to drop at an onset Deborah number of 0.4 and continues to decrease with increasing De. At higher values of the Deborah number, the apparent permeability reaches an asymptotic value.

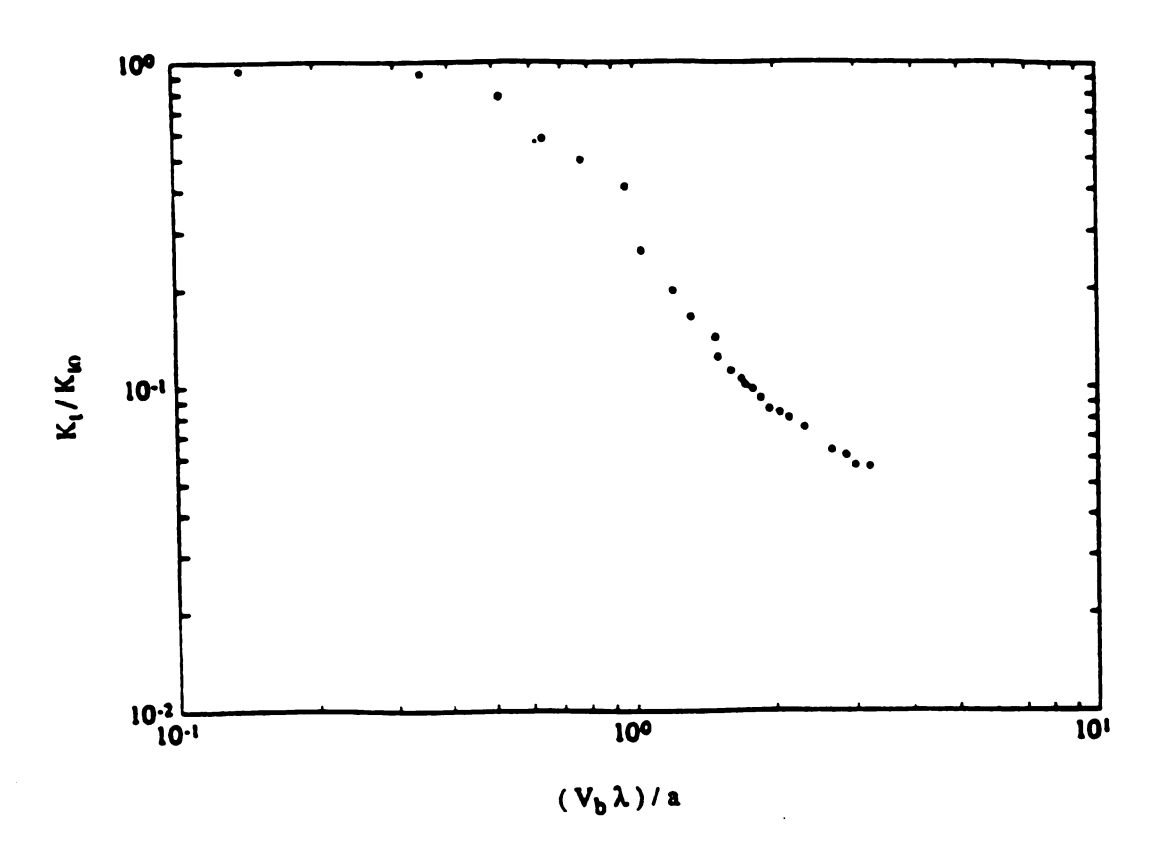


Figure 3.4 Apparent transverse permeability Vs. viscoelasticity - Hexagonal array

3.2.2 THE MATHEMATICAL MODEL

The one dimensional flow along the y -direction transverse to the fiber axis in the fiber array, is described by the following equations. First we define a coordinate moving with the front

$$\xi \equiv z - z_f \tag{3-3}$$

where z_f denotes the location of the front. Then, we obtain

Continuity
$$\frac{\partial U_o}{\partial \xi} = 0$$
 Permeation
$$\frac{\partial P}{\partial \xi} = -\frac{U_o}{m_a}$$
 (3-4) Motion of front
$$\frac{dz_f}{dt} = \frac{U_o}{\varepsilon}$$

 U_{o} is the superficial velocity through the fiber array, ϵ is the porosity of the array and m_{a} is the apparent mobility defined by

$$m_a \equiv \frac{K_t}{\mu} \tag{3-5}$$

the apparent permeability K_{t} and the viscosity μ .

The boundary conditions for operation at constant inlet pressure are

$$P = P_o$$
 at $\xi = -z_f$
 $P = 0$ at $\xi = 0$ (3-6)

Analysis Of Model Equations: Three different regions are identified on the basis of apparent resin mobility, which is the ratio of apparent permeability through the fiber

preform, to the viscosity of the resin. The mobility of fluid flowing through the first region close to the inlet is uniform because the shear viscosity is constant and the Deborah number is lower than the onset value for viscoelastic effects. The mobility of fluid flowing through the second region decreases towards the front only because of the increasing shear viscosity. The mobility of fluid flowing through the third region is affected by both variations in extensional viscosity and increasing shear viscosity.

The analysis of the filling process is presented for two different situations: filling with constant mobility and filling with the first two types of regions. For the purpose of this dissertation, the viscoelastic effects are not considered. It was observed by Gonzalez-Romero and Macosko (1985) that the viscosity of several polyurethane systems is independent of the shear rate, i.e. Newtonian behavior of the polymeric fluids may be assumed, up to the gel point. Since the viscoelastic regime does not begin until the viscosity is quite high, this assumption is made for these resins also.

The solution for the first situation is classic (Collins, 1961). In the other situation, analytical expressions are developed for the resin pressure distribution and for the velocity at any given time by assuming an exponential variation of mobility over each subregion. These expressions are combined with numerical integration over time for the location of the front and of the crossover planes for onset of shear viscosity increases. The constant inlet pressure condition leads to progressively lower superficial velocities with time so that the residence time corresponding to a location in the mold increases with time. In other words, after the start of the filling operation, fluid elements entering the mold at any time undergo the same rheology changes at shorter distances from the gate.

Filling With Constant Mobility: The mobility is constant throughout the resin up to time t₁

from the start of the filling operation and is described by

$$m_a \equiv m_I = \frac{K_{to}}{\mu_o} \tag{3-7}$$

The front has advanced for a time period less than $t_{\rm I}$, the solution to the model equations (eq. 3-4) is readily obtained as

$$P = -\frac{P_o \xi}{z_f} = \frac{P_o}{z_f} (z_f - z)$$

$$z_f = \left[\frac{2m_I P_o t}{\varepsilon} \right]^{\frac{1}{2}}$$

$$U_o = \frac{m_I P_o}{z_f}$$
(3-8)

The location of the front at time t_I , denoted by y_A , may be found from the above equation as

$$y_A = \left[\frac{2m_I P_o t_I}{\varepsilon}\right]^{\frac{1}{2}} \tag{3-9}$$

The velocity at the onset of rheology changes is $m_I P_o/y_A$. This velocity will be used as a reference velocity for analysis of the second region.

Filling With Shear Viscosity Changes: Over the time period t_I to t_{II} , the region behind the advancing front may be divided into two subregions -- one of uniform mobility m_I and another where the mobility varies because of the changing shear viscosity alone. The mobility at the front m_f is then given by

$$m_f = \frac{K_{to}}{\mu(t)}$$
 for region II (3-10)

The viscosity is evaluated at the time corresponding to z_f . The location of

crossover between the two subregions, termed y_I , also varies with time. It is convenient to fit the variation in mobility from this crossover plane to the front in region II with an exponential at any given front location or a given time. This choice has been validated by the final converged values of residence times at different locations behind the advancing front. The velocity U_0 at a given front location is then obtained from the following equation.

$$\frac{m_I P_o}{y_A U_o} = \frac{y_I}{y_A} + \left(\frac{z_f - y_I}{y_A}\right) LMMDR[f, I]$$
 (3-11)

This equation involves four dimensionless groups. The group $[m_IP_o/(U_oy_A)]$ represents a factor by which the velocity is reduced from the velocity at the onset of rheology changes. The group (z_f/y_A) is the current location of the front relative to its location at the onset of rheology changes. The group (y_I/y_A) is the current location of the crossover between the first two regions. The final group termed LMMDR [f,I] is the ratio of a logarithmic mean mobility difference (between the crossover plane and the front) to the mobility at the front; this group is given by the following expression.

$$LMMDR[f,I] = \frac{1}{m_f} \frac{m_f - m_I}{\ln\left(\frac{m_f}{m_I}\right)}$$
(3-12)

If there were no changes in fluid rheology during the filling process ($m_f = m_I = constant$), this group would have a value of 1.

The increments in front location and in the crossover location corresponding to increments in time are determined by integrating eq. (3-4) and an analogous equation for y_1 with the trapezoidal rule.

$$\Delta z_f = \Delta t \quad \frac{U_o^{old} + U_o^{new}}{2 \ \varepsilon}$$
 (3-13)

These equations are combined with Eq. (3-11) to determine the velocity at the next time value.

3.2.3 DISCUSSION OF COMPUTED RESULTS

The expressions derived above have been used to compute the motion of the front and of the different crossover planes, as well as the evolving pressure distribution, for several cases. These cases are represented by different values of the characteristic velocity $m_I p_o/y_A$ ranging from 3.59 mm/s to 6.22 mm/s. Scaling all displacements by y_A and the pressure by the inlet pressure P_o then yields one curve for each of these quantities that covers all values of inlet pressure and of Newtonian liquid permeability (K_{to}) provided the rheology variation with time is given; something in the nature of a master curve is obtained.

Penetration: The resin penetration into the fiber bundle is plotted against time on Figure 3.5. The front crosses over at 0.5 min into the region of changing shear viscosity and into the region of developing modulus at a time of 2 min and a location 1.94y_A. Between 0.5 min and 2 min, the change in shear viscosity leads to a 20 percent higher drop in velocity than would be obtained with unchanging mobility. At longer times -- 4 min, the changing rheology leads to a 94 percent higher drop in velocity than would be obtained with the mobility fixed at the value corresponding to 2 min. The dimensionless plot of velocity on Figure 3.6 shows these trends. It must be kept in mind that the sharper drop at greater

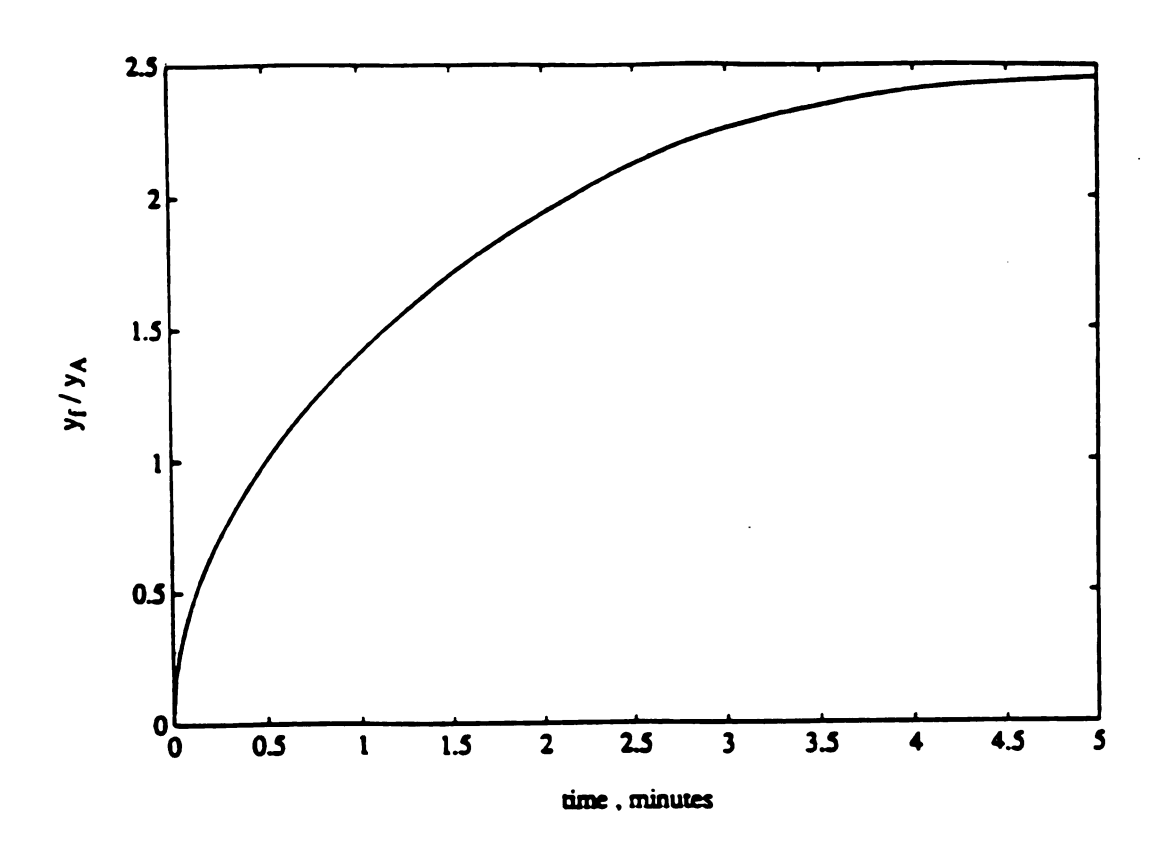


Figure 3.5 Resin penetration into fiber bundles

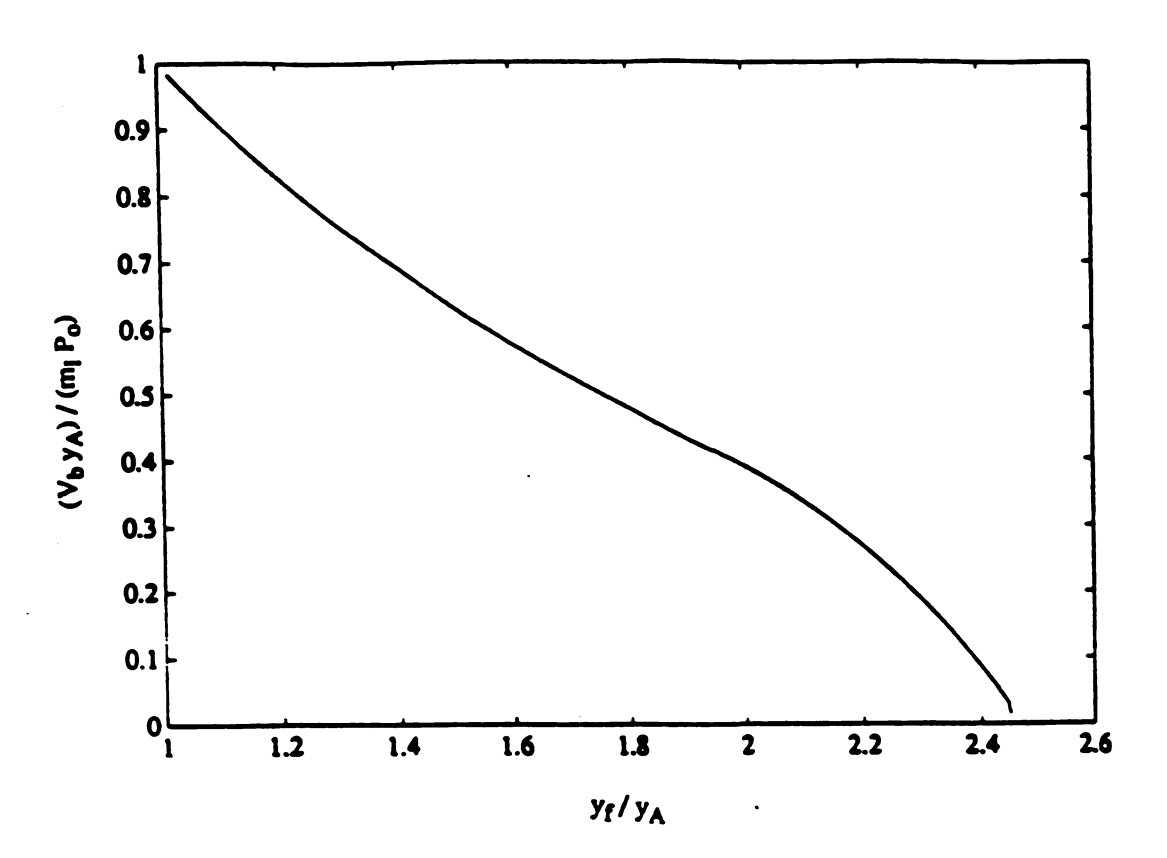


Figure 3.6 Dimensionless superficial velocity at various flow front positions

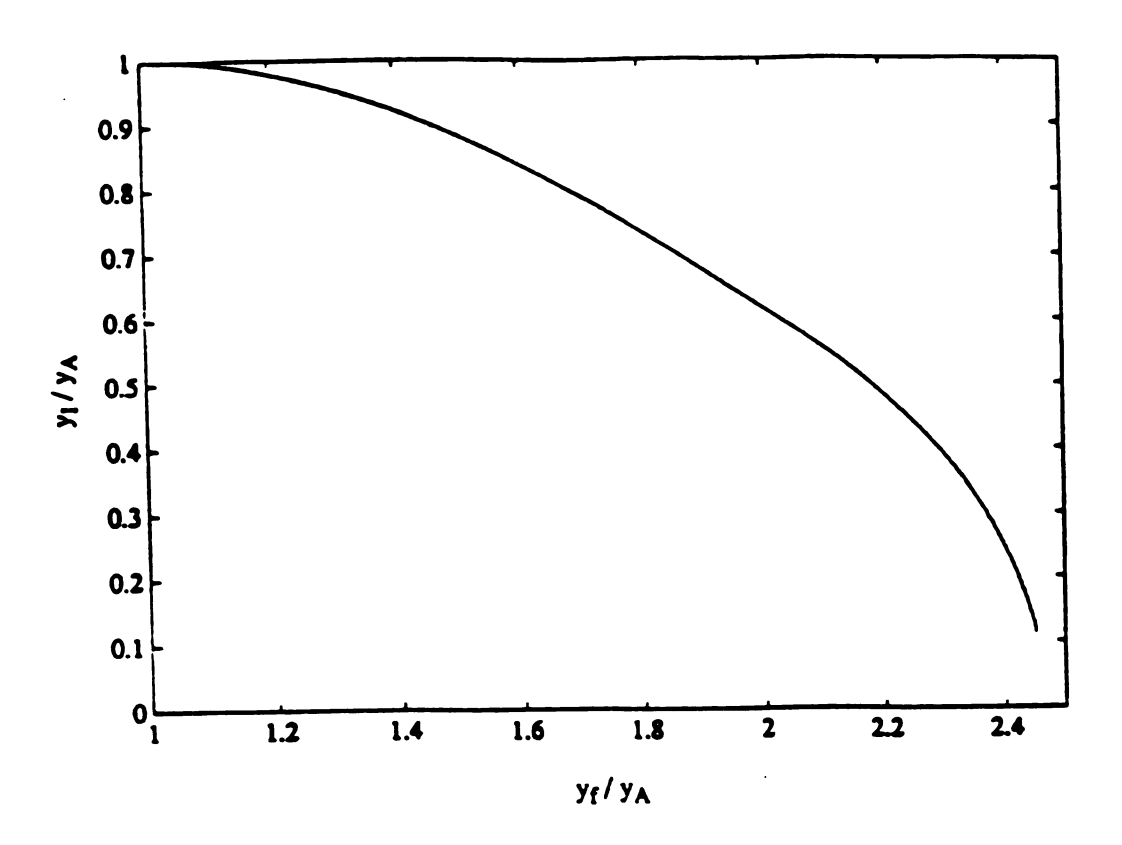


Figure 3.7 Location of y_I at various positions of the flow front

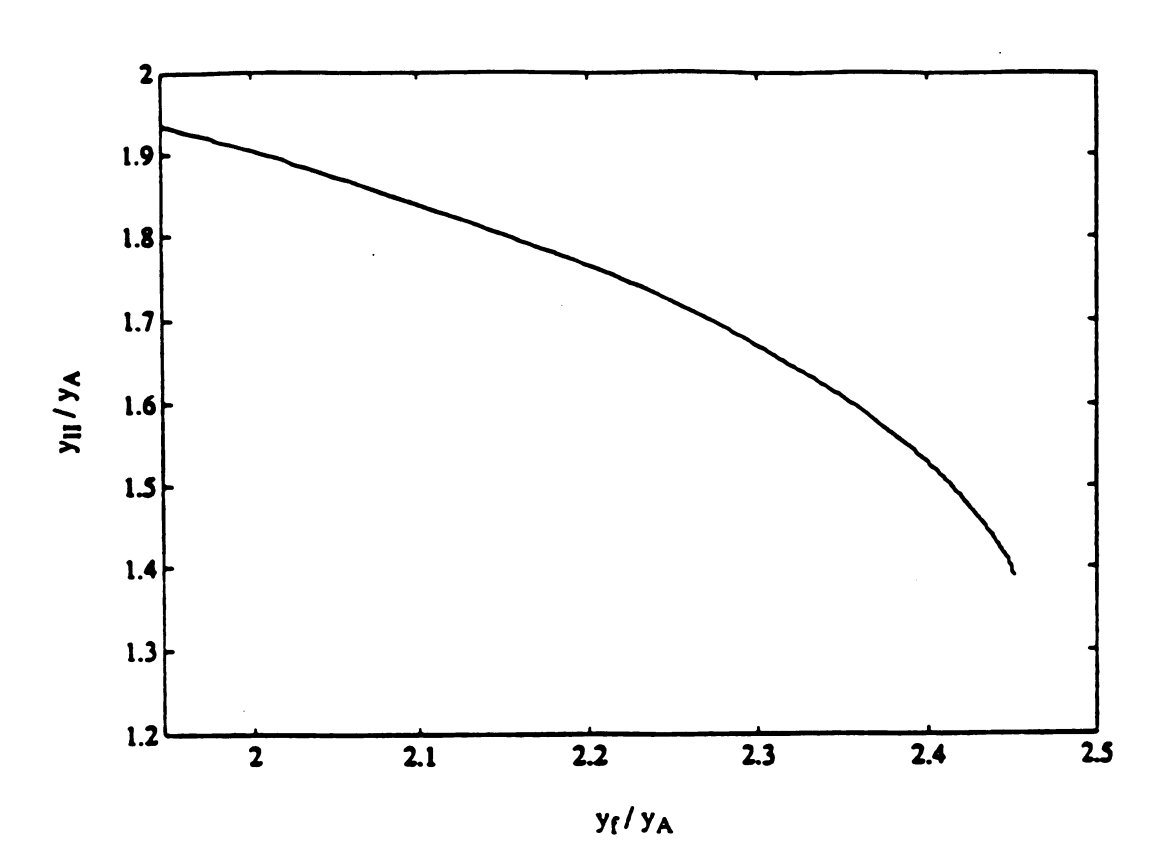


Figure 3.8 Location of $y_{I\!I}$ at various positions of the flow front

times is caused not just by permeability drops in the third region but also by the expanding region of changing fluid rheology.

Figures 3.7 and 3.8 show the location of the two crossover planes with time. From these curves, it is seen that the extent of region with changing fluid rheology expands to the entire filled region at the end of 4 min. As the front moves forward, the location of y_I , which marks the beginning of rheology changes, is seen to move towards the inlet port of the mold. This is shown in Figure 3.7. Once the front enters the third region, this onset plane for all rheology changes moves more rapidly toward the inlet; given sufficient time for this filling operation, y_I would be expected to reach the inlet port, depending on the nature of rheology of the resin. Once the front has reached y_{II} , the third regime begins, which corresponds to an increasing elastic behavior of the fluid. As the front progresses, however, the location of y_{II} , i.e., the onset plane for extensional viscosity effects moves toward the inlet of the mold. Again, with progressing flow front, the rate at which y_{II} moves toward the inlet increases, as shown in Figure 3.8.

A Unified Correlation: A very simple relation is obtained between the logarithmic mean mobility difference ratio and a velocity reduction factor. The latter quantity is defined as follows. The hypothetical velocity that would be obtained for constant mobility throughout is given by eq. (3-8). The ratio of this quantity to the actual superficial velocity is termed the velocity reduction factor. The velocity reduction factor is plotted against LMMDR [f,I] on Figure 3.9. This figure shows that the two quantities are identical over most of the region (though not exactly same). This may also be seen from equation 3-11 after some simplification. Hence, the effect of changing fluid rheology on the filling

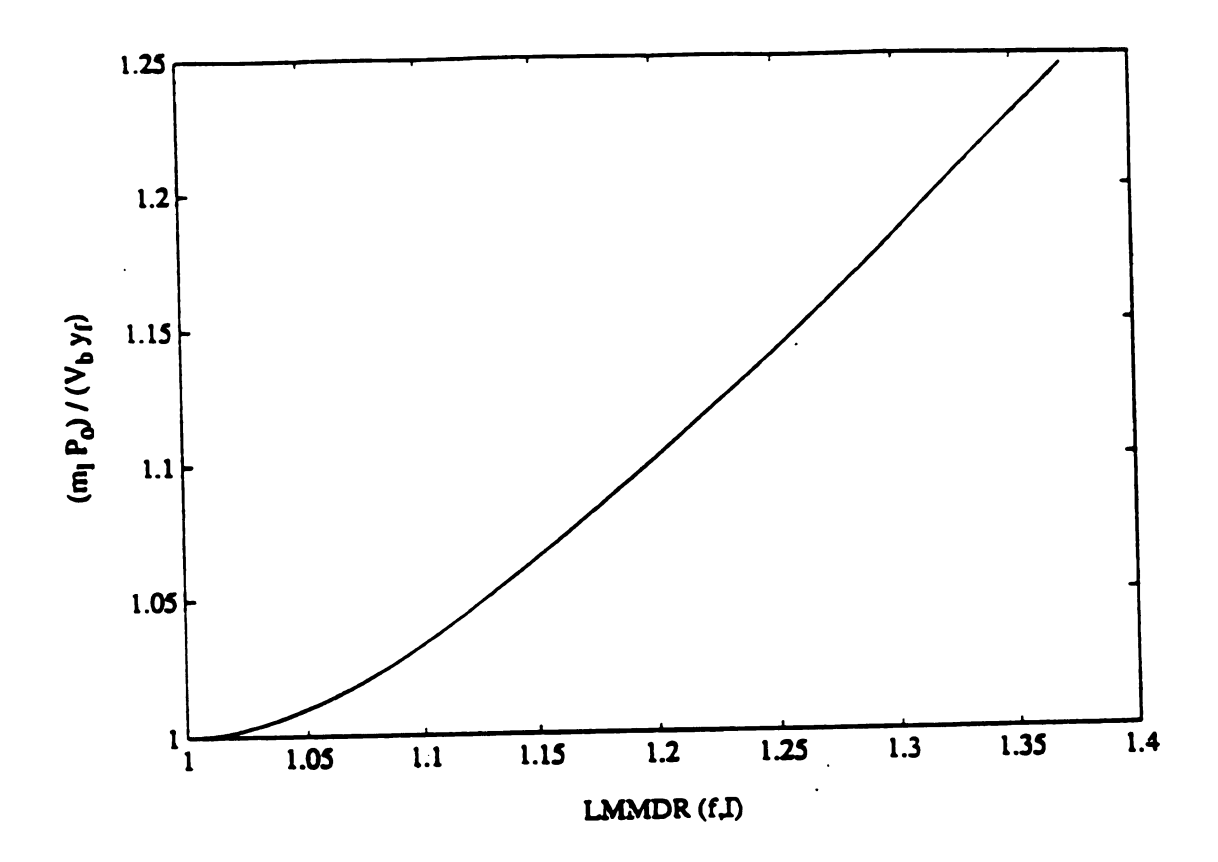


Figure 3.9 Velocity reduction factor Vs LMMDR [f,I]

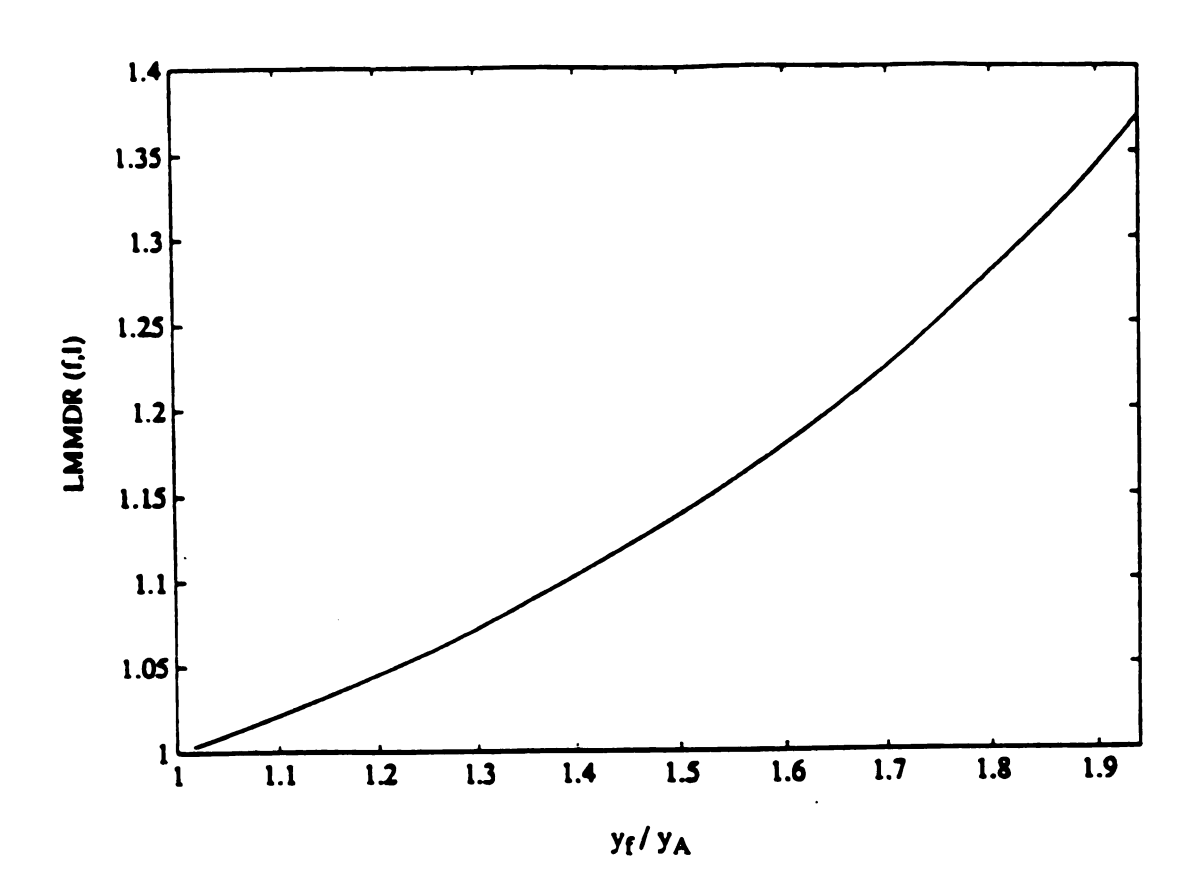


Figure 3.10 LMMDR [f,I] at various positions of the flow front - regime II

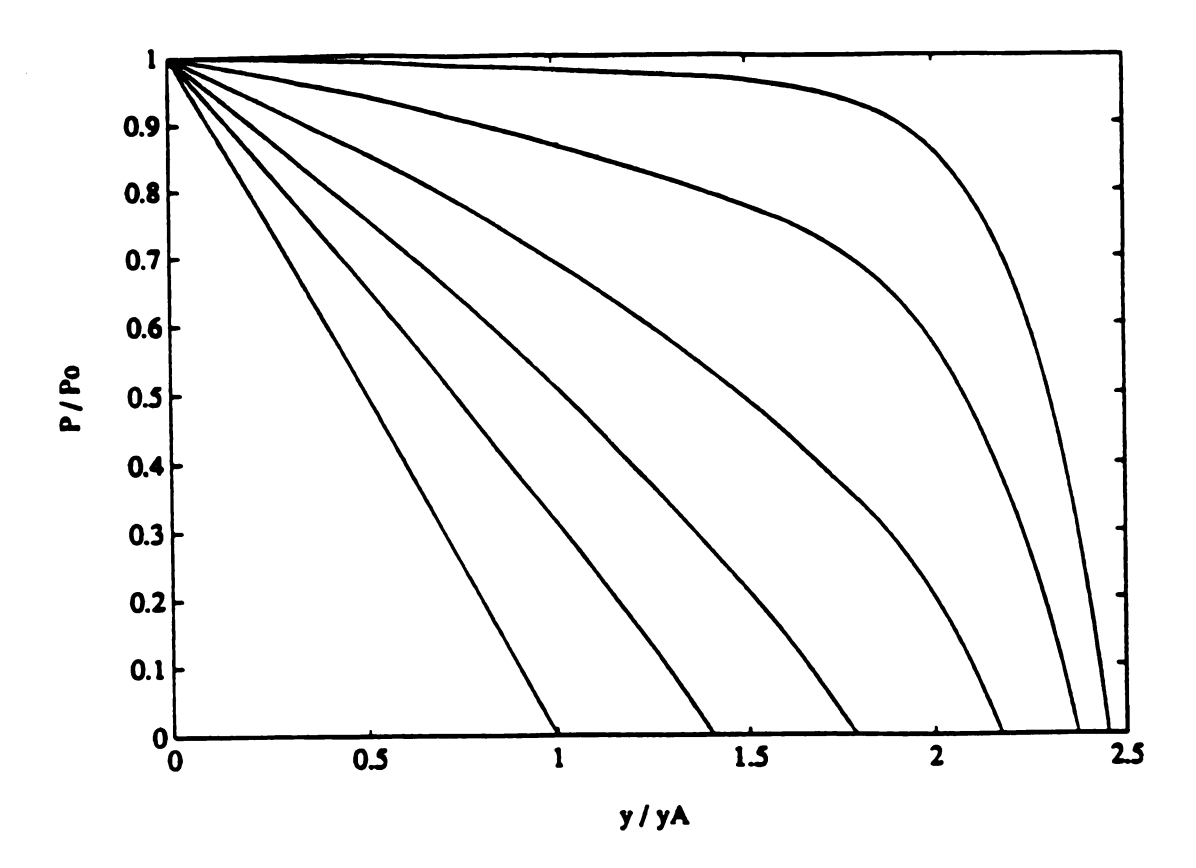


Figure 3.11 Pressure profiles at various locations of the flow front

process can be correlated effectively by comparing these two quantities. Figure 3.10 shows the LMMDR's at various front locations.

Pressure Distribution: For the constant inlet pressure process, the pressure profiles at various instants of filling time in the mold are shown in Figure 3.11. When the front is at locations up to y_A, the entire saturated portion contains resin of uniform rheology and so the pressure profile is linear, as seen in the innermost curve in this figure. As the front moves further, the rheology changes in the second regime and the pressure in this region is considerably higher than what it would have been if the rheology had not changed. The pressure drop is still fairly linear in the first regime. The curve begins to become increasingly convex, as the front moves forward, and the pressure drop across a small portion of the fluid, close to the front, is large. That is, the pressure gradients in the bulk of the fluid are lower than those at the moving front. As the front enters the third regime, the pressure profile becomes increasingly flatter in the bulk and steeper closer to the front.

This type of pressure distribution with a steep drop near the front is significant for practical operation with clusters of filaments making up the preform. The driving force for longitudinal wetting of individual filaments in a cluster would be uniformly high in the present instance over the bulk of the region swept by the front. In contrast, without rheology changes, this driving force decreases linearly.

3.2.4 SUMMARY

The motion of the front, and the pressure distribution, have been tracked in the

above analysis, by modeling the measured viscosity profile in a simple fashion. The effect of rheological changes on the reduction of the flow velocity, in a constant injection pressure situation, have been represented by a simple relation between two quantities - a velocity reduction factor and a ratio of the logarithmic-mean mobility difference versus the mobility at the front.

CHAPTER 4 VISCOUS FINGERING DURING REACTIVE FILLING OF FIBER
PREFORMS: EFFECT OF CHEMICAL REACTION

4.1 INTRODUCTION

It has been found that viscous fingering occurs during mold filling in liquid molding operations (Losure, 1994). This phenomenon is attributed to growth of disturbances inside the flow domain, hence to instabilities of the flow process involved in the mold filling stage. The disturbances themselves arise due to minute variations in any of the variables, such as velocity, conversion, viscosity, etc., occurring due to inhomogeneities in the porous medium or in resin mixing.

The viscosity of the polymeric resin, coupled with the polymerization reaction, has an effect on the stability of the miscible displacement process occurring during mold filling. A linear stability analysis is done to obtain the criteria for flow stability. The onset of instabilities arising from adverse viscosity gradients of displacement processes without reactive coupling is compared to that with reaction in this chapter. It is found that, in the absence of dispersion, the reactive coupling mechanism tends to stabilize the lower wave number disturbances. The effect of varying permeability is also considered.

Most of the available literature on fingering, cited in chapter 1, refers to displacement processes occurring in the context of secondary recovery of oil from subterranean formations. Liquid molding is a means of manufacturing polymer composite materials, with major applications in the automotive and aviation industry. In this process,

a polymeric resin flows through a bed of reinforcing fibers placed inside a mold. After filling, the mold is left to cure, during which time the resin hardens; subsequently the part is removed from the mold. An important qualitative requirement in these industries is the avoidance of voids and/or inhomogeneities in the manufactured part, since they would weaken the structure. Disturbances arising during the filling stage, over a range of wavenumbers, can grow with time at various growth rates, resulting in fingers. The properties of the resin in the fingers would be different from those of the resin in its vicinity, due to possible differences in the degrees of crosslinking from different ages. Upon curing, then, these fingered structures would be retained in the final part as inhomogeneities.

Before entering the mold, the resin is in an unreacted (monomeric constituent) state and the polymerization reaction begins as soon as the fluid enters the mold. The bed of fibers is a preform and may be random with isotropic permeability or aligned with anisotropic permeability. The concentration of the fresh fluid entering the mold is different from that of the older fluid, as the latter has already begun to polymerize. Thus the incoming fluid, which pushes the older fluid, is less viscous than the latter, creating an adverse viscosity gradient - a filled region, in the mold, of increasing viscosity in the flow direction. It is to be noted that the displaced and displacing fluids in liquid molding, differing only in the degree of polymerization, are completely miscible. Also, the viscosity gradients in the mold filling problem are continuous across the entire flow domain (due to a continuous base state concentration profile), while earlier literature considered abrupt changes in viscosity at an interface (a step profile of base state concentration). Mobility, defined as a ratio of permeability and viscosity, would thus decrease in the direction of

miscible displacement (for uniform permeability in the flow direction), causing fingering instabilities. The mechanism of generation of fingers under an adverse viscosity gradient has already been dealt with in chapter 1.

Due to the nature of the fluids and the physical processes considered, earlier literature has dealt only with the effects of dispersion, surface tension, permeability and gravity on fingering. Since liquid molding uses reactive flow systems, the stability of the flow process is also affected by the nature of the polymerization reaction. The effect of reaction and anisotropic permeation on flow stability during reactive filling, in the absence of dispersion, is explored in this chapter.

Hickernell and Yortsos (1986) presented the linear stability behavior of miscible displacement processes in porous media, in infinite domain, in the absence of dispersion. In their paper, upper and lower bounds on the growth rate were derived when dispersion was absent, and these bounds were found to be directly dependent on the lowest and highest values of the viscosity gradients in the domain of the problem. The inherent instability of the miscible displacement process, in the presence of an adverse viscosity gradient, is observed and appropriate stability criteria are derived in their theoretical paper. Disturbances of all wavelengths are seen to be unstable. In our problem, too, dispersion is absent; however there are two major differences. First, the domain of their problem is infinite, while the liquid molding problem discussed in this chapter is finite. Secondly, in the current problem, chemical reaction plays a major role in both generation of the viscosity gradient and growth/decay of disturbances; the problem investigated by Hickernell and Yortsos (1986), however, involved no chemical reaction.

Polymerization reactions may follow various types of kinetics (see chapter 2);

reactions having simple n-th order kinetics are considered (e.g. polyurethanes follow simple second order kinetics). Conditions under which the filling process would be stable to infinitesimal disturbances will be presented, as marginal stability curves. A frozen profile approximation, valid when the growth rate of the disturbances is much greater than the rate of change of the base state (the moving front), is used. The problem is formulated and described in the next section, where the governing equations are presented, the base case solution is discussed and the eigen value problem obtained from the stability analysis is presented and discussed. The solution approach is described in Section 4.3, followed by a description of the results and their discussion in Section 4.4. Some important conclusions that emerge from this study are listed in Section 4.5.

4.2 PROBLEM FORMULATION

4.2.1 THE GOVERNING EQUATIONS

Figure 4.1 shows the flow situation being considered. Fiber bundles are placed inside the mold and the resin enters the mold at an end-gate across the entire cross section. The figure shows the advancing flow front at some instant of time. A constant injection rate is considered, which means that the pressure drop along the mold varies as the mold is filled. This is in contrast to the problem investigated in chapter 3, where a constant injection pressure was used. Another major difference from the problem discussed in section 3.2 is the contribution of polymerization kinetics to the resin rheology. In that section, the effect of changing rheology was included directly with the help of rheological data obtained on the resin as it cures within the gap of a rheometer. In the following

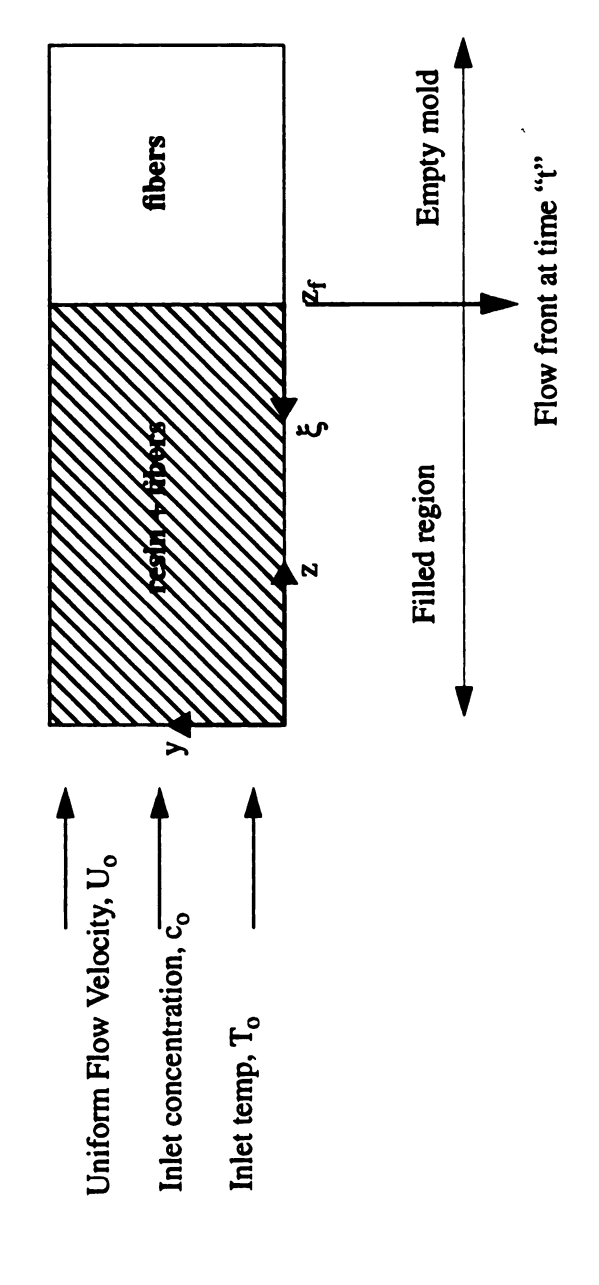


Figure 4.1 Schematic of reactive filling, frozen at time "t", in an end-gated mold

discussion, however, these kinetic parameters are included explicitly in a component balance equation. One more distinction from section 3.2 that has to be kept in mind is the arrangement of fibers inside the mold: in section 3.2 the fibers were all oriented transverse to the flow of the resin, in ordered arrays, while this section deals with a more realistic fiber preform. It is assumed, for the purpose of this analysis, that the fiber and resin in the filled region are at the same temperature, as would occur if the heat transfer coefficient at the fiber-resin interface were extremely large. The thermal parameters of the resin and fibers are also lumped as a volume fraction weighted average for the filled region. Another important assumption is the absence of dispersion; this yields the effect of chemical reaction on the growth of disturbances, independent of the dispersive effects seen by Tan and Homsy (1986).

Since the fluid moves with a constant velocity U_0 in the z-direction, a Lagrangian frame of reference is used for convenience, based on the location of the flow front at any time; the length coordinate in the flow direction, in the moving frame of reference is, then,

$$\hat{\xi} = \hat{z} - \hat{z}_f \equiv \hat{z} - U_o \hat{t} \tag{4-1}$$

The impregnation of the fiber arrays is treated as flow through porous media, and is described by Darcy's law.

$$\hat{\boldsymbol{u}} = \hat{\boldsymbol{q}} + U_o \tilde{i}_3 = -\left(\frac{1}{\hat{\boldsymbol{\mu}}}\right) (\hat{\boldsymbol{K}} \bullet \nabla \hat{\boldsymbol{P}})$$
 (4-2)

where u and q are the velocities in the fixed and moving frames of reference respectively.

The permeation equation (Darcy's law) involves a permeability tensor, which would be diagonal if the principal axes are assumed to lie along the coordinate directions. Also, the permeability is assumed to be equal in both the transverse directions, yielding just two

independent terms in the permeability tensor,

$$\hat{K} = \begin{bmatrix} \hat{K}_x & 0 & 0 \\ 0 & \hat{K}_y & 0 \\ 0 & 0 & \hat{K}_{\underline{l}} \end{bmatrix}$$
 (4-3)

The equation of continuity, the reactant mass balance and the energy balance, lumping the fiber and resin temperatures together and assuming an adiabatic process with no heat transfer with the surroundings, in the moving frame of reference, would be

Continuity
$$\nabla \bullet \hat{q} = 0$$
Reactant Mass Balance
$$\frac{\partial \hat{c}}{\partial \hat{t}} + \hat{q} \bullet \nabla \hat{c} = -\hat{R}(\hat{c}, \hat{T})$$
Energy Balance
$$\frac{\partial \hat{T}}{\partial \hat{t}} + \hat{q} \bullet \nabla \hat{T} = \beta \hat{R}(\hat{c}, \hat{T})$$
where
$$\beta = \frac{-\Delta H_R}{\rho C_p} = \frac{\Delta T_{ad}}{c_o}$$
(4-4)

The adiabatic temperature rise, ΔT_{ad} , is given by (βc_o) and will be the scaling factor for temperature in this dissertation.

To demonstrate the theory being developed in this chapter, a polyurethane resin system is chosen. The reaction is of second order kinetics and the viscosity of the resin has an Arrhenius' type dependence on the temperature. The various kinetic, thermal and rheological properties are taken from Castro and Macosko (1982) and are listed in Table 4.1. The reaction rate and viscosity for this resin are given by the equations:

$$\hat{R}(\bar{\alpha}, \hat{T}) = k_o c_o^2 (1 - \bar{\alpha})^2 \exp\left[\frac{E_a}{R_g \hat{T}}\right]$$

$$\hat{\mu} = A_{\mu} \left(1 - \frac{\bar{\alpha}}{\alpha_{gel}}\right)^{-(1.5 + \bar{\alpha})} \exp\left[\frac{E_{\mu}}{R_o \hat{T}}\right]$$
(4-5)

Table 4.1 Thermal, kinetic and rheological data for the resin and glass fibers

	RESIN	GLASS
C _p (J/kg K)	1,840	790
$\rho (kg/m^3)$	1000	2,500
$k_0 (m^3/mol s)$	10,560	
E _a (J/mol)	53,200	
c _o (mol/m ³)	2,410	
$-\Delta H_r$ (J/mol)	96,300	

Viscosity described by an Arrhenius' type equation:

$$\mu(T,\alpha) = A_{\mu} \exp\left[-\frac{E_{\mu}}{RT}\right]$$

where

E_{μ} (J/mol)	41,300		
A _µ (Pa-s)	10.3 x 10 ⁻⁸		
$\alpha_{\mathbf{g}}$	0.65		

Lumped value of (ρC_p) for the resin-filled fiber mat = 1.9 x 10^6 J/m³ K.

4.2.2 SCALING

All the quantities in the preceding equations are dimensional and appropriate scales are chosen to make them dimensionless. The chosen scaling factors for the different variables are listed in Table 4.2. Reaction is the important physical phenomenon in this problem, so the time and length scales are based on the reaction rate at the inlet composition and a reference temperature. The scale for temperature is the adiabatic temperature rise, ΔT_{ad} . Viscosity is scaled with the viscosity at the reference temperature. Using these scales, the equation of continuity, the component mass balance and the energy balance, in dimensionless form, yield

Continuity
$$\nabla \cdot \mathbf{q} = 0$$

Reactant Mass Balance $\frac{\partial \alpha}{\partial t} + \mathbf{q} \cdot \nabla \alpha = R(\alpha, T)$

Energy Balance $\frac{\partial T}{\partial t} + \mathbf{q} \cdot \nabla T = R(\alpha, T)$ (4-6)

while the permeation equation becomes

$$q = -\lambda \ K \bullet \nabla P - \tilde{i}_3 \tag{4-7}$$

where

$$K = \begin{bmatrix} b_1 & 0 & 0 \\ 0 & b_2 & 0 \\ 0 & 0 & 1 \end{bmatrix}$$

$$\lambda = \frac{1}{\mu}$$

$$b_1 = \frac{\hat{K}_x}{\hat{K}_l} \qquad b_2 = \frac{\hat{K}_y}{\hat{K}_l}$$

$$(4-8)$$

In these equations b_1 and b_2 are measures of the anisotropic nature of the medium permeability, while λ is the dimensionless mobility, whose gradient will be seen to have

Table 4.2 Scaling factors for different variables

Concentration:

$$\hat{c} = c_o \cdot (1 - \alpha)$$

Permeability:

$$\hat{K} = \hat{K}_l \cdot K$$

Pressure:

$$\hat{P} = \left(\frac{\mu_o U_o}{\hat{R}_l}\right) \cdot \left(\frac{U_o c_o}{\hat{R}(c_o, T_{ref})}\right) \cdot P$$

Velocity:

$$\hat{q} = U_o \cdot q$$

Reaction:

$$\hat{R}(\hat{c}, \hat{T}) = \hat{R}(c_o, T_{ref}) \cdot R$$

Temperature:

$$\hat{T} = \Delta T_{ad} \cdot T$$

Time:

$$\hat{t} = \frac{c_o}{\hat{R}(c_o, T_{ref})} \cdot t$$

Length:

$$\hat{z} = \frac{U_o c_o}{\hat{R}(c_o, T_{ref})} \cdot z$$

Viscosity:

$$\hat{\mu} = \mu_o \cdot \mu$$

Activation energy:

$$E_R = \frac{E_a}{R_g \Delta T_{ad}};$$

$$E_R = \frac{E_a}{R_g \Delta T_{ad}}; \qquad E_{\mu} = \frac{\hat{E}_{\mu}}{R_g \Delta T_{ad}}$$

considerable importance later in this chapter.

4.2.3 THE BASE STATE EQUATIONS

(NOTE: All base state quantities are identified by an overbar.)

Since the only velocity component is U_0 in the z-direction (one-dimensional flow), the base state solution for the velocity vector, in the moving frame of reference (see equation 4-2), is

$$\bar{q} = 0 \tag{4-9}$$

The base state solutions for the conversion, temperature and pressure profiles are obtained by solving the following simplified forms of equations 4-6 and 4-7.

$$\frac{\partial \overline{\alpha}}{\partial t} = R(\overline{\alpha}, \overline{T})$$

$$\frac{\partial \overline{T}}{\partial t} = R(\overline{\alpha}, \overline{T})$$

$$-\overline{\lambda}(\overline{\alpha}, \overline{T}) \frac{\partial \overline{P}}{\partial \xi} = 1$$
(4-10)

The boundary conditions to be used in conjunction with the above equations are:

$$\overline{P} = 0$$
 at $\xi = 0$ front
 $\overline{\alpha} = 0$; $\overline{T} = T_o$ at $\xi = -z_f$ inlet
 $\overline{\alpha} = 0$; $\overline{T} = T_o$ at $t = 0$

For an isothermal process, the equations are independent of temperature and only the first and third equations of (4-10) need to be solved. For an adiabatic reaction, the first two equations of (4-10), when combined using the inlet conversion and temperature as the initial conditions, yield

$$\bar{T} = \bar{\alpha} + T_{\alpha} \tag{4-12}$$

Thus, taking

$$\Re(\overline{\alpha}) \equiv R(\overline{\alpha}, \overline{T}) \equiv R(\overline{\alpha}, T_o + \overline{\alpha}) \tag{4-13}$$

we can rewrite the first equation of (4-10) as:

$$\frac{\partial \overline{\alpha}}{\partial t} = \Re(\overline{\alpha}) \tag{4-14}$$

The rate of reaction and viscosity, after scaling, is given by

$$R(\bar{\alpha}, T) = (1 - \bar{\alpha})^{2} \exp\left[\frac{-E_{a}}{R_{g}\Delta T_{ad}}\left(\frac{1}{T} - \frac{1}{T_{o}}\right)\right]$$

$$\mu(\bar{\alpha}, T) = \left(1 - \frac{\bar{\alpha}}{\alpha_{gel}}\right)^{-(1.5 + \bar{\alpha})} \exp\left[\frac{\hat{E}_{\mu}}{R_{g}\Delta T_{ad}}\left(\frac{1}{T} - \frac{1}{T_{o}}\right)\right]$$
(4-15)

Incorporating Eq. 12 for an adiabatic process and using definitions for the dimensionless activation energies for reaction and viscosity growth, E_R and E_μ respectively, shown in Table 4.2, we get the following equations for the dimensionless reaction rate and viscosity:

$$\Re = (1 - \overline{\alpha})^{2} \exp\left[\frac{E_{R}\overline{\alpha}}{T_{o}(T_{o} + \overline{\alpha})}\right]$$

$$\mu = \left(1 - \frac{\overline{\alpha}}{\alpha_{gel}}\right)^{-(1.5 + \overline{\alpha})} \exp\left[\frac{-E_{\mu}\overline{\alpha}}{T_{o}(T_{o} + \overline{\alpha})}\right]$$
(4-16)

The rate of reaction is plotted as a function of the conversion, for a range of values of the activation energy E_R , in Figure 4.2. Setting ER = 0 yields the isothermal case. For low values of E_R (up to a value of about 14.26), the derivative ($dR/d\alpha$), described in later sections, is negative, while at higher values the plot goes through a peak, corresponding to a change in sign of the derivative. The effect of this derivative on the flow stability will be discussed after the stability analysis has been presented.

Figure 4.3 shows the viscosity profile as a function of conversion, for different

values of E_{μ} , the dimensionless activation energy for viscosity. E_{μ} =0 corresponds to the isothermal case, since the thermal dependence vanishes. For E_{μ} <16.45, the viscosity is always increasing with conversion. As E_{μ} is increased, the viscosity corresponding to a given conversion becomes lower. Also, for higher values of E_{μ} , the viscosity gradient changes sign for increasing conversion. This implies that V, the gradient of the viscosity defined later in this chapter, changes sign somewhere in the filled region, affecting the stability of the flow process.

4.2.4 THE BASE STATE SOLUTION

To obtain the base state conversion profiles, the initial value problem described by equation 4-14 is solved for different positions of the flow front, z_f , with the initial condition given in (4-11). The independent variable, time, corresponds to a location (z) in the filled portion of the mold, since

$$\hat{z} = U_o \hat{t}$$

$$\Rightarrow z = t \tag{4-17}$$

The base case is a plug flow for which every location in the filled portion of the mold would correspond to a unique conversion and temperature with given inlet conditions.

Since it is a constant injection process, all fluid elements spend the same amount of time to reach a given location in the mold and, therefore, would attain the same conversion when they reach this location.

For an isothermal process the initial value problem can be solved analytically, since the exponential term in equation 4-16 vanishes. For an adiabatic process, due to this exponential factor, a numerical approach is needed. Once the conversion profile is

Figure 4.2 Non-dimensional reaction rate for polyurethane resin: isothermal and adiabatic cases, $T_o = 325^{\circ}K$

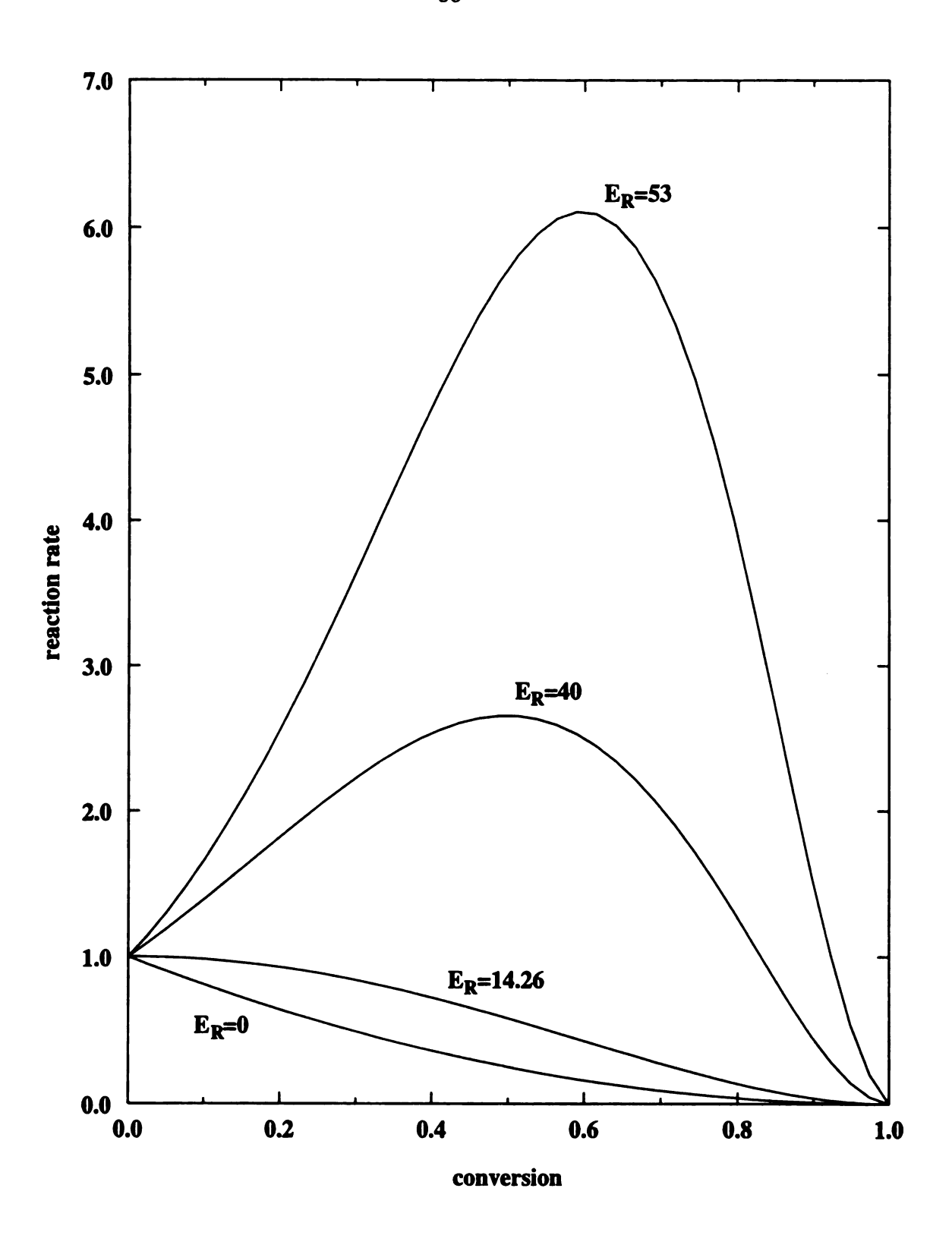


Figure 4.2

Figure 4.3 Non-dimensional viscosity for polyurethane resin: isothermal and adiabatic cases, $T_0 = 325^{\circ}K$

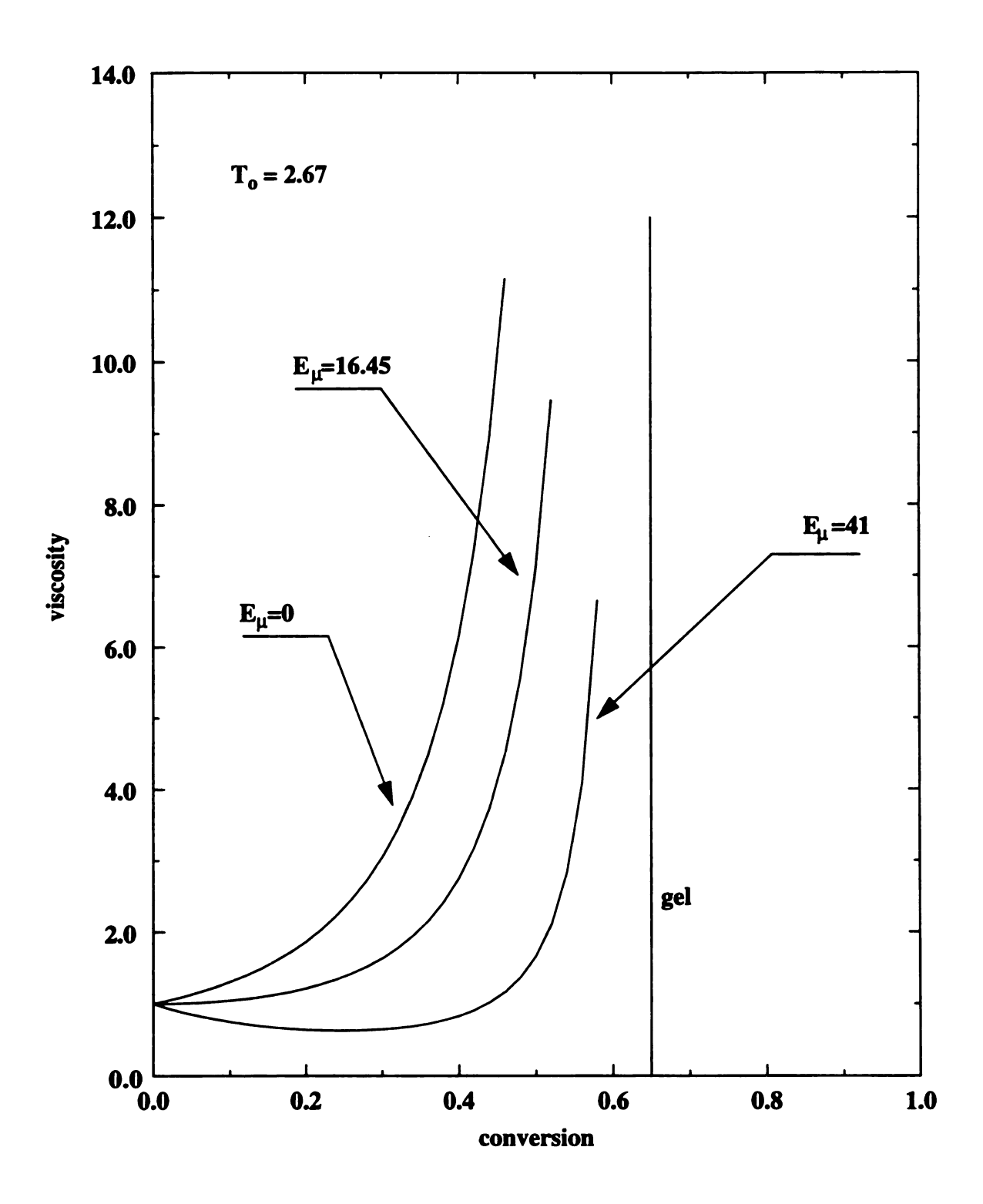


Figure 4.3

available, the temperature profile is easily computed in the adiabatic case using equation 4-12.

The solution to equation 4-14 is shown in Figure 4.4, for several values of the dimensionless activation energy and for a fixed inlet temperature, as a plot of conversion versus the dimensionless distance from the mold inlet. The range of values for E_R is obtained by varying the activation energy E_a . The case of $E_R = 0$ corresponds to "isothermal" filling, since the temperature dependence of the reaction rate vanishes. For this case the fluid travels a larger distance in the mold before reaching the gel point, compared to a case of high E_R . Thus, as the process moves away from the "isothermal" state, gel conversion is reached much faster and the length of mold that can be filled by the resin is much smaller.

The solution to Darcy's law, given in equation 4-10, is now obtained using the conversion profiles of Figure 4.4. The pressure profiles are shown in Figure 4.5, for the adiabatic case under the following conditions: $E_R = 53$; $E_\mu = 41$; gel conversion = 0.65; Inlet temperature = 325° K. The base state pressure is plotted against the dimensionless distance, z, from the mold inlet, for several flow front positions, z_f . As the mold gets filled, the pressure at the inlet rises due to the increasing resin viscosity. This means that the pressure at which the resin is pumped into the mold is continuously increasing, for a constant injection rate to be maintained. For isothermal filling, however, the conversion profile indicates a slower approach to gelation. The corresponding pressure profile for the isothermal case would be expected to show lower injection pressures for the same extent of mold filling.

The derivative of the reaction rate w.r.t. conversion, $(dR/d\alpha)$, is termed S and is

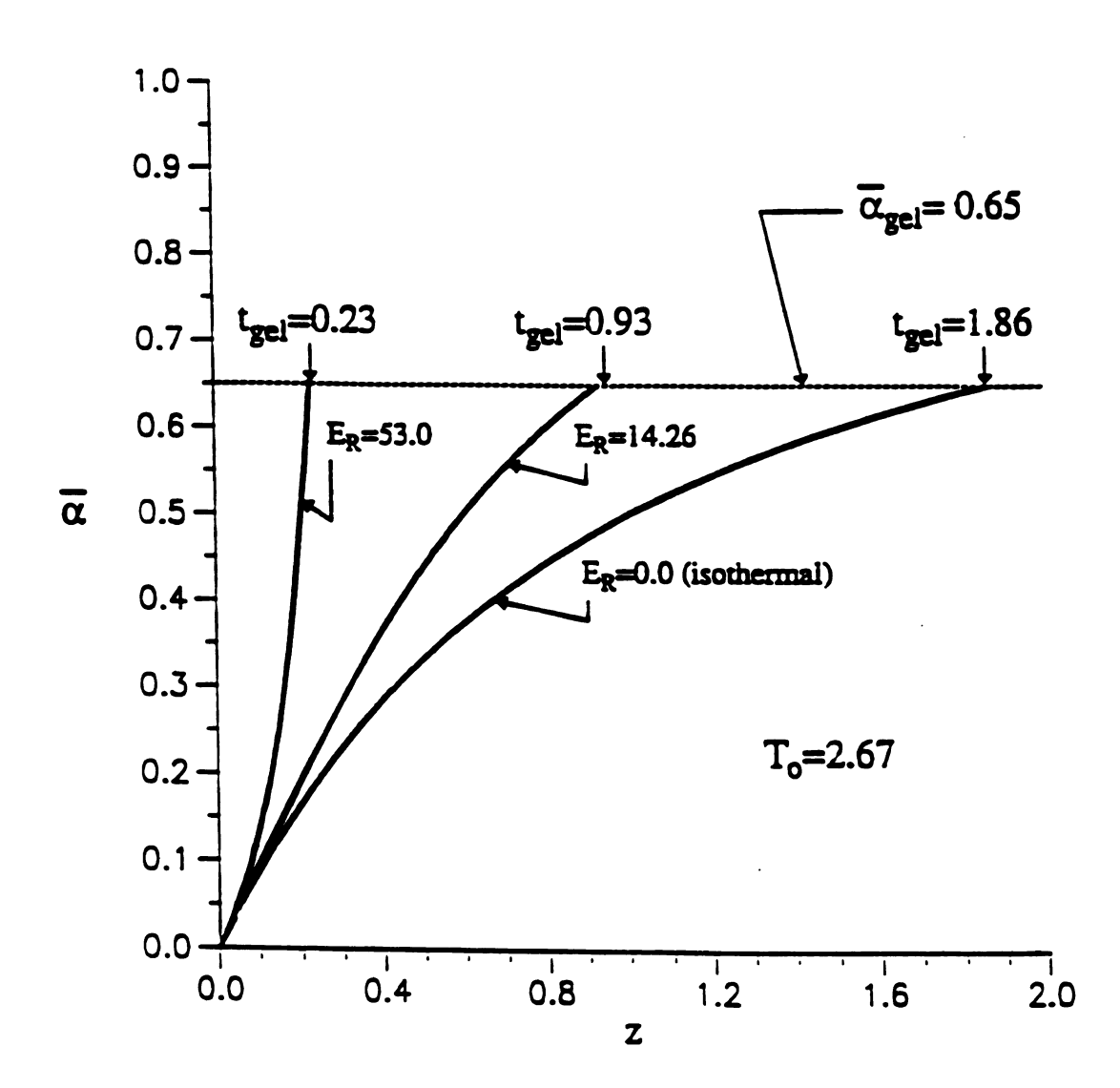


Figure 4.4 Base state conversion profiles: isothermal and adiabatic cases, $T_0 = 325^{\circ}$ K

Figure 4.5 Base state dimensionless pressure profiles: adiabatic case, E_R = 53, E_μ = 41, α_{gel} = 0.65, T_o = 325°K

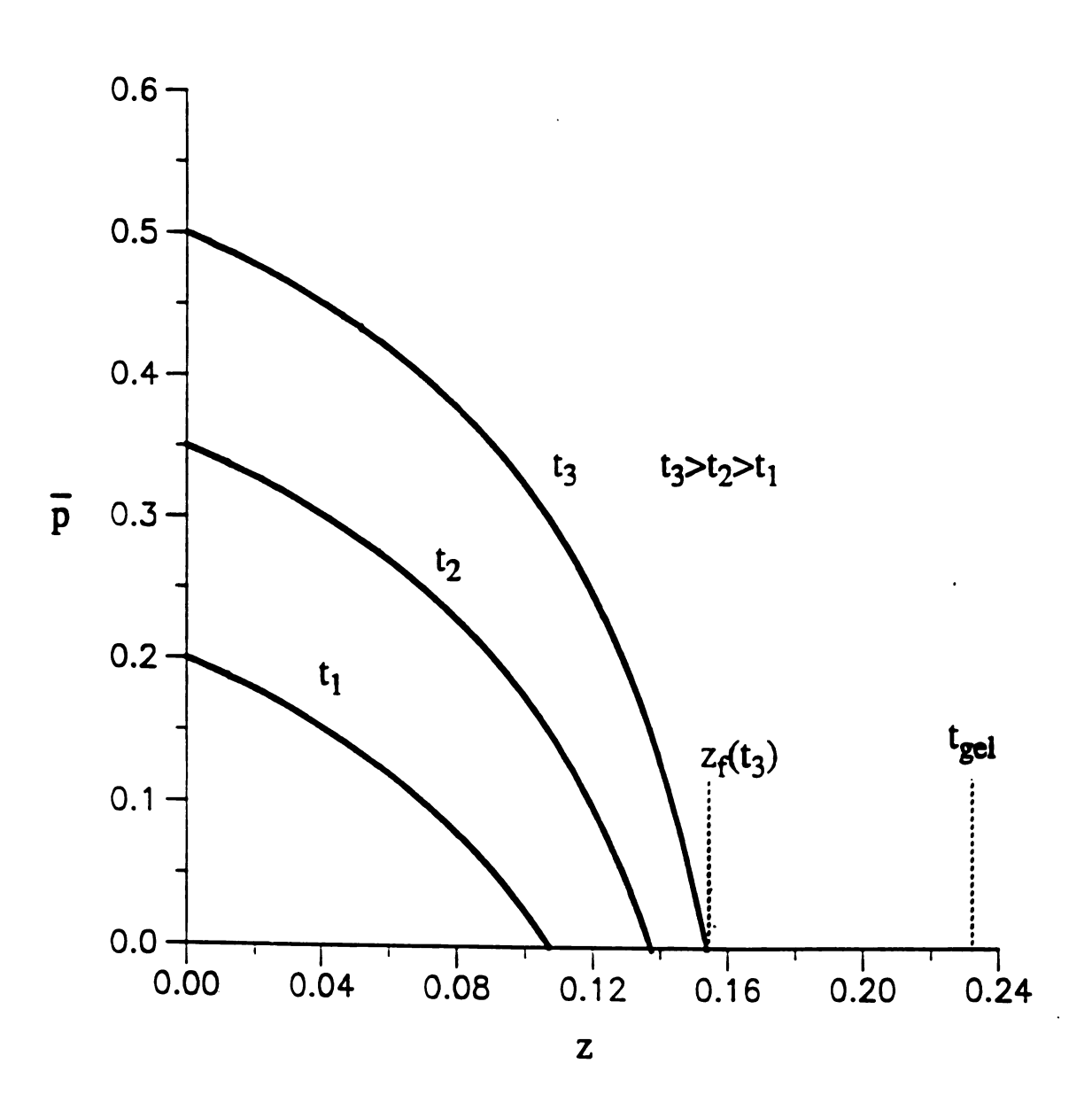


Figure 4.5

E_µ=4!.

found to have a significant role on the stability of the flow process. Figure 4.6 shows S and the mobility gradient V, (defined as $d[\ln \overline{\lambda}]/d\xi$), for the polyurethane resin up to a conversion of about 0.6, under isothermal conditions. By this time the viscosity has risen to a fairly large value (gel conversion is 0.65). As will be explained in a later section, S < 0 is a necessary condition for stability and $V \neq 0$ in the domain of the problem is a sufficient condition for real growth rates (from an exchange of stabilities analysis). It is seen that both S and V are negative throughout the domain for the isothermal case, which means that the growth rate is real and negative for at least some wave numbers (in the small wavenumber region). The quantities S and V are calculated and plotted for the adiabatic case with E_R=52.67 and an inlet temperature of 325°K in Figure 4.7. For this case while S is always positive, V changes sign in the flow domain considered. Hence it is expected that at all lengths of filling (z_f), the flow would be unstable to disturbances. The behavior of S, for different values of E_{R} , may also be seen from an inspection of the plot of rate versus conversion (Figure 4.2). For small values of the dimensionless activation energy, i.e. for E_R less than about 14.26, the reaction rate curves have a negative slope at all conversions. This suggests stability of the flow process under these conditions.

4.2.5 STABILITY ANALYSIS

In order to study the growth behavior of infinitesimal disturbances that the filling process may be subjected to, a linear stability analysis is to be performed on the model equations in (4-6). Perturbations on each of the variables are introduced into the problem, described by:

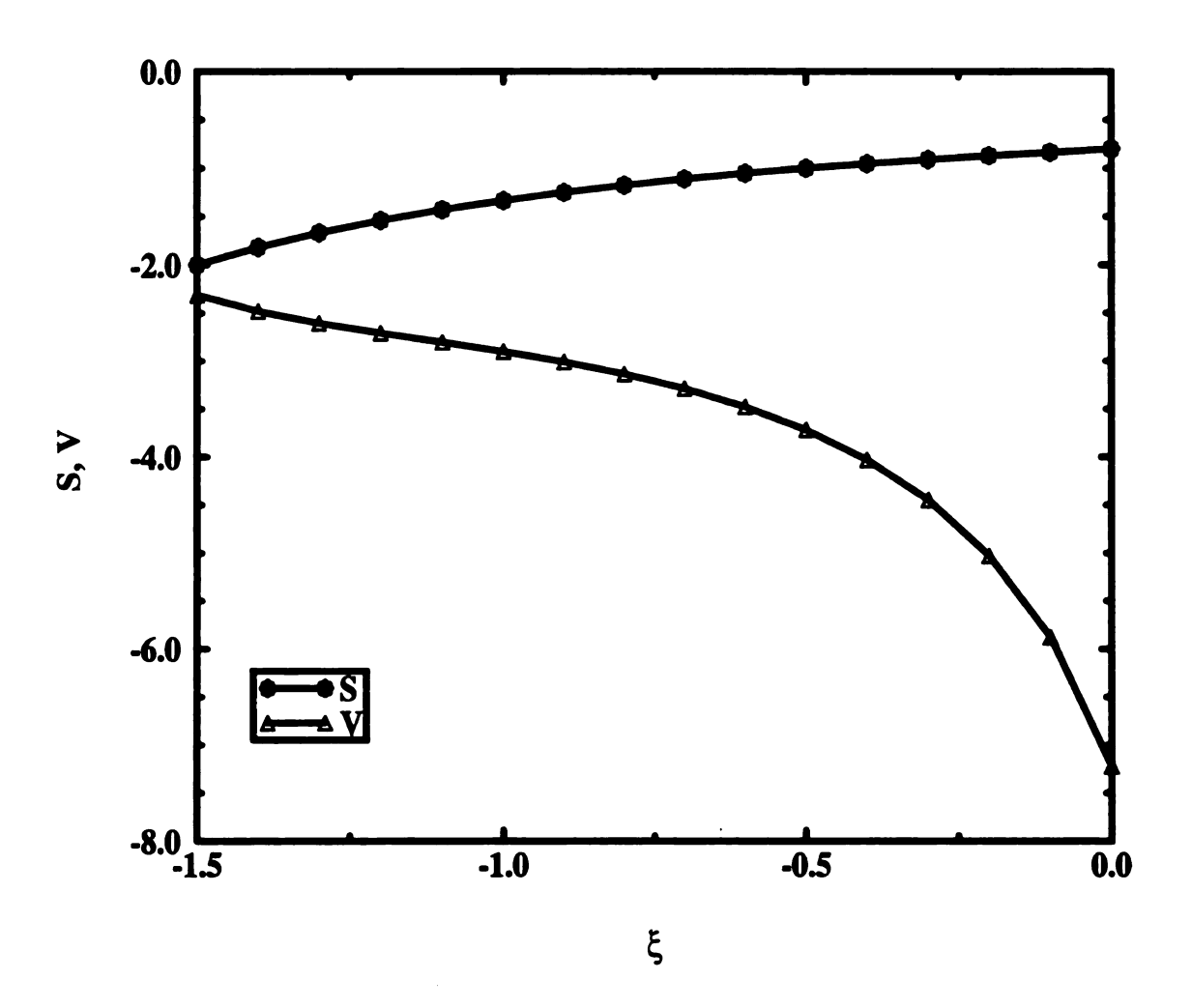


Figure 4.6 S, V profiles for isothermal filling: $E_R = 53$, $E_{\mu} = 41$, $\alpha_{gel} = 0.65$, $T_o = 325^{o}K$

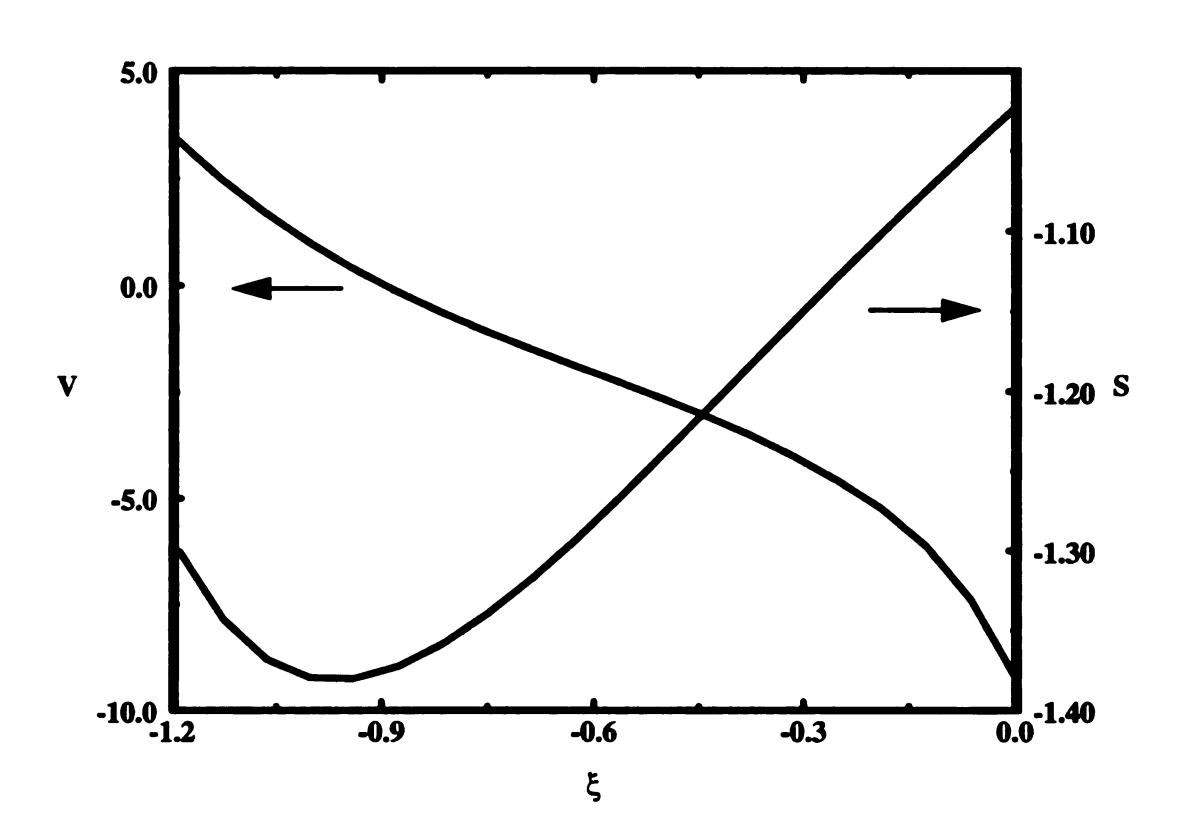


Figure 4.7 S, V profiles for adiabatic filling: $E_R = 5$, $E_{\mu} = 41$, $\alpha_{gel} = 0.65$, $T_o = 325^o K$

$$P = \overline{P}(\xi, t) + P'(x, y, \xi, t)$$

$$\lambda = \overline{\lambda}(\xi, t) + \lambda'(x, y, \xi, t)$$

$$\alpha = \overline{\alpha}(\xi, t) + \alpha'(x, y, \xi, t)$$

$$q = \overline{q}(\xi, t) + q'(x, y, \xi, t)$$

$$T = \overline{T}(\xi, t) + T'(x, y, \xi, t)$$
(4-18)

Here the base state variables are dependent only on one space variable (ξ) and time, while the disturbances (primed quantities) are three dimensional and time dependent. All the variables in equations 4-6 and 4-7 are replaced by the representation given in (4-18) and the equations are then linearized. For an adiabatic reaction, the lumped energy balance may be combined with the component mass balance and equation 4-12 for the base state solution, to yield the following relation between the temperature and conversion perturbations: $T' = \alpha'$. This is valid for reactions that are much faster than the rate at which heat transfer takes place. Linearization of the continuity equation incorporating Darcy's law yields

$$\bar{\lambda} \left(b_1 \frac{\partial^2}{\partial x^2} p' + b_2 \frac{\partial^2}{\partial y^2} p' \right) + \frac{\partial}{\partial \xi} \left(\bar{\lambda} \frac{\partial p'}{\partial \xi} - \frac{\lambda'}{\bar{\lambda}} \right) = 0$$
 (4-19)

while linearization of the reactant mass balance results in

$$\frac{\partial \alpha'}{\partial t} + \left(\frac{\lambda'}{\bar{\lambda}} - \bar{\lambda} \frac{\partial p'}{\partial \xi}\right) \frac{\partial \bar{\alpha}}{\partial \xi} = \frac{d\Re}{d\bar{\alpha}} \alpha' \tag{4-20}$$

Frozen profile approximation: It may be noted that the base state in the filling problem is time dependent. It is assumed that the growth rate of disturbances is much faster than the rate of change of base state. That is, a quasi-steady state is assumed and the stability analysis is done with time frozen at t_0 . The rate of change of the base state, $d\alpha/dt$, may be

:

represented by the reaction rate R, which provides a bound for the time of applicability of the quasi-steady state approximation. For times of the order of about ln(R) and lower, the QSSA is inapplicable. From the conversion profiles in Figure 4.4, at large values of E_R , $d\overline{\alpha}/dt$ is much higher than at low E_R . This suggests that the quasi-steady state approximation may possibly be invalid at large values of E_R .

In the limit of applicability of the QSSA, the disturbances are, decomposed into Fourier components:

$$\alpha' \sim A(\xi) \exp[i(k_x x + k_y y) + \sigma(t_o)t]$$

$$p' \sim p(\xi) \exp[i(k_x x + k_y y) + \sigma(t_o)t]$$

$$\lambda' \equiv \frac{d\bar{\lambda}}{d\bar{\alpha}} \alpha' \sim \frac{d\bar{\lambda}}{d\bar{\alpha}} A(\xi) \exp[i(k_x x + k_y y) + \sigma(t_o)t]$$
(4-21)

Here, it is noted that λ' is tied to the conversion disturbance α' since viscosity is directly related to conversion. In these equations k_x and k_y are the wavenumbers of the disturbances in the respective directions and are, later, combined into a single wavenumber, k. $\sigma(t_0)$ is the quasistatic growth rate of the disturbance, evaluated at time t_0 and is a complex quantity. If σ has a negative real part the disturbances would decay with time, while they would grow if it has a positive real part. If the imaginary part of the growth rate is non-zero, then it indicates an oscillatory trajectory for the disturbances with time. It may be shown that it is a real quantity for this eigenvalue problem (Appendix A).

Using the above definitions of the disturbances, we get from eq. 4-19,

$$\frac{\partial}{\partial \xi} \left[\bar{\lambda} \frac{\partial p}{\partial \xi} - \frac{1}{\bar{\lambda}} \frac{d}{d\bar{\alpha}} \bar{\lambda} A(\xi) \right] = \bar{\lambda} (bk^2) p$$

$$where \qquad bk^2 = b_1 k_x^2 + b_2 k_y^2$$
(4-22)

A relation obtained by substituting the Fourier expansions of the disturbances into

eq. (4-20) is

$$A(\xi) \equiv \frac{\left(\bar{\lambda} \frac{dp}{d\xi}\right) \frac{\partial}{\partial \xi} \bar{\alpha}}{\sigma - S + V} \tag{4-23}$$

This equation relates the amplitudes of conversion and pressure disturbances and is a useful relation in simplifying the equations at a later stage.

Combining eqs. 4-22 and 4-23 we get:

$$\frac{\partial}{\partial \xi} \left[\bar{\lambda} \frac{dp}{d\xi} \frac{(\sigma - S)}{(\sigma - S + V)} \right] = bk^2 \bar{\lambda} p \tag{4-24}$$

where S, V are defined by

$$S = \frac{d\Re}{d\bar{\alpha}}$$

$$V = \frac{1}{\bar{\lambda}} \frac{d}{d\xi} \bar{\lambda} = \frac{1}{\bar{\lambda}} \frac{d}{d\bar{\alpha}} \bar{\lambda} \cdot \frac{d}{d\xi} \bar{\alpha}$$
(4-25)

In equations 4-25, S and V are the quantities referred to during the discussion of the base state solution. The former is the derivative of the reaction rate w.r.t. concentration (conversion) and the latter is a viscosity gradient. Both these quantities are seen to be associated with the growth rate σ , which is also the eigen value in equation 4-23, and so determine the stability characteristics of the filling process. An analysis of the exchange of stabilities for the eigen value problem indicates that a sufficient condition for the growth rate to be a real quantity is a non-zero V, or that V does not change sign in the entire domain. It may be shown that a sufficient condition for the quasistatic growth rate, σ , to be a real quantity is that V does not change sign in the entire domain, and is non-zero.

The boundary conditions used in solving the eigen value problem are

$$\frac{dp}{d\xi} = 0 \qquad at \qquad \xi = -z_f$$

$$p = 0 \qquad at \qquad \xi = 0$$
(4-26)

The first condition is obtained by taking the disturbance in conversion to be zero (i.e. A=0) at the mold inlet and using eq. (4-22), while the second boundary condition implies an undisturbed pressure at the flow front.

The transformation

$$\bar{\lambda} \ p = \frac{d\psi}{d\xi}$$
 with $\psi = 0$ at the inlet

leads to the following simplified eigenvalue problem:

$$\frac{d^{2}\psi}{d\xi^{2}} - V \frac{d\psi}{d\xi} - b k^{2} \left[\frac{\sigma - S + V}{\sigma - S} \right] \psi = 0$$
 (4-28)

with the boundary conditions

$$\psi = 0 at \xi = -z_f$$

$$\frac{d\psi}{d\xi} = 0 at \xi = 0$$
(4-29)

Equation 4-28 may be compared to the eigenvalue problem developed by Hickernell and Yortsos (1986) in eq. (2.19) in their paper, rewritten as:

$$\frac{d^2 \Psi}{d\xi^2} - V \frac{d\Psi}{d\xi} - k^2 \left[\frac{\sigma + V}{\sigma} \right] \Psi = 0$$
 (4-30)

This equation is subject to decay of the disturbance at infinite distances on either side of the interface. It is easily seen that the main difference between equations 4-28 and 4-30 is the factor (-S) added to the growth rate in equation 4-28. The boundary conditions in our problem simply refer to decay of the pressure and conversion disturbances at the inlet and

front respectively. When we take a chemical reaction with S = 0, i.e. a zeroth order reaction, then, the behavior of the fingers would be predicted by the results in their paper, i.e. the growth rate is bound by the values of the viscosity gradient:

$$\frac{inf \ V < \sigma < sup \ V}{\xi} \qquad \qquad \xi \tag{4-31}$$

That is, the growth rates are bound by the infemum and supremum values of V in the domain of the problem. If V is positive everywhere in the domain, the flow process is unstable for all wavenumbers.

When the chemical reaction is of a higher order, however, a direct comparison cannot be made. Even though S is being subtracted from the growth rate (in equation 4-28), the fact that S, unlike the growth rate, is dependent on the location, ξ , complicates the problem; if S were independent of the location, $(\sigma - S)$ could be combined into a new, reduced, growth rate and the results of Hickernell and Yortsos (1986) applied.

4.3 NUMERICAL APPROACH

The results of the stability calculations are presented as growth rate data and marginal stability curves, solving the eigen value problem (equation 4-28), using the boundary conditions in equation 4-29. This equation is solved using an orthogonal collocation scheme on finite elements (Finlayson, 1980).

The numerical procedure is illustrated in the schematic shown in Figure 4.8. The flow domain is divided into two elements based on the viscosity profile. The interface between the two elements, depicted by $z_{\rm I}$ in the figure, is the location in the flow domain where the viscosity gradient increases sharply. The number of collocation points in each

.

Figure 4.8 Schematic of the numerical scheme - orthogonal collocation on finite elements with Legendre polynomials

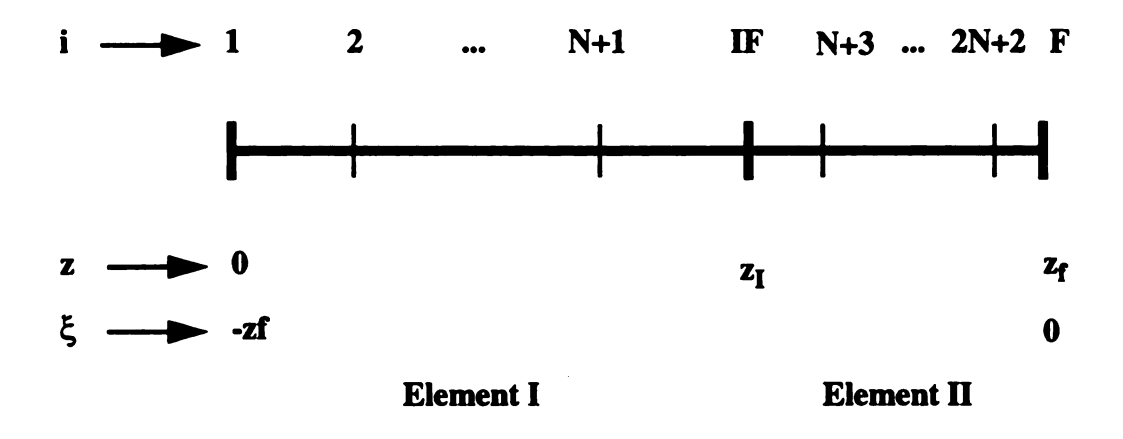


Figure 4.8

element is N. The index "i" in this figure denotes each collocation point. Legendre' polynomials are used to approximate the solution in each element. The domain in each element is then transformed into the Legendre' domain where the boundary locations are at 0 and 1. Thus we have 2N collocation points at which the eigenvalue problem (equation 4-28) is applied. The boundary conditions in equation 4-29 are applied at the left end of the first element (z = 0, the inlet) and at the right end of the second element ($z = z_f$, the front). The solution from each element is matched at the interface between the two elements (location z_f); that is, the solution ψ and its first derivative from each element are equated). We obtain a system of linear, homogeneous, algebraic equations with the unknowns being the values of ψ at each collocation point, as well as the eigen value, σ .

$$M_{(2N+2)\times(2N+2)} \bullet \underline{\Psi}_{(2N+2)\times 1} = \underline{0}_{(2N+2)\times 1}$$
(4-32)

That is, we have (2N+2) equations with (2N+2) unknowns. There are two other parameters: the wavenumber, k, and the quasistatic growth rate, σ . A nontrivial solution for this system of equations requires that the coefficient matrix, M, of the linear system be singular. The resulting characteristic equation for σ solved at a range of chosen values for the parameter, k and the most dominant root is taken as the growth rate. The eigenvalue problem is solved for several values of N, the number of collocation points in each element and convergence was observed for N=6.

The cutoff wavenumber is defined as the wavenumber at which the growth rate changes its sign. This is computed directly from the characteristic equation by setting $\sigma = 0$ and solving the resulting polynomial in (k). The characteristic equation has also been used to obtain marginal stability plots on a variety of parameter planes.

4.4 RESULTS AND DISCUSSION

The base state solution, as obtained for a polyurethane resin with second order kinetics, was discussed in section 4.3. The solution of the eigen value problem is presented and discussed in this section as growth rate and marginal stability curves. Some of the operating conditions and properties of the resin are then varied and their effect on the flow stability of each of these new formulations is examined.

4.4.1 ISOTHERMAL REACTION

It is instructive to consider the $E_R = 0$ limit of isothermal reactive filling at first. This limit is more representative of thermosetting polyester resins, for which the gel conversion is very low and the heat liberated by reaction is low upto the gel point.

The growth rate σ is evaluated for this case at a few locations (z_f) of the flow front and plotted against the wave number (represented by $b^{1/2}k$) in Figure 4.9. It is seen that, for any z_f , the growth rate is negative at low wavenumbers and becomes positive for larger values of (k). This implies that the process is stable for disturbances of large wavelength.

The results for isothermal filling are shown in Table 4.3 where the cutoff wavenumbers are tabulated for varying filling time and gel conversion. The range of wavenumbers over which the flow is stable may be shown on a plot of the cutoff wavenumbers. Figure 4.10 is one such plot, in which the cutoff wavenumbers are plotted as a function of the Damkohler number, which is the ratio between flow and reaction time scales. It can easily be shown that the Damkohler number (Da) is equivalent to the length of the mold that has been filled by the resin. It is seen that the flow becomes unstable for a

Figure 4.9 Growth rate curves for isothermal filling of polyurethane resin: z_f = 0.8, 1.0, 1.2, 1.5; E_R = 53, E_μ = 41, α_{gel} = 0.65, T_o = 325°K

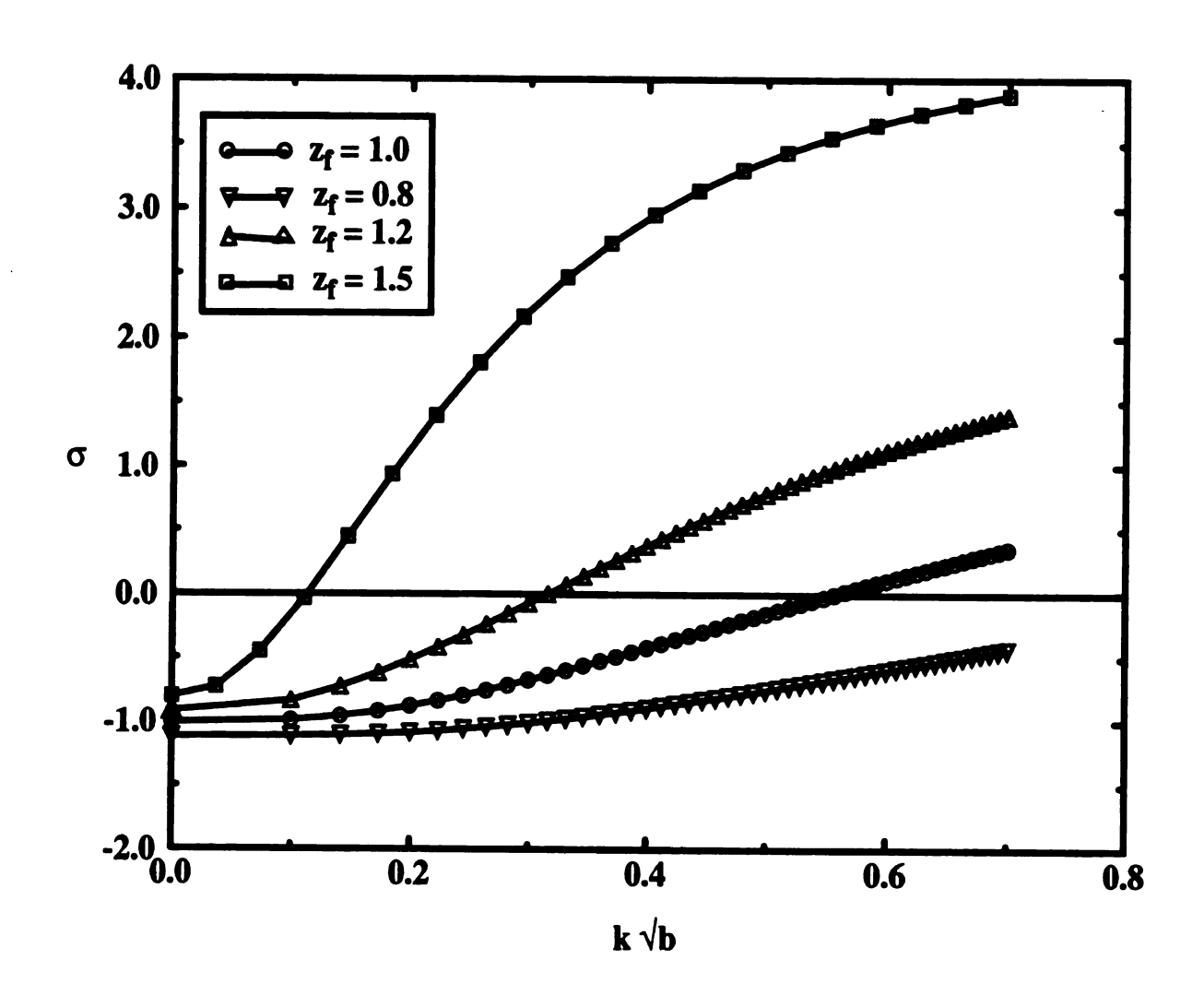


Figure 4.9

Table 4.3 Computational results for isothermal reaction

$$T_o = 325^{\circ}\text{K}; E_R = 52.64; E_{\mu} = 40.68$$

$$-\Delta H_R = 96,300 \text{ J/mol-}^{\circ}\text{K}; (\rho C_p) = 1.9092 \times 10^6 \text{ J/m}^3 \text{-}^{\circ}\text{K}$$

$$\Delta T_{ad} = 121.56^{\circ}\text{C}$$

α_{g}	z _f	$lpha_{ m f}$	(bk ²) _c	k _c (b=1.0)	k _c (b=0.1)		
	VARYING EXTENT OF FILLING (z _f)						
0.65	0.5	0.3333	6.1760	2.4852	7.8588		
0.65	0.7	0.4118	1.6992	1.2920	4.0856		
0.65	0.9	0.4737	0.5449	0.7382	2.3343		
0.65	1.2	0.5455	0.1016	0.3187	1.0080		
0.65	1.5	0.6000	0.0132	0.1150	0.3637		
VARYING GEL CONVERSION							
0.65	1.5	0.6000	0.0132	0.1150	0.3637		
0.73	1.5	0.6000	0.0986	0.3140	0.9930		
0.8	1.5	0.6000	0.2597	0.5096	1.6115		
0.9	1.5	0.6000	0.7700	0.8775	2.7749		

Figure 4.10 Marginal stability curve for isothermal filling, data from figure 9: Damkohler number (Da = flow time / reaction time)

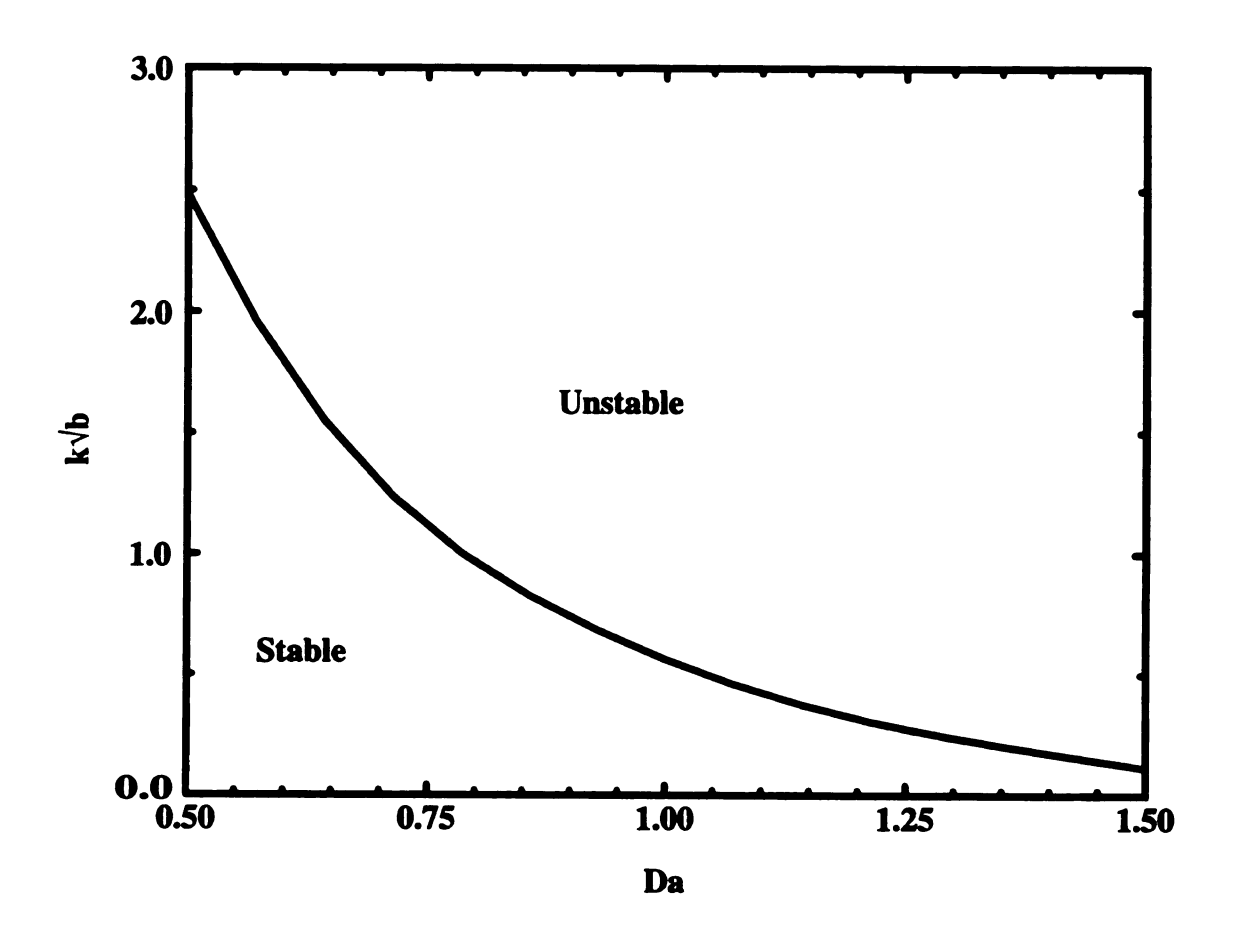


Figure 4.10

wider range of wave numbers, with increasing z_f. This implies that, as the mold gets filled to a greater length, the flow becomes increasingly unstable. At the larger filling times, the degree of conversion is larger than at small filling times; from Figure 4.6, it may be seen that at these larger conversions, the magnitude of S is lower (sign of S is negative). Since the flow is more stable when S is more negative, the results of Figure 4.10 are understandable. In terms of the ratio of the time scales, a small Da indicates a slower chemical reaction in comparison to the flow rate.

Effect of anisotropic permeability: The effect of anisotropic permeability is seen by comparing the ordinate in Figure 4.10 for several values of the degree of anisotropy, b. It is clear from this figure that when the transverse permeability is smaller than the permeability in the longitudinal direction (b < 1), the cutoff wavenumber, k_c , is larger than it is for the isotropic case (b = 1). That is, the range of wavenumbers for which the flow becomes stable is greater when the transverse permeability is small. This may be understood from an inspection of equation 4-19 which is a combination of the equation of continuity and Darcy's law for disturbances. When the transverse permeability is small, i.e. when b_1 and b_2 are small, conservation of mass dictates that for a disturbance to survive or propagate, the spatial pressure gradients in the disturbances have to be very large. This means that only sharp fingers (disturbances of large wavenumbers) would grow, while those of small wavenumbers are eliminated. Thus anisotropy with low transverse permeability helps in elimination of large fingers.

Effect of order of reaction and S: The dependence of reaction rate on conversion, i.e. the

order of reaction, governs the stability of the flow process. To understand the effect of reaction on the stability of the system, we compare the growth rates of the second order reaction system with the solution to the eigen value problem with S=0. The latter situation corresponds to a reaction with zeroth order kinetics with the same inlet and front conversions, and the same viscosity profile. Figure 4.11 is a plot of the growth rate curves a resin with the same viscosity behavior but with S=0. It is seen that for this case the growth rate is always positive, while for S < 0 it was negative for large disturbances. Thus, if the same converison profile is obtained with a zeroth order reaction, there is no stable region. Only when S<0 (for the second order reaction), do we get a stable region.

In Figures 4.9 and 4.11, the plots approach a finite growth rate asymptotically, for large wavenumbers. These asymptotic limits are plotted for various flow front positions for both S=0 and S<0, termed ultimate growth rate (σ_u), in Figure 4.12. This ultimate growth rate is seen to be higher for the no-reaction case, again indicating the dependence of flow stability on the order of reaction.

The results from an analysis of the isothermal mold filling, thus, provide us an idea of the behavior of the flow process governing mold filling, and it is expected that adiabatic operation of liquid molding would lead to similar results.

4.4.2 ADIABATIC REACTION

Some liquid molding operations can be carried out under adiabatic conditions.

Mathematically this is slightly more complex, due to the involvement of an additional balance equation (energy balance); however the adiabatic nature simplifies the equations

Figure 4.11 Growth rate curves for S = 0 for isothermal filling for identical base state viscosity profiles as for Figure 9

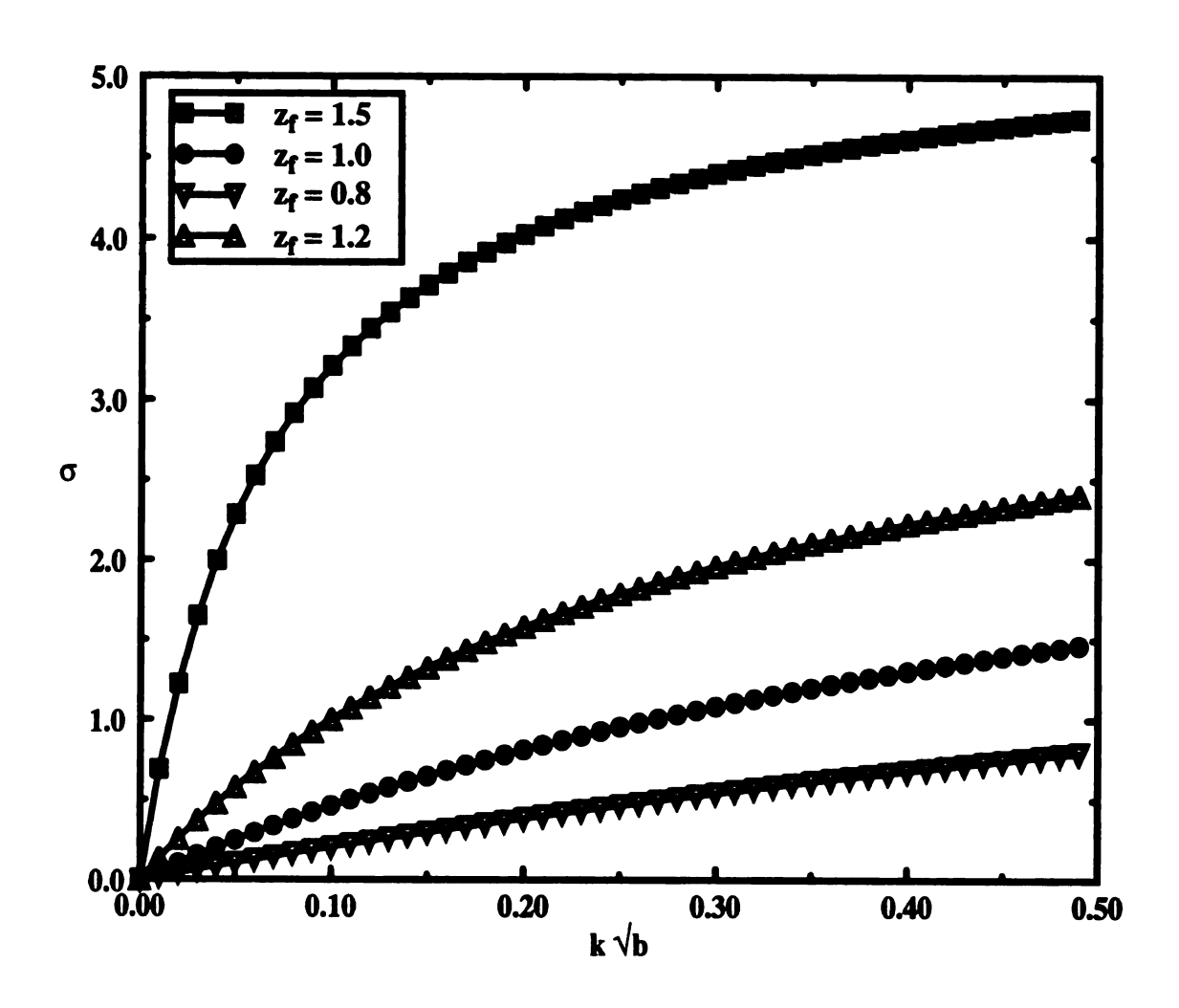


Figure 4.11

Figure 4.12 Upper limit of growth rate Vs Damkohler number for isothermal filling, T_o = 325^o K

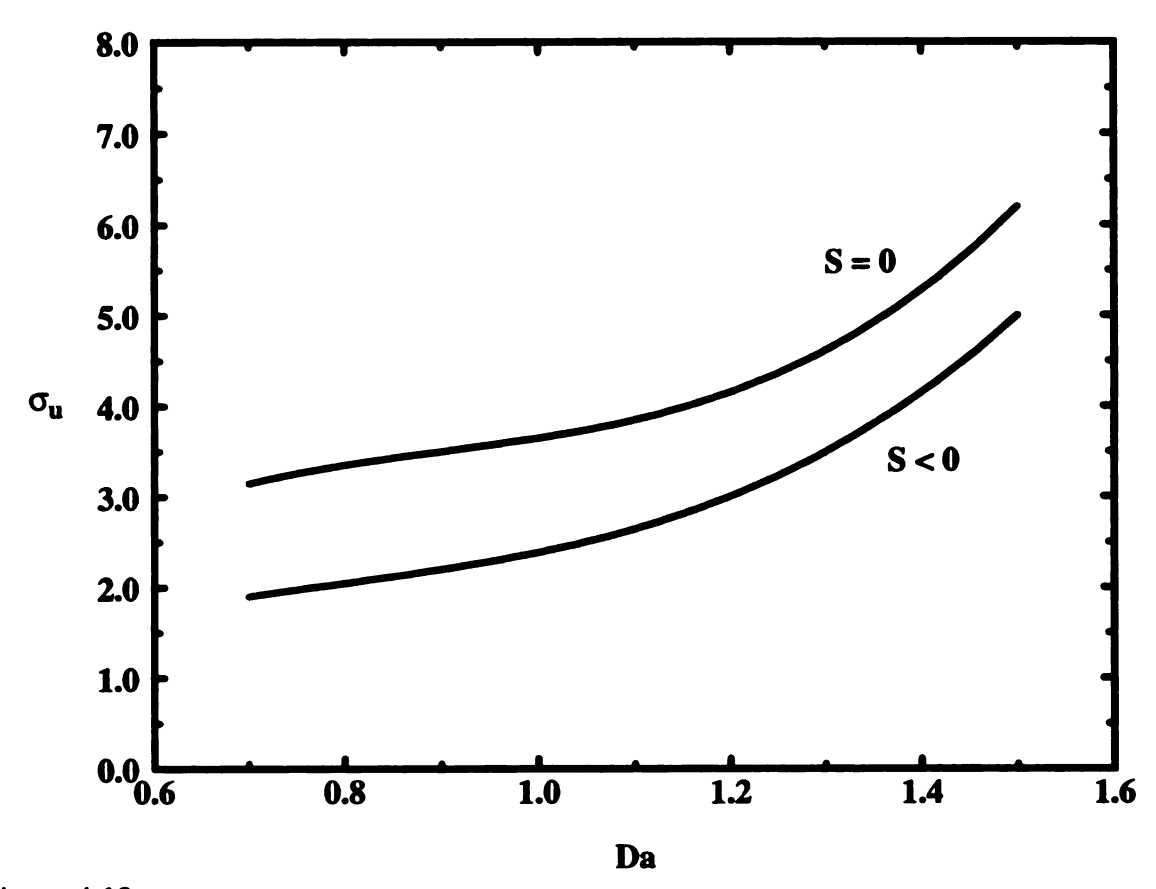


Figure 4.12

to some extent, as seen in section 4.3. To be even more realistic, fully non-isothermal equations would have to be solved, which render the model equations and their stability analyses, and consequently their solution, more complicated.

The results of the computations are now presented for mold filling under adiabatic conditions. Figure 4.13 shows the growth rate curves for several values of E_R . E_R may be altered by modifying the resin formulation to one with a different activation energy or a different heat of reaction. It is seen that for small values of E_R , there exists a range of wavenumbers with a negative growth rate, corresponding to a stable regime. This leads us to examine the stability characteristics of other formulations of the polyurethane resin, obtained by altering the kinetic and rheological parameters. The stability of the filling process may be affected by the thermochemical properties of the resin and the operating conditions. In the following analysis, several parameters are varied independently and the flow stability examined. In each of these cases, except for the case of varying z_f , the mold is filled to the same length enable comparison. The effect of varying the inlet temperature is also presented. The results are presented in the form of marginal stability plots.

Dependence of stable regime on various parameters:

For the adiabatic case, the parameters that may be varied are the fill time (which is equivalent to the Damkohler number), adiabatic temperature rise (ΔT_{ad}) (which may be changed by choosing appropriate values of the inlet concentration (c_0) and the heat of reaction (ΔH_R)), the kinetic activation energy (E_a), the inlet temperature (T_0) of the resin and the gel conversion (α_{gel}) of the polymer system. Most of these parametric studies have been done for a resin with the following properties:

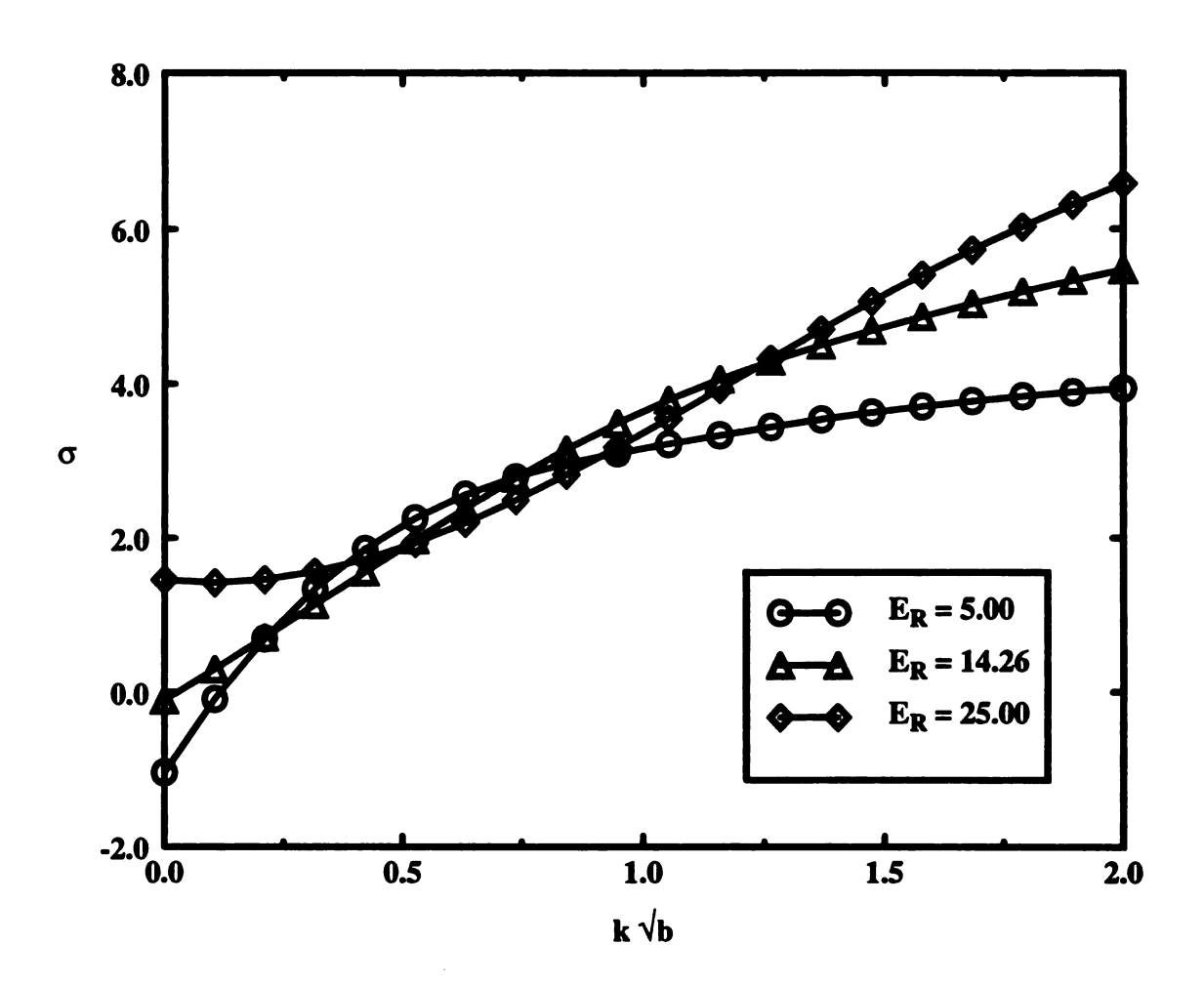


Figure 4.13 Growth rate curves for varying activation energy during adiabatic fill

 E_m = 131.17; E_R = 168.96; ΔT_{ad} = 37.87°K; α_{gel} = 0.8; reference temperature = 370°K. The activation energy and initial concentration of the resin were not changed from the values taken for earlier calculations but the heat of reaction was altered from 96,300 J/mol to 30,000 J/mol, which changed the adiabatic activation energy. For this lower exotherm, it was found that the viscosity gradient, V, did not change sign, thus satisfying the condition for exchange of stabilities. The results of the computations are presented in Tables 4.4 and 4.5.

- a) The effect of changing the dimensionless activation energy, E_R , on the stability at a fixed inlet temperature, noted earlier in Figure 4.13, is shown in Figure 4.14 as a marginal stability plot. As observed earlier, a decrease in E_R leads to an expansion of the range of stable wavenumbers, in the low-wavenumber region. This change in E_R may be accomplished by decreasing the kinetic activation energy, E_a . A higher activation energy means that more energy is required for the polymerization reaction to occur, which makes it more difficult for the viscosity on either side of the edge of an incipient finger to rise. This, in turn, means that the driving force available for finger growth (pressure drop across the edge of the disturbance) does not reduce as fast as it would for a lower E_a case, making it more stable than the case of a higher E_a .
- b) Figure 4.15 depicts marginal stability plots for changing Da (= t_F/t_R) and varying inlet temperature, in adiabatic mold filling using a resin with $E_R = 14.26$, which does have a stable regime as seen in Figure 4.14. The plot indicates, as in the isothermal case, that the

Table 4.4 Computational results for adiabatic reaction

					·····				
No.	$(\Delta T)_{ad}$	E _R	T _o	α_{gel}	E_{μ}	t			
Varying E _R with fixed T _o									
1.	121.56	52.67	2.67	0.65	40.86	0.206			
2.	121.56	25.00	2.67	0.65	40.86	0.527			
3.	121.56	14.26	2.67	0.65	40.86	0.801			
4.	121.56	5.00	2.67	0.65	40.86	1.194			
Varying α_{gel}									
5.	37.87	168.96	9.242	0.65	131.17	0.85			
6.	37.87	168.96	9.242	0.80	131.17	0.85			
7.	37.87	168.96	9.242	0.90	131.17	0.85			
Varying T _o									
8.	37.87	168.96	8.58	0.80	131.17	0.85			
9.	37.87	168.96	8.98	0.80	131.17	0.85			
10.	37.87	168.96	9.242	0.80	131.17	0.85			
11.	37.87	168.96	9.51	0.80	131.17	0.85			
Varying Exotherm, which alters both $(\Delta T)_{ad}$ and E_R , hence T_o									
12.	25.25	253.45	13.86	0.80	196.73	0.85			
13	37.87	168.96	9.24	0.80	131.17	0.85			
14.	50.50	126.72	6.93	0.80	98.36	0.85			
Varying filling time									
15.	37.87	168.96	9.242	0.8	131.17	0.535			
16.	37.87	168.96	9.242	0.8	131.17	0.750			
17.	37.87	168.96	9.242	0.8	131.17	0.850			
18.	37.87	168.96	9.242	0.8	131.17	0.950			

Table 4.5 Cutoff wavenumber data for adiabatic reaction

No.	$(\Delta T)_{ad}$	E _R	T _o	E_{μ}	t	(bk ²)c			
Varying T _o									
1.	37.87	168.96	8.58	131.17	0.85	0			
2.	37.87	168.96	8.98	131.17	0.85	0			
3.	37.87	168.96	9.242	131.17	0.85	0.47096			
4.	37.87	168.96	9.51	131.17	0.85	0.5435			
Varying filling time									
5.	37.87	168.96	9.242	131.17	0.535	3.2122			
6.	37.87	168.96	9.242	131.17	0.750	0.9041			
7.	37.87	168.96	9.242	131.17	0.850	0.47096			
8.	37.87	168.96	9.242	131.17	0.950	0.2281			

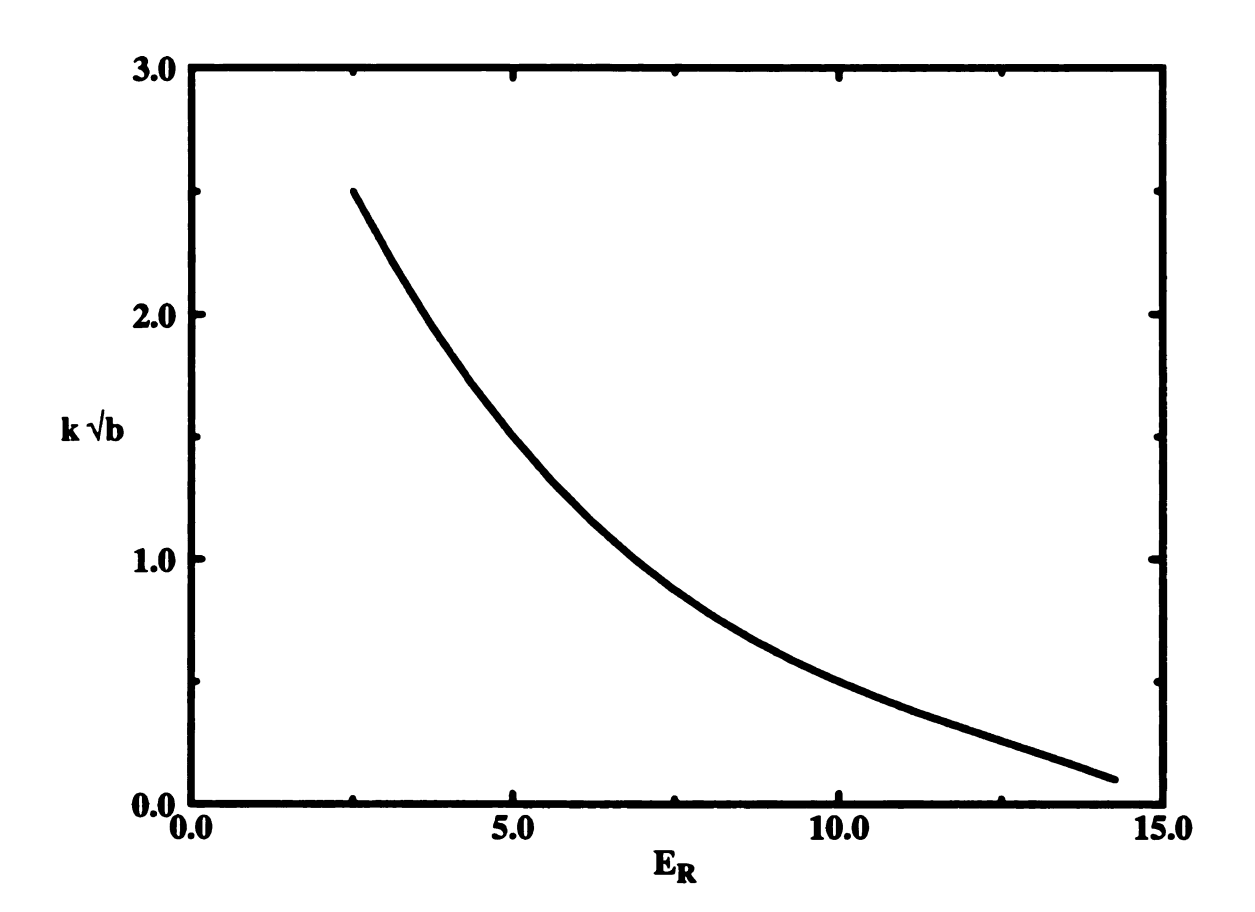


Figure 4.14 Marginal stability curve for adiabatic filling: activation energy

region of stability becomes smaller with increasing fill time. The reason for this behavior follows exactly from that discussed in the isothermal case. Also, an increase in the inlet temperature is found to expand the range of stable wavenumbers of fingers. The higher temperature would make the reaction go faster, thus making the viscosity profile less steep. This reduces the pressure drop across the edge of the disturbance, making the process less unstable. This effect is opposite to that of the activation energy.

- c) The effect of anisotropic permeability in adiabatic filling is seen, as in the isothermal case, by looking at the ordinate in Figure 4.15 for various values of the degree of anisotropy, b. The range of wavenumbers over which fingers are damped is much larger for the case with lower transverse permeability.
- e) Figure 4.16 depicts the effect of gel conversion on the stability of the mold filling process. A larger gel conversion implies stability over a wider range of wavenumbers. At lower gel conversions, the viscosity increase with conversion is faster, and makes the molecules less mobile. The number of sites available for further reaction, as a consequence, is much lower and this causes the driving force for finger growth to decrease at a slower rate, making the process more unstable.

Geometric limitations: The wavenumbers (k) referred to above may be converted to appropriate wavelengths of the fingers (λ_w), using the relation ($k = 2\pi l_{sc}/\lambda_w$), where l_{sc} is the length scale for the problem. To illustrate the significance of these results, the finger wavelengths corresponding to the cutoff wavenumbers are compared to the actual physical

Figure 4.15 Marginal stability curve for adiabatic filling: fill time and varying temperature; $E_R = 169$, $E_{\mu} = 131$, $\alpha_{gel} = 0.80$, $\Delta T_{ad} = 38^{o}K$

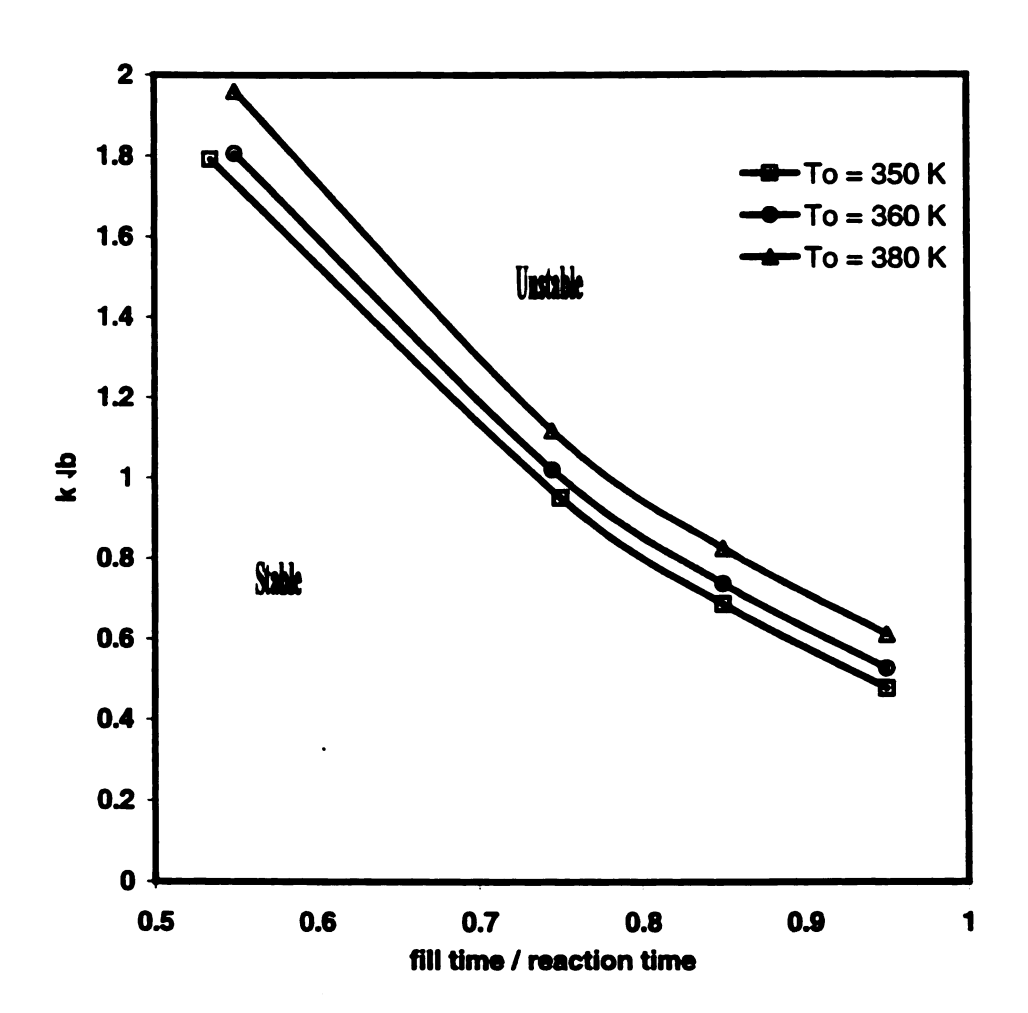


Figure 4.15

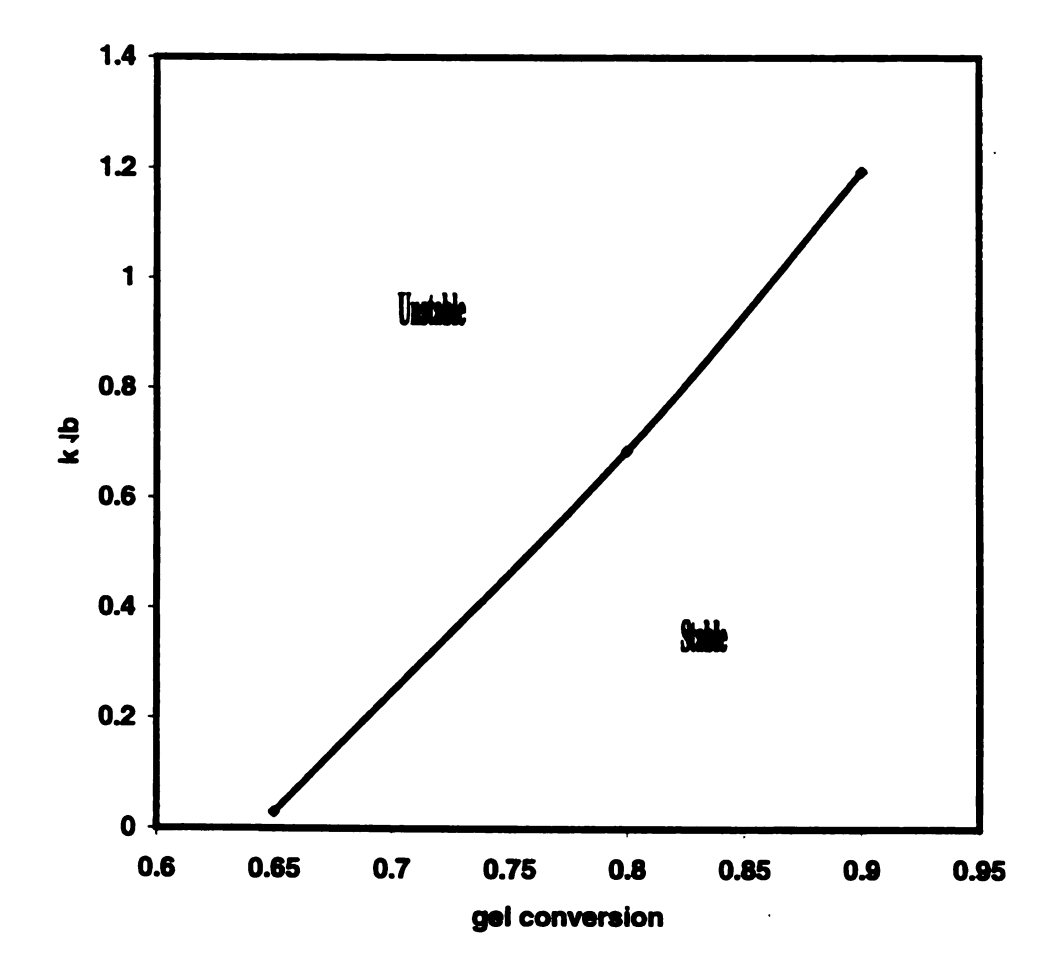


Figure 4.16 Marginal stability for adiabatic filling: gel conversion

dimensions of the mold. The thickness of the mold, B, represents the largest possible finger size, while the diameter of the fiber tow, d_1 , is the smallest possible finger width.

Representative values are chosen as below:

Mold thickness, B: 10mm

Fiber tow diameter, d_t: 0.1mm

Injection velocity, U₀: 0.5 cm/s

The data for polyurethane resins given in Table 4.1 are used, to obtain a length scale (l_{sc}) of 0.0637 mm.

The results of Figure 4.16 are now transformed into wavelengths. From Table 4.5, the cutoff wavenumber when z_f is 0.535 is $k_c = 1.79$. When converted to dimensional finger widths, this corresponds to $\lambda_c = 0.22$ mm. All fingers narrower than 0.22 mm will grow; conversely, all fingers wider than this are eliminated. This limiting finger width is now compared to the physical dimensions B and dt. It is seen that the tow diameter is much less than $\,\lambda_c;\,$ similarly, the mold thickness is much larger than this cutoff value. While very large fingers are eliminated, small fingers are undamped. A similar analysis may be done for other values of z_f , and it is clear that, as the mold gets filled, even fingers of large sizes tend to grow.

The above discussion was done for the case of isotropic permeability (b=1). As dicussed earlier, if the transverse permeability is less than the longitudinal permeability (b < 1), the cutoff wavenumbers are larger, which means that a wider range of disturbance wavelengths is stabilized. For example, when b=0.1, we get $k_c = 5.67$, which corresponds to a wavelength of $\lambda_c = 0.07$ mm. All disturbances wider than this are eliminated. Since

this is less than the fiber tow diameter, it may be concluded that any disturbance that is generated by the adverse viscosity gradient is damped out due to the low transverse permeability.

4.5 MECHANISM OF STABILIZATION

4.5.1 EFFECT OF S ON THE GROWTH RATE

Eq. 4-23 may also be expressed, using Eq. 4-27, as

$$\left[\frac{\sigma - S}{\sigma - S + V}\right] \bar{\lambda} \frac{dp}{d\xi} = b k^2 \psi \tag{4-33}$$

From this equation it is seen that when the wavenumber is zero, for non-zero amplitudes of the disturbances, the growth rate is equal to S. The necessary condition for dampening of disturbances is, then,

$$S < 0 \tag{4-34}$$

This means that there is a possibility of stabilizing disturbances of small wavenumbers (large finger widths) when the criterion in equation (4-34) is satisfied.

The effect of S on the growth rate is demonstrated by the schematic shown in Figure 4.17, which represents an incipient disturbance at some instant. The line AA' is the base state solution. Before the onset of the disturbance (t<0), the points M-, M+ are at the same, base state, conversion. The deviation from the base state, shown in the figure, corresponds to an increase in conversion (positive amplitude, A(ξ)); at this time (t=0), the conversions at M-, M+ are in an increasing order.

If there were no disturbance, then the fluid particles at the two points would react at the same rate and remain at the base state conversion at t > 0. In the presence of the

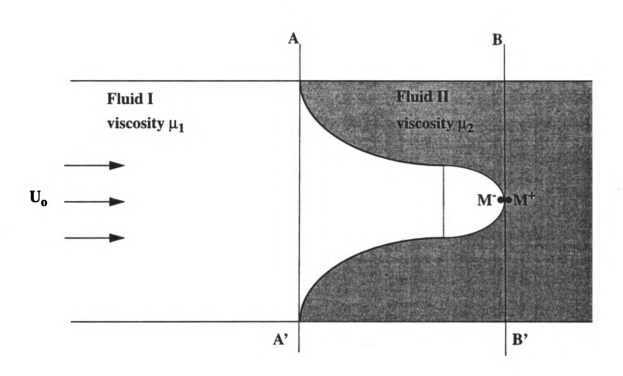


Figure 4.17 Schematic representation of the effect of S on growth rate

disturbance, however, several possibilities exist for the behavior of the disturbance at t > 0, depending on the shape of the reaction rate curve (Figure 4.2).

- i) If S < 0, since the conversion at M- is lesser than that at M+; thus the polymerization rate at M- is higher than that at M+, bringing the conversions at the two points closer. This decreases the amplitude of the disturbance at t > 0.
- ii) If S > 0, the higher conversion at M+ results in a higher rate of polymerization than at M-, widening the gap in conversion between the two points at longer times, t > 0. Thus the disturbance grows with time for positive values of S.

The above discussion was presented by taking k = 0, to demonstrate the effect of S on the growth rate. However, it has to be remembered that the viscosity gradient, V, also dictates the stability behavior of fingers.

4.5.2 STABILIZATION OF LARGE FINGERS

It was seen that chemical reaction, in addition to creating an adverse viscosity gradient that causes fingers, can couple with the flow process to stabilize large fingers but not small fingers. The mechanism for this inability to eliminate small fingers may be explained by plotting the growth rate against the ratio, κ , between a reference growth rate and the reaction rate. The former is the growth rate, at a given wavenumber, for a hypothetical fluid with the same viscosity and conversion profiles as the resin, but with S=0, i.e. a zeroth order reaction. A low value of the ratio κ , then, corresponds to a fast reaction in comparison to disturbance growth rate. In addition the reference growth rate, as seen in Figure 4.11, increases with an increasing wavenumber; thus a small value of κ implies small wavenumbers and vice versa. To illustrate the mechanism, the growth rate vs

Figure 4.18 Effect of S on growth rates for identical conversion and viscosity profiles in the base state

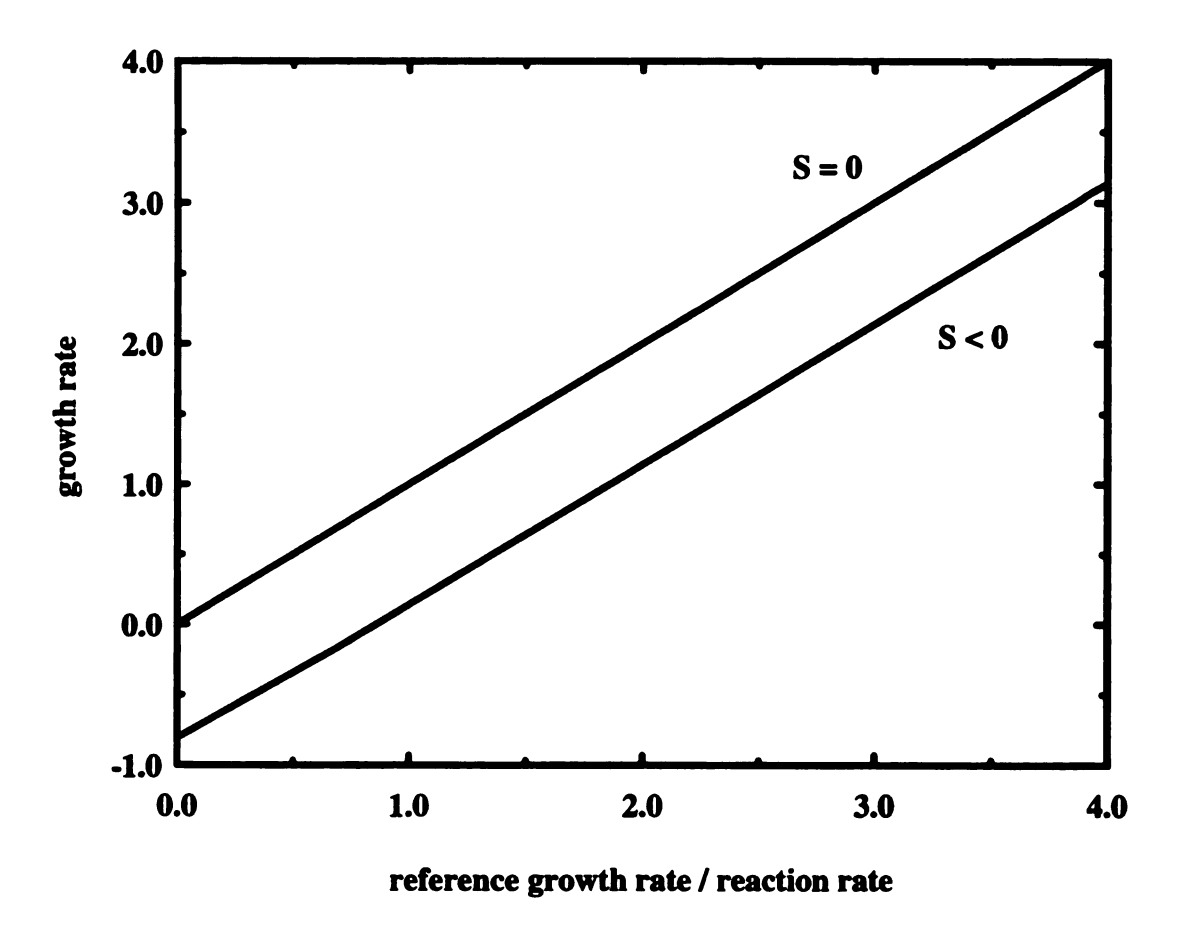


Figure 4.18

 κ plot for a specific case is shown in Figure 4.18. It is seen that the growth rate is negative for small κ and becomes positive at large κ . At large values of κ (short wavelengths), the time scale for finger growth is much smaller than the reaction time scale. This means that the growth of fingers occurs faster than chemical reaction can damp them out. Since large values of κ correspond to small finger widths, we may conclude that small fingers cannot be eliminated by the reactive coupling mechanism. On the other hand, at low κ (large wavelength), the reaction time scale is small, which means that the chemical reaction is faster than the rate at which the finger would grow; this enables damping of these large fingers.

4.6. SUMMARY

Flow of reacting resin through a fiber preform located in a a mold produces a continuous distribution of resin age from the inlet to the advancing resin front. The effect of this age distribution on fluid mixing within the fille dregion has been examined with a linear stability analysis. The results of this analysis for isothermal and adiabatic reactive filling indicates that the role of reaction is two fold. In the first place, it generates an adverse viscosity gradient, which leads to generation of fingers. Secondly, it contributes to stabilization of these fingers at smaller wavenumbers.

The effect of reactive coupling on the fingering is derived as an eigen value problem, the largest eigen values of which are the growth rates used to determine the stability behavior of the filling process. Reactive coupling occurs in the form of a quantity S, defined as a gradient of the reaction rate with conversion, and V, the viscosity gradient.

For positive values of S, the process is always unstable and disturbances of all wavelengths would grow; for polymeric systems with a negative S throughout the flow domain, mold filling can be stable and large disturbances can be damped. Thus the kinetics of the polymerization reaction determines the stability of the mold filling process.

The stability characteristics of a polyurethane resin have been investigated for a variety of parameter planes. It is seen that the resin may be reformulated suitably, altering the kinetics or rheological properties, to reduce the amount of fingering during mold filling. The gel conversion, adiabatic temperature rise and transverse permeability may be increased to help eliminate fingers, while the process becomes less stable as the mold gets filled. Stabilization may also be achieved by raising the inlet temperature.

CHAPTER 5 VISCOUS FINGERING DURING REACTIVE FILLING OF FIBER
PREFORMS: EFFECTS OF DISPERSION AND REACTION

5.1 INTRODUCTION

Mold filling in liquid composite molding processes involves the flow of a polymerizing liquid mixture through an anisotropic porous medium comprised of fiber reinforcements. The work of Homsy and co-workers has established that dispersion within the porous medium is a stabilizing influence at higher wavenumbers or narrower finger widths. In the present application, spatial variations in monomer concentration are brought about not only by dispersion but also by the polymerization reaction within the porous medium. Hence it is important to understand the influence of these two factors on the finger widths most likely to grow during the mold filling process.

The fiber bed is, in general, anisotropic both for permeation of the resin through the preform and dispersion of the monomer in the reaction mixture. The permeability of the preform is determined by its physical structure and can vary according to the kind of fiber arrangement chosen, viz. random or aligned. The effective dispersion coefficient is dependent on the characteristics of both the porous medium and the resin. Due to the polymerization reaction, the molecular weight of the resin increases with time; this affects the dispersion of the monomeric resin (of low molecular weight) through the polymerized resin. The bulk dispersion depends on the injection velocity as well as the length scale of the fiber bed.

The object of this chapter is to analyze viscous fingering during reactive filling of an end gated mold containing a pre-located porous fiber bed. The mechanism for growth or attenuation of fingers in flow of a reacting liquid mixture through a porous medium is explored here. This mechanism is directly related to the reaction kinetics of the resin and dispersion characteristics of the monomer through the polymerized resin and will also lead to criteria for attenuation of fingers in the presence of reactive and dispersive effects.

5.2 MODEL PROBLEM AND EQUATIONS

In order to study the combined effect of dispersion and reaction on the generation of fingers, the flow situation is described by a simplified model problem. The physical problem is posed in the context of multiple shot injection of two-component resins, mixed in-line, into a mold. A batch of fluid is injected into the mold and allowed to react for some time, during which it undergoes polymerization, with a rise in viscosity. At a later time (t=0), another shot of resin is injected. Due to the difference in ages of the two shots of fluid, a step jump $\Delta\alpha$ in the extent of reaction is observed at the interface of the two shots. This multiple shot approach was used by Losure (1994) to prepare molded composites with a variety of fingered microstructure; the mechanical properties of such composite specimens were found to be affected significantly by the details of the microstructure. It may also be noted that the step jump in the extent of reaction is quite different from the continuous conversion profile seen in actual liquid molding operations, as discussed in chapter 4. The purpose of this chapter is to present a simplified analysis of the combined effects of dispersion and chemical reaction on the stability of the mold

filling process. A more realistic problem would involve a continuous conversion profile (hence, viscosity profile), which will not be part of this dissertation.

In order to delineate clearly the effect of chemical reaction on fingering, mathematically, we pose the problem in an infinite porous medium, as in the work of Tan & Homsy (1986) which addressed dispersion alone. The locations far from an incipient disturbance, in this analysis, are assumed to be unaffected by it and, therefore, may be assumed to correspond to infinity with no significant loss of accuracy. Figure 5.1a depicts the flow domain at the initial time t=0. Region I in this figure is resin that has been injected and allowed to react till an extent of reaction α_1 (corresponding to viscosity μ_1). The instant of time when fresh resin with an extent of reaction α_2 (viscosity μ_2) is injected is termed (t = 0) for the purposes of this analysis. The velocity of injection is a constant, U_0 .

The defining equations for this model problem are the equation of continuity,

Darcy's law (for flow through porous media), an equation for the location of the moving

flow front and a component mass balance written for the monomer concentration. The

bulk flow is, as in chapter 4, in the z-direction. The differential balance equations

governing this problem, expressing the velocity as a three dimensional vector since it is

required for the later stability analysis, are

Continuity
$$\nabla \bullet \hat{\underline{u}} = 0$$

$$Darcy's \ Law \qquad \qquad \hat{\underline{u}} = -\frac{1}{\varepsilon \ \hat{\mu}} \hat{K} \bullet \nabla \hat{P}$$

$$Reactant \ Mass \ Balance \qquad \frac{\partial \hat{c}}{\partial \hat{t}} + \hat{\underline{u}} \bullet \nabla \hat{c} = -\hat{R} + \nabla \bullet [\hat{D} \bullet \nabla \hat{c}]$$

$$(5-1)$$

The velocity vector in Darcy's Law represents the local velocity inside the porous medium. In the reactant mass balance equation, the change in concentration both due to

Figure 5.1a Flow of reacting liquid through a porous medium (moving frame)

Figure 5.1b Profiles of conversion, viscosity and S at t=0

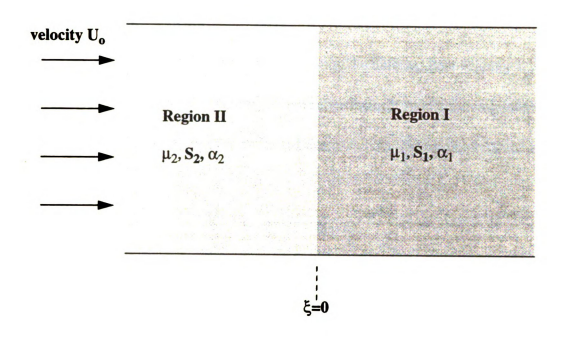


Figure 5.1a

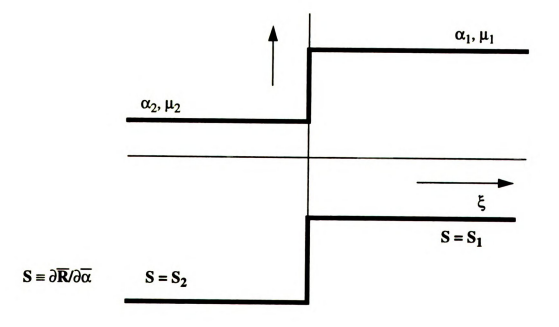


Figure 5.1b

mass dispersion and chemical reaction are included; the former was missing in the balance equations dealt with in chapter 4.

A moving frame of reference is defined, using the uniform flow velocity U_0 and the location of the interface z_I , introducing the new coordinate ξ . In this moving reference frame, the x- and y- coordinates are unaltered due to the one-dimensional nature of the bulk flow.

$$\hat{\xi} = \hat{z} - \hat{z}_I \equiv \hat{z} - U_o \hat{t} \tag{5-2}$$

The velocity vector in the moving frame of reference has a corresponding change.

$$\hat{q} = \hat{\underline{u}} - U_o \tilde{i}_3 \tag{5-3}$$

The model equations may then be rewritten, in the moving reference frame, as

Continuity
$$\nabla \bullet \hat{q} = 0$$

$$Darcy's \ Law \qquad \qquad \hat{q} + U_o \quad \tilde{i}_3 = -\frac{1}{\varepsilon \ \hat{\mu}} \quad \hat{K} \bullet \nabla \hat{P}$$

$$Reactant \ Mass \ Balance \qquad \frac{\partial \hat{c}}{\partial \hat{t}} + \hat{q} \bullet \nabla \hat{c} = - \quad \hat{R} + \nabla \bullet [\hat{D} \bullet \nabla \hat{c}] \qquad (5-4)$$

Figure 5.1b schematically shows the profiles of conversion and viscosity at the initial time, t=0, when the second shot of fluid has been injected. Both these quantities see a step jump at ξ =0. (The quantity S on both Figures 5.1a and 5.1b will be discussed in section 5.4.)

5.3 SCALING AND DIMENSIONLESS FORM OF THE EQUATIONS

Appropriate scales are used to make these equations dimensionless. The problem discussed in chapter 4 had chemical reaction as the only important physical phenomenon,

which made the choice of scales for length and time rather easy. In this problem, however, both mass dispersion and chemical reaction are dominant mechanisms. As a result we have two possible choices for the length and time scales: one based on the reaction kinetics and another based on dispersion. In keeping with the work of Tan and Homsy (1986) and others, who solved similar problems but with no chemical reaction, the length and time scales for this problem are based on the dispersion characteristics of the porous medium and are taken to be, respectively, D/U₀ and D/U₀²; this choice eliminates the Peclet number from the equations. (A brief discussion on the choice of scaling factors is given in Appendix B.) In dimensionless quantities, then, eq. (5-4) may be rewritten as

$$\nabla \bullet \underline{q} = 0$$

$$q = -\overline{\lambda} \quad K \bullet \nabla P - \widetilde{i}_{3}$$

$$\frac{\partial \alpha}{\partial t} + \underline{q} \bullet \nabla \alpha = \theta \quad R(\alpha, T) + \nabla^{2} \alpha$$
(5-5)

In these equations, the permeability has been normalized by the longitudinal permeability K_1 , with $K = K_D/\epsilon = (1/\epsilon) \times (K/K_1)$. In addition, as in chapter 4, $\overline{\lambda} = 1/\overline{\mu}$.

The component mass balance, then, is left with only one non-dimensional parameter, θ , which is the product of the Damkohler number and the Peclet number. The Damkohler number (Da = t_f/t_R) is the ratio of flow time scale to reaction time scale. The Peclet number (Pe = t_D/t_f) is the ratio of the dispersive time scale to the flow time scale. The product of these two, θ , represents a ratio of the dispersive time scale to the reaction time scale ($\theta = t_D/t_R$). A large value of θ corresponds to a small value of t_R in comparison to t_D , which implies that the chemical reaction is much faster than the rate at which dispersion takes place; in other words, the effect of a large θ is a smothering of dispersion

effects by chemical reaction. The choice of dispersive scales has, thus combined the Peclet and Damkohler numbers into a single dimensionless quantity.

5.4 STABILITY ANALYSIS

Linear stability analysis leads to the following eigenvalue problem with two coupled equations. The analysis is similar to that presented in chapter 4 for the reaction-only case, with the same forms of base state and perturbation variables (eq. 4-18), linearization of the perturbed equations and decomposition of the disturbances into Fourier components (eq. 4-21).

$$\left[D^{2} + \rho(\xi) \frac{\partial \overline{\alpha}}{\partial \xi} D - k^{2}\right] q_{\xi} = \frac{k^{2} \rho(\xi)A}{(\Delta \alpha)}$$

$$\left[\sigma - \theta \frac{\partial \overline{R}}{\partial \xi} + k^{2} - D^{2}\right]A = -(\Delta \alpha) \frac{\partial \overline{\alpha}}{\partial \xi} q_{\xi}$$
(5-6)

 q_{ξ} is the amplitude of the velocity disturbance and A is the amplitude of the conversion disturbance. It must be noted that, in these equations, the base state conversion has been normalized by $(\Delta\alpha)$, the initial step change in conversion across the interface. That is, $\overline{\alpha} = (\overline{\alpha}^{o}/\Delta\alpha)$. This yields $d\overline{\alpha} = (1/\Delta\alpha) d\overline{\alpha}^{o}$, where $\overline{\alpha}^{o}$ is the un-normalized base state conversion. This ensures that the limits of the conversion are 0 - 1 and enables direct comparisons to the results of Tan and Homsy (1986) as a limiting case.

The two coupled equations in eq. (5-6) are combined to obtain

$$\begin{bmatrix} \sigma - \theta & \frac{\partial \overline{R}}{\partial \overline{\alpha}} & + k^2 - D^2 \end{bmatrix} L \quad q_{\xi} = -\frac{\partial}{\partial \xi} \overline{\alpha} \quad k'^2 \quad q_{\xi}$$

$$where \qquad L \equiv \left[\frac{1}{\rho(\xi)} \left(D^2 + \rho(\xi) \right) \frac{\partial}{\partial \xi} \overline{\alpha} \quad D - k'^2 \right]$$

$$and \qquad \rho(\xi) = -\frac{1}{\overline{\lambda}} \frac{d}{d\overline{\alpha}} \overline{\lambda}$$
(5-7)

L is an operator as defined above, while $\rho(\xi)$ is related to the quantity V defined in chapter 4 (eq. 4-25).

In this problem, σ is the exponential growth rate of disturbances and is the eigenvalue, and k is the wavenumber. The boundary conditions associated with the eigenvalue problem are the decay conditions at ∞ (the effect of the disturbances is not felt by the fluid at locations far from the interface), and continuity conditions at the interface, on disturbances in velocity, conversion and pressure (Tan and Homsy, 1986). These boundary and continuity conditions are discussed in greater detail in section 5.5.2

Other groups arising in the scaled eigenvalue problem are $S = (\partial \overline{R}/\partial \overline{\alpha})$ — the incremental rate of reaction with increasing extent, discussed in chapter4; and $\rho = -d(\ln \overline{\lambda})/d\overline{\alpha}$, where $(-\rho)$ x $(d\overline{\alpha}/d\xi) = V$ represents the gradient of mobility $(\overline{\lambda})$ along the flow direction (also discussed in chapter 4). As explained in chapter 2, the type of resin polymerization affects the stability of the mold filling process, through the parameter S. Figure 5.1b shows a sample profile of S at time t=0; given the step jump in conversion profile, S also follows a similar pattern. Some polymerization reactions involve consumption of inhibitor almost up to the gel point, the rate of which is independent of the monomer concentration (Gonzalez-Romero & Macosko, 1985). For this zeroth order reaction, S=0, and the stability of the mold filling process is unaffected by the chemical reaction. In other polymerization reactions, the initial stage of the network forming

process is of first order kinetics, which leads to a constant value of S. For many polymerization reactions S is negative and it becomes increasingly negative as the reaction progresses. For example, polyurethanes follow second order kinetics (Castro & Macosko 1982). Figure 2-2 shows the behavior of S for different types of chemical reactions, schematically, and has been discussed in more detail in chapter 2.

5.5 INITIAL GROWTH RATE

Thu purpose of this study is to describe the combined effect of dispersion and chemical reaction on the stability of the process. The solution of the complete form of the model equations for the base state (from eq. 5-5) and that of the eigenvalue problem (eq. 5-7) is quite involved and would require extensive numerical computations. The problem is more involved than that of Tan and Homsy (1986) and that presented in chapter 4, where only one of dispersion and reaction was present. In the current problem, both dispersion and chemical reaction terms, and the corresponding Damkohler number, in the component balance equations. However, a description of the disturbances in their initial period of existence is very important, and governs their subsequent behavior. A study of the initial growth rates is important and tells us a great deal about the stability of the flow process. In addition, the initial growth rates may be studied relatively easily; some simplifications may be made that make the equations amenable to mathematical analysis with comparatively less, simple, numerical computations. Therefore, the following sections of this dissertation chapter will present a semi-analytical solution to the eigenvalue problem at small times after the two shots of fluid are brought into contact.

5.5.1 DERIVATION OF THE PROBLEM

This section presents the steps involved in the derivation of eq. (5-7) at t = 0 to yield the eigen value problem for initial growth rate analysis. The most important feature of this initial growth rates analysis is the representation of the conversion profile in the domain of the problem as a Heaviside step function $(H(\xi))$, shown schematically in Figure 5.1b.

Using the initial (step) conversion profile, i.e. $\alpha(\xi) = (\Delta \alpha) H(\xi)$, we get $\partial \overline{\alpha}/\partial \xi = (\Delta \alpha) \delta(\xi)$. Also, the definition $\rho(\xi) = -(1/\overline{\lambda}) (d\overline{\lambda}/d\overline{\alpha})$ was used. This yields, from equation (5-6),

$$[D^{2} + \rho(\xi) \quad (\Delta\alpha) \quad \delta(\xi)D - k^{2}] \quad q_{\xi} = \frac{k^{2} \quad \rho(\xi)A}{(\Delta\alpha)}$$

$$[D^{2} - \sigma - k^{2} + \theta \quad S]A = (\Delta\alpha) \quad (\Delta\alpha) \quad \delta(\xi) \quad q_{\xi}$$
(5-8)

Eliminating A from these equations, we get

$$[D^{2}-\sigma-k^{2}+\theta S]\left\{\frac{\Delta\alpha}{k^{2}\rho(\xi)}\left[D^{2}+\rho(\xi)(\Delta\alpha)\delta(\xi)D-k^{2}\right]q_{\xi}\right\}$$

$$=(\Delta\alpha)(\Delta\alpha)\delta(\xi)q_{\xi}$$
(5-9)

Since $\Delta \alpha$ and k' are independent of ξ , this gives

$$[D^{2}-\sigma-k^{2}+\theta \ S]\left\{\frac{1}{\rho(\xi)} \ [D^{2}+\rho(\xi) \ (\Delta\alpha) \ \delta(\xi)D-k^{2}] \ q_{\xi}\right\}$$

$$= k^{2} \ (\Delta\alpha) \ \delta(\xi) \ q_{\xi}$$
(5-10)

or

$$[D^2 - \sigma - k^2 + \theta \ S] \ Lq_{\xi} = k^2 \ (\Delta \alpha) \ \delta(\xi) \ q_{\xi}$$
 (5-11)

where the operator L is given by

$$L = \frac{1}{\rho(\xi)} [D^2 + \rho(\xi) (\Delta \alpha) \delta(\xi) D - k'^2]$$
 (5-12)

Tan and Homsy (1986) solved a similar problem where they assumed a viscosity that varied exponentially with concentration. This means that ρ is independent of $\overline{\alpha}$, hence ξ . (Note that the viscosity itself does depend on ξ ; it is only the first derivative of the natural logarithm of viscosity, i.e. the mobility gradient, that is invariant.) Mobility is defined as the ratio between permeability and viscosity. The mobility ratio, given by m_R , is then $m_R = mob_2/mob_1 = \mu_1/\mu_2 = exp(\rho)$ (where μ_1 is the viscosity of the fluid to the right of the interface).

In this problem, too, an exponential viscosity profile is chosen as a representative example. This makes equations (5-11), (5-12) amenable to analytical solution at t=0; if the ξ -dependence of ρ were retained, these equations would be far more complicated and would require numerical solution for the initial growth rate as well. This choice of viscosity profile facilitates comparison of limiting case (h = 0) results of this analysis with those obtained by Tan and Homsy (1986).

Thus, taking ρ to be independent of ξ , the eigenvalue problem becomes

$$[D^2 - \sigma - k^2 + \theta \ S][D^2 + \rho(\xi) \ (\Delta \alpha) \ \delta(\xi)D - k^2]q_{\xi} = k^2 \ \rho \ (\Delta \alpha) \ \delta(\xi) \ q_{\xi} \ (5-13)$$

5.5.2 BOUNDARY CONDITIONS

Due to the discontinuity at the interface, this fourth order o.d.e. has to be solved separately on either side of the interface ($\xi < 0$ and $\xi > 0$) and the two solutions matched at the interface. Two of the conditions are given by the decay of the q_ξ disturbance as $\xi \rightarrow$

 $\pm\infty$. That leaves us with two more conditions, needed to solve the fourth order o.d.e. In the absence of any other simple, independent boundary conditions on q_{ξ} , we use four matching conditions on the disturbances at the interface. All these conditions are now presented.

I. The decay of disturbances is given by:

$$At \quad \xi = \pm \infty \qquad q_{\xi} = 0 \tag{5-14}$$

- II. The matching conditions at the interface are given by:
 - a) Matching of the velocity disturbance.

$$At \quad \xi = 0 \qquad q_{\xi}(0^{+}) = q_{\xi}(0^{-}) \qquad (5-15)$$

b) Matching of the conversion disturbance.

$$At \quad \xi = 0 \qquad A(0^+) = A(0^-)$$
 (5-16)

c) Matching of the pressure disturbance.

Using the equation of continuity, Darcy's law and the Fourier expansions for disturbances, the pressure disturbance $p(\xi)$ may be expressed in terms of the velocity disturbance q_{ξ} . This relation is obtained as

$$p(\xi) = -\frac{1}{(bk^2)} \frac{dq_{\xi}}{\bar{\lambda}}$$
 (5-17)

Using the continuity of pressure at the interface, $p(0^+) = p(0^-)$, we get

$$m_R \left. \frac{dq_{\xi}}{d\xi} \right|_{0^+} = \left. \frac{dq_{\xi}}{d\xi} \right|_{0^-} \tag{5-18}$$

where m_R is the mobility ratio defined earlier.

III. The final condition involves integration of the o.d.e. (equation 5-13) across the

$$\int_{0^{-}}^{0^{+}} [D^{2} - \sigma - k^{2} + \theta \ S][D^{2} + \rho(\xi) \ (\Delta \alpha) \ \delta(\xi)D - k^{2}]q_{\xi} \ d\xi$$

$$= k^{2} \rho \ (\Delta \alpha) \int_{0^{-}}^{0^{+}} \delta(\xi) \ q_{\xi} \ d\xi$$
(5-19)

The eigenvalue problem to be solved, thus, consists of the o.d.e. in equation (5-13), the boundary conditions (5-14) and the matching conditions (5-15), (5-16), (5-18), (5-19).

5.5.3 ANALYTICAL SOLUTION

The initial growth rate for an exponential viscosity-concentration relationship, with a step jump in concentration at time t=0, was analyzed by Tan & Homsy (1986). A similar approach has been used in this work to obtain the initial growth rates (at t=0) for the model problem with combined reaction and dispersion. The particular case in which viscosity varies exponentially with conversion, i.e. ρ =constant, is chosen for the following analysis.

The first step is the representation of the solution for $\xi \neq 0$, using the decay conditions. Since the base state profile is a step function, for $\xi \neq 0$, the Dirac delta function in eq. (5-13) vanishes and the equation may be simplified to

$$[D^{2} - m^{2}] [D^{2} - k^{2}]q_{\xi} = 0$$
where $m^{2}(\xi) = \sigma + k^{2} - \theta S(\xi)$ (5-20)

The solution to equation (5-20), on either side of the interface, is given by

$$q_{\xi} = A_1 \exp[m_{\xi}] + B_1 \exp[k'\xi]$$
 for $\xi < 0$
 $q_{\xi} = A_2 \exp[-m_{\xi}] + B_2 \exp[-k'\xi]$ for $\xi > 0$ (5-21)

The constants A₁, A₂, B₁, B₂ are to be determined using the matching conditions.

Applying eq. (5-15), i.e. matching of the velocity disturbance, on eq. (5-21), we get

$$A_1 = A_2 + B_2 - B_1 \tag{5-22}$$

Applying eq. (5-18), i.e. matching of the pressure disturbance, on eq. (5-21), and using the relation (5-22), we get

$$A_1 = \frac{1}{k' - m} [(k' + m_+ m_R) A_2 + (k' + k' m_R) B_2]$$
 (5-23)

In applying eq. (5-16), i.e. matching of the conversion disturbance, since $A \equiv Lq_{\xi}$, we get

$$[D^{2} + \rho \ (\Delta \alpha) \ \delta(\xi)D - k^{2}]q_{\xi}|_{0^{-}}^{0^{+}} = 0$$
 (5-24)

In this equation, using eq. (5-21), the first term (taking the second derivatives of q_E) yields

$$D^{2}q_{\xi}\Big|_{0^{-}}^{0^{+}} = (A_{2}m_{+}^{2} - A_{1}m_{-}^{2}) + (B_{2} - B_{1})k^{2}$$
 (5-25)

The second term, due to the presence of the dirac delta function $\delta(\xi)$, vanishes. The third term also gives, using eq. (5-22),

$$-k'^2 q_{\xi} \Big|_{0^-}^{0^+} = 0 ag{5-26}$$

Thus (5-24) may be simplified, using (5-22) and (5-23), as

$$B_2 = -A_2 \left[\frac{m_+^2 + m_+ m_R (k' + m_-) + m_- k'}{k'^2 + k' m_R (k' + m_-) + m_- k'} \right]$$
 (5-27)

Three of the matching conditions have been used above, to obtain a simple relation between two of the constants. The integral boundary condition (5-19) is now applied on eq. (5-21) to get another relation between A_2 and B_2 . The integral equation is rewritten as

$$\int_{0^{-}}^{0^{+}} [D^{2} - \sigma - k^{2} + \theta \ S] Lq_{\xi} \ d\xi = k^{2} \rho (\Delta \alpha) \int_{0^{-}}^{0^{+}} \delta(\xi) \ q_{\xi} \ d\xi$$
 (5-28)

a) The first term in the integral on the left hand side yields

$$\int_{0^{-}}^{0^{+}} D^{2}(Lq_{\xi}) d\xi = D(Lq_{\xi}) \Big|_{0^{-}}^{0^{+}}$$
 (5-29)

Using the definition of LqE, this gives

$$D(Lq_{\xi})\Big|_{0^{-}}^{0^{+}} = D^{3}q_{\xi}\Big|_{0^{-}}^{0^{+}} + \rho(\Delta\alpha)\delta'(\xi)Dq_{\xi}\Big|_{0^{-}}^{0^{+}} + \rho(\Delta\alpha)\delta(\xi)D^{2}q_{\xi}\Big|_{0^{-}}^{0^{+}} - k'^{2}Dq_{\xi}\Big|_{0^{-}}^{0^{+}}$$
(5-30)

Now, using the properties of the dirac delta function

$$\delta |_{0^{-}} = \delta |_{0^{+}} = 0$$

$$\delta' |_{0^{-}} = \delta' |_{0^{+}} = 0$$
(5-31)

the second and third terms in eq. (5-30) vanish. We are now left with

$$D(Lq_{\xi})\Big|_{0^{-}}^{0^{+}} = D^{3}q_{\xi}\Big|_{0^{-}}^{0^{+}} - k^{2}Dq_{\xi}\Big|_{0^{-}}^{0^{+}}$$
 (5-32)

Using eq. (5-21), then, we get

$$D(Lq_{\xi})\Big|_{0^{-}}^{0^{+}} = A_{2}m_{+}[m_{+}^{2} + k'^{2}] - A_{1}m_{-}[m_{-}^{2} - k'^{2}]$$
 (5-33)

- b) The second and third terms on the l.h.s. of eq. (5-28) vanish.
- c) The right hand side of eq. (5-28) yields

$$k^{2} \rho (\Delta \alpha) \int_{0^{-}}^{0^{+}} \delta(\xi) q_{\xi} d\xi = k^{2} \rho (\Delta \alpha) q_{\xi}|_{\xi=0}$$

$$= k^{2} \rho (\Delta \alpha)[A_{2} + B_{2}]$$
(5-34)

Equations (5-33) and (5-34) are now plugged into eq. (5-28) to give, after simplifying,

$$B_2 = \frac{A_2}{k'^2 \rho(\Delta \alpha)} \left[-m_+^3 + m_+ k'^2 - k'^2 \rho(\Delta \alpha) + m_- k'^2 - m_- m_+^2 \right]$$
 (5-35)

(5-27) and (5-35) are now combined to eliminate the constants A_2 and B_2 , yielding a simple, algebraic equation involving the eigenvalue, σ , of the problem.

$$\frac{(m_{+}+m_{-}) (k^{2}-m_{+}^{2})-k^{2} \rho \Delta \alpha}{k' \rho \Delta \alpha} = -\frac{k'(m_{-}+m_{+}M)+m_{+}(m_{+}+m_{-}M)}{(k'+m_{-}) (1+M)} (5-36)$$

where

$$M = \exp(\rho)$$

$$k^{2} = bk^{2} = b_{1}k_{x}^{2} + b_{2}k_{y}^{2}$$

$$m_{+}^{2} = \sigma + k^{2} - \theta S_{1}$$

$$m_{-}^{2} = \sigma + k^{2} - \theta S_{2}$$
(5-37)

The parameters in the growth rate curves are θ , S_1 and S_2 . The cutoff wavenumbers are defined as the wavenumbers at which the growth rate changes sign, implying a transition between stable and unstable regimes. Eq. (5-36) may be solved for the cutoff wavenumbers k_c by setting σ =0. The roots of the algebraic equations in either case are obtained by Newton-Raphson iterations. The initial guesses must be close to the roots, to obtain convergence of the numerical scheme. Suitable guesses for the lower cutoff wavenumber are obtained from the results of two different analyses. One was performed by Hickernell & Yortsos (1986) for non-dispersive displacement through porous media, and another was done for reactive filling without dispersion (Jayaraman et al 1992).

5.5.4 RESULTS

For consistency with the data used in chapter 4, a second order reaction is chosen to

investigate the behavior of the initial growth rate profiles. For any n-th order reaction, the first derivative of the reaction rate R w.r.t. α , i.e. $S = dR/d\alpha$, is S = -k n $(1-\alpha)^{n-1}$. Since both k (reaction rate constant) and n (order of the reaction) are positive quantities, and so is $(1-\alpha)$, it follows that S is always negative and that at larger conversions the magnitude of S is smaller. That is, $|S_1| < |S_2|$ (see Figure 5.1b). In addition, for a second order reaction (as in polyurethanes), the range of possible values of S is $\{-2k$ to $0\}$, which in dimensionless terms is $\{-2$ to $0\}$. The choice of $\Delta\alpha$ is also important. When $\Delta\alpha = 1.0$ and in the limiting case of $\theta = 0$, the results would correspond to those obtained by Tan & Homsy, 1986. In the physical problem under consideration, however, this is not practical since it would require the fluid on the right of the interface to be completely reacted; hence this particular case is only of academic interest.

For the purpose of illustration of this analysis, $\Delta\alpha$ has been chosen to be 0.2. Specifically, the first shot of fluid is allowed to react till a conversion of 0.2 is reached and then the second shot is injected, at which time we take t=0. The corresponding values of S are $S_2 = -2.0$ and $S_1 = -1.6$ (see Figure. 5.1b). Thus the conversion and S follow step profiles and possess a discontinuity at ξ =0. As discussed in section 5.5.1, an exponential viscosity profile has been chosen, and the value of ρ , the gradient of viscosity w.r.t. conversion, has been taken to be 3.0. The parameter θ is then varied and equation (5-36) solved for the growth rate σ as a function of the wavenumber k. The parameters used in this computation are, then:

time instant, t = 0

 $\rho = 3;$

 $\Delta \alpha = 1.0$

Table 5.1 Computational results from eq. (5-36); Parameters: $\Delta \alpha = 0.2$; $\rho = 3.0$; $S_1 = -1.6$; $S_2 = -2.0$

Table 5.1

_		_	_
"		41	41
-	_		

σ	k ₁	k ₂
0	0	0
0.001	0.0038	0.1448
0.002	0.0081	0.1393
0.003	0.0130	0.1333
0.004	0.0186	0.1268
0.006	0.0328	0.1107
0.007	0.0429	0.0996
0.008	0.0617	0.0800

$\theta = 0.002$

σ	k ₁	k ₂
0	0.0105	0.1353
0.001	0.0159	0.1290
0.002	0.0220	0.1219
0.003	0.0293	0.1138
0.004	0.0384	0.1038
0.005	0.0520	0.0894
0.0052	0.0563	0.0849
0.0054	0.0628	0.0782

$$\theta = 0.003$$

σ	k ₁	k ₂
0	0.0172	0.1268
0.001	0.0237	0.1194
0.002	0.0314	0.1108
0.003	0.0415	0.0999
0.004	0.0589	0.0818
0.0041	0.0626	0.0779

$\theta = 0.004$

σ	k ₁	k ₂
0	0.0254	0.1169
0.001	0.0337	0.1078
0.002	0.0449	0.0958
0.0025	0.0533	0.0870
0.0027	0.0583	0.0818
0.0028	0.0620	0.0780

p=idi

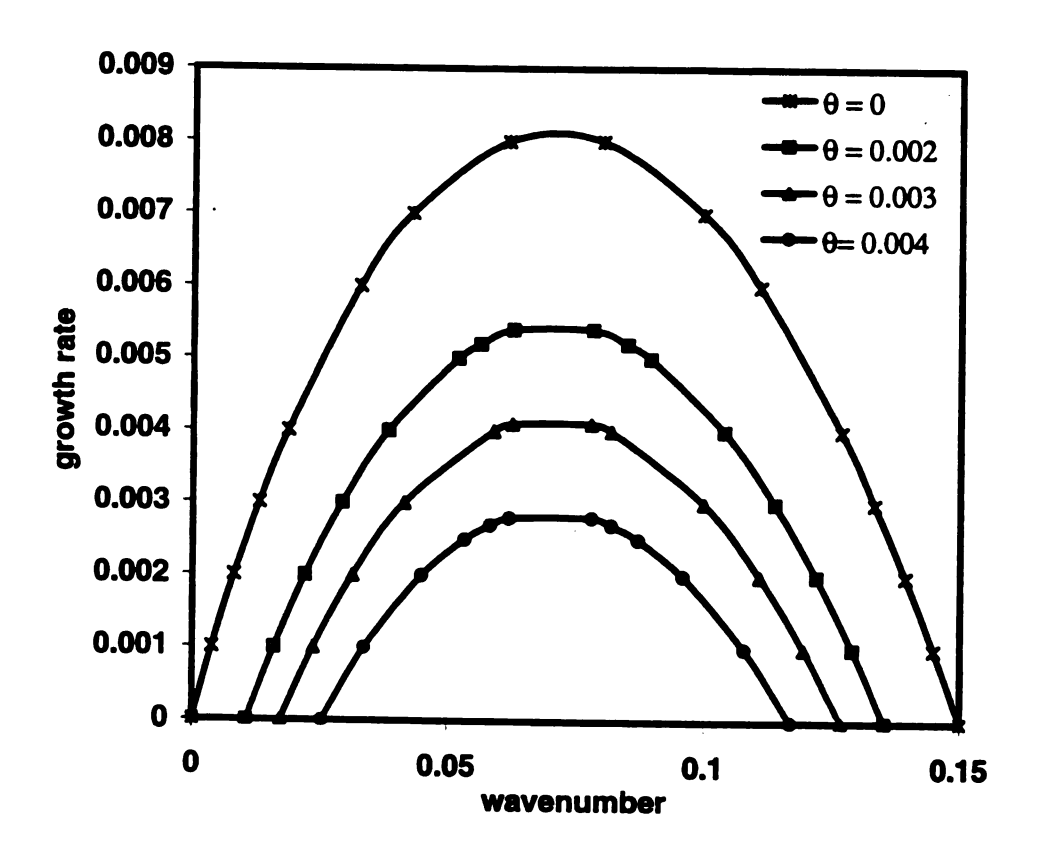


Figure 5.2 Initial growth rate curves - varying θ

Table 5.2 Cutoff wavenumber data at several values of θ ; Parameters: $\Delta \alpha = 0.2$; $\rho = 3.0$; $S_1 = -1.6$; $S_2 = -2.0$

Table 5.2

θ	k _{c,1}	k _{c,2}
0	0	0.1500
0.001	0.0048	0.1430
0.002	0.0105	0.1353
0.003	0.0172	0.1266
0.004	0.0254	0.1169
0.005	0.0360	0.1045
0.006	0.0539	0.0851
0.0062	0.0617	0.0769

eters: Ja=1.

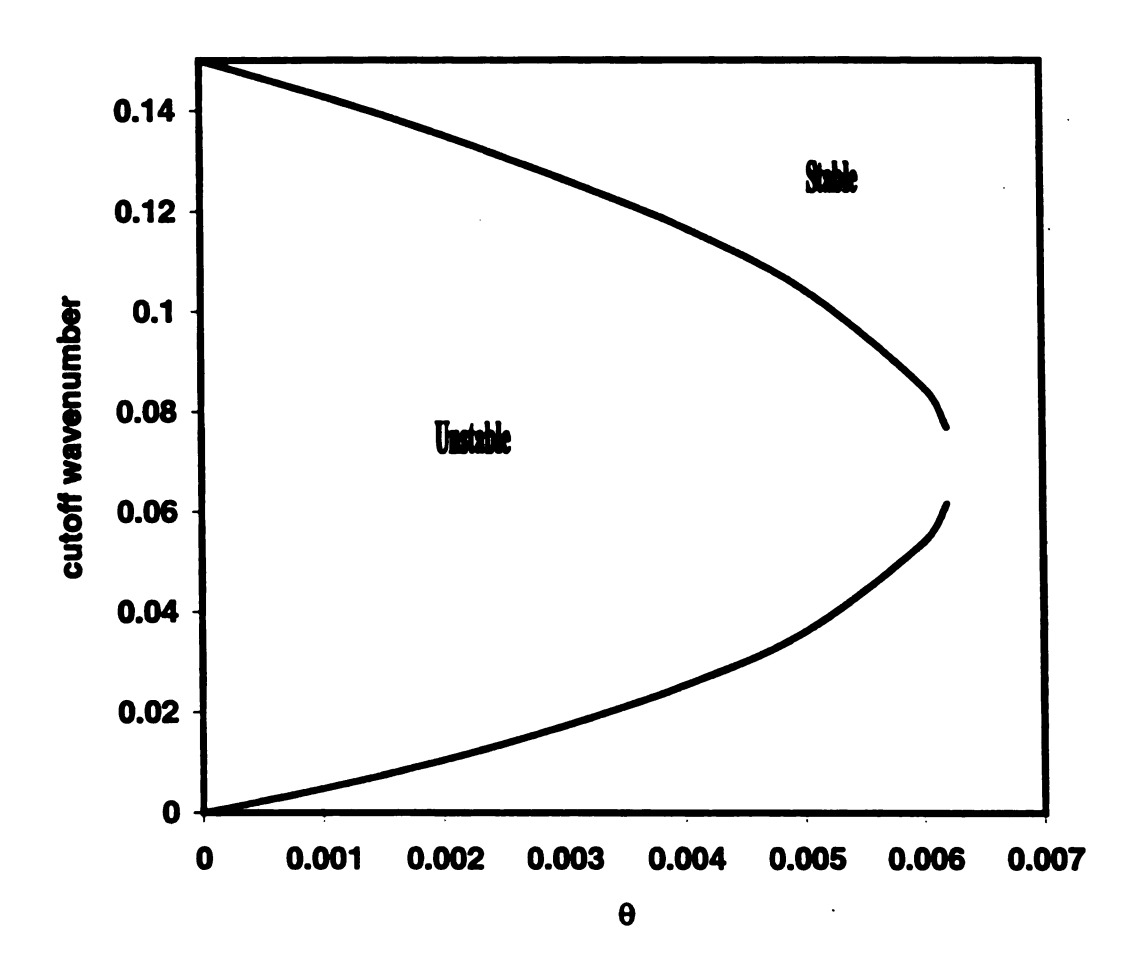


Figure 5.3 Marginal stability: θ

$$S_1 = -1.6;$$

$$S_2 = -2.0$$

The values of θ are raised from θ =0 and the two solutions for the wavenumber k are evaluated at increasing σ . These results are tabulated in Table 5.1. The values of the initial growth rate, σ , are plotted against the wave number, k, for the different values of θ as shown in Figure 5.2. The curve for θ =0 corresponds to the flow process dominated by dispersion. It matches up well with the result of Tan & Homsy (1986). For this case, small fingers get smeared out due to dispersion, while large fingers remain undamped. This is in contrast to the case of θ >0, where two different non-zero cutoff wavenumbers may be identified. As the rate of chemical reaction is increased relative to the rate of dispersion, by increasing θ , it is seen that only a small range of intermediate finger sizes are unstable. The polymerization reaction combined with dispersion thus stabilizes a broader range of fingers. For the chosen values of S_1 , S_2 and ρ (-1.6, -2.0 and 3.0 respectively) it is seen that, when the rate of reaction is about two hundred times the rate of dispersion (θ > 0.005), disturbances of all sizes decay.

The marginal stability curve is plotted in Figure 5.3. The cutoff wavenumbers k_c at the different values of θ are shown in Table 5.2. For a given θ , fingers of wavenumbers within the envelope would grow, while the rest are damped out. The width of the unstable region decreases with a rise in θ . These results may be compared to results reported earlier for miscible displacement without reaction or dispersion. Hickernell and Yortsos (1986) have reported that without dispersion, any incipient fingers would invariably grow.

The wavenumbers (k) referred to above may be converted to appropriate finger widths (λ), using the relation (k = $2\pi l_{sc}/\lambda$), where l_{sc} is the length scale for the problem.

To illustrate the significance of these results, the finger widths corresponding to the cutoff wavenumbers are compared to the actual physical dimensions of the mold. The thickness of the mold, B, represents the largest possible finger size, while the diameter of the fiber tow, d_t , is the smallest possible finger width. Representative values are chosen as below:

Mold thickness, B: 10mm

Fiber tow diameter, d_t: 0.1mm

Dispersion coefficient, D: 0.001 cm²/s (after Losure, 1994)

Injection velocity, U₀: 0.5 cm/s

This yields a length scale (l_{sc}) of 0.0002 mm.

From Table 5.2, the cutoff wavenumbers when θ is 0.004 are $k_{c1} = 0.0254$ and $k_{c2} = 0.1169$. When converted to dimensional finger widths, these correspond to $\lambda_1 = 4.95$ mm and $\lambda_2 = 1.075$ mm. All fingers of sizes between these values will grow; conversely, all fingers of widths outside this range are eliminated. These limiting finger widths are now compared to the physical dimensions B and d_t . It is seen that the tow diameter is much lesser than the lower limit λ_2 . This means that all fingers with widths of the order of tow diameter will be eliminated. Similarly, the mold thickness is much larger than the upper limit, λ_1 . While very large fingers are eliminated, there is an intermediate range of finger widths that are undamped.

For the case of $\theta=0.001$, Table 5.2 lists $k_{c1}=0.0048$ and $k_{c2}=0.1430$. These correspond to $\lambda_1=26.25$ mm and $\lambda_2=0.88$ mm. It is clearly seen for this case that the mold thickness is much lesser than the upper limit on unstable finger widths, λ_1 , and the tow diameter is smaller than the lower limit, λ_2 . This means that fingers of sizes of the

order of tow diameter will be eliminated, while all fingers larger than λ_2 will grow. A similar analysis may be done for other values of θ , and it is clear that, as chemical reaction becomes more significant in comparison to the dispersion mechanism, the range of sizes of growing fingers becomes smaller.

For the hypothetical case where the parameters S_1 and S_2 are both positive, chosen as +3 and +1 respectively, which corresponds to a reaction with autocatalytic kinetics, the unstable range of wavenumbers is larger with reaction than without reaction as seen in Figure 5.4. This computation has been performed to confirm the necessary condition for stabilization, S < 0, obtained in chapter 4. Compared to the no-reaction case (θ =0), the upper cutoff wavenumber is greater for higher θ . Also, for any given wavenumber of the disturbance in the unstable range, the growth rate is higher for the $\theta>0$ case. This means that positive S_1 and S_2 destabilize the flow process.

5.6 SUMMARY

The combined effects of chemical reaction and dispersion on the growth of flow instabilities in reactive flow through a fiber bed are strikingly different from the effect of dispersion alone, or that of reaction alone, on fingering. The model problem to make this study was inspired by a multiple-shot injection experiment done by Losure (1994). Since the initial growth rates govern subsequent behavior of any incipient disturbances, the stability analysis of the model problem was simplified to obtain the initial growth rates, and their behavior investigated. An analytical solution of the eigen value problem was possible, under the conditions chosen.

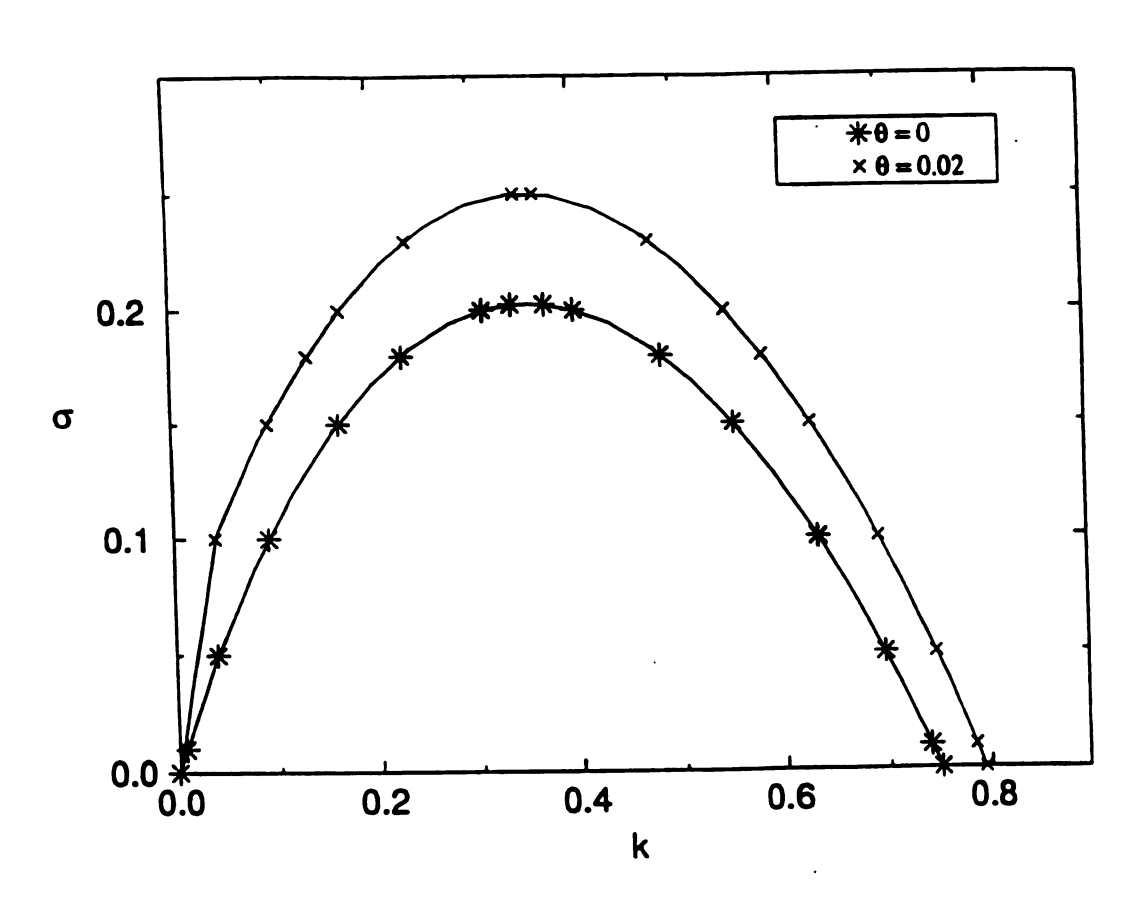


Figure 5.4 Initial growth rate curves - positive values of S

It is seen that the result depends on the type of reaction as seen in the incremental rate of reaction with increasing extent of reaction, S. As the rate of chemical reaction is increased relative to the rate of dispersion, the process becomes increasingly more stable. If S is increasingly negative along the flow direction, and the reaction rate is several times the rate of dispersion, it is possible to eliminate fingers entirely. When S is positive, the unstable range of wavenumbers is increased with reaction. These effects are more pronounced when the spatial variation in S is steeper. The wavenumbers may also be converted to finger widths, and predictions on the growth or elimination of fingers may be made by comparing the cutoff finger widths to the dimensions of the mold and fiber tows used.

CHAPTER 6 CONCLUSIONS

6.1 SUMMARY AND CONCLUSIONS

A study of the flow of reactive, polymeric liquids through fiber bundles has been presented in this dissertation. Following the observation of fingers during the mold filling process and subsequent investigation of their deleterious effects on some of the mechanical properties of the final parts (Losure, 1994), this work attempts to obtain theoretical criteria that enable prediction of the generation and growth of these fingering instabilities.

A simple model has been developed to track the motion of the flow front and the pressure distribution inside the filled region of the mold at any time. The effect of rheological changes on the reduction in flow velocity, in a constant pressure scenario, have been represented by two quantities - a velocity reduction factor and the log-mean mobility difference ratio (LMMDR). These analyses were done using representative rheological data for an epoxy resin and a vinyl ester resin. The data enabled division of the entire flow domain into three regimes - one with an invariant viscosity, another with a changing viscosity, and a third regime where elastic effects come into play. The pressure distributions, after the viscosity increase significantly, are steep very near the flow front and provide greater driving force for fiber wet out, i.e. penetration of the resin into the fiber tows to wet individual fibers is facilitated.

Since the resin in liquid molding operations is continuously undergoing polymerization reaction, the viscosity of the resin also increases along the flow direction towards the advancing front. An adverse viscosity gradient is known to generate fingers.

However, the coupling between the evolving reaction and the viscosity gradient complicates the mechanism and produces some stabilization at larger length scales. In the moving frame of reference, the cutoff wavenumbers when the viscosity gradient is steady are different from those when the viscosity gradient is produced by an evolving chemical reaction. The study of the generation and subsequent behavior of disturbances is done by performing a linear stability analysis on the equations describing the system. It is found that a necessary condition for damping of fingers is given by equation 4-31, i.e. S < 0. The effect of various parameters on finger growth has also been investigated. The thermochemical properties of the resin, like the activation energy, gel conversion and reaction exotherm, may suitably be altered to eliminate fingers during mold filling. In addition, the operating conditions (resin inlet temperature, injection velocity, etc.) may be changed to affect finger growth. The ranges of stable wavenumbers in each case are presented in the form of marginal stability curves. The effect of anisotropy of permeability has also been presented.

Disturbances of small wavenumbers, i.e. large finger widths, have been found to be stabilized by the coupling of chemical reaction with the flow process. This is in contrast to the stabilizing effect of dispersion for fingers of small widths (Tan and Homsy, 1986). The complementary nature of the two mechanisms of damping of fingers is utilized in chapter 5 to obtain the ranges of stable wavenumbers in the presence of both mechanisms. The combined effect of mass dispersion and chemical reaction, on the fingering process, was examined in the context of a multiple-shot injection where the interface between resins of different ages is examined. It has been found that the individual effects of chemical reaction alone (chapter 4) and dispersion alone (Tan and Homsy, 1986) are both seen in

this case. That is, disturbances at both ends of the spectrum of wavenumbers are stabilized. In addition, it is found that an increase in chemical reaction rate increases the range of stable wavenumbers; so much so, that at certain levels of reaction rates in comparison with dispersion rates, all disturbances die out. The necessary condition discussed earlier, i.e. S < 0, for stabilization is also confirmed by this analysis.

The sizes of fingers generated are limited by the geometric dimensions of the mold and of the fiber tows used in the preform. In the case of an end-gated mold, the thickness of the mold represents the largest finger size possible, while the diameter of the fiber tows corresponds to the smallest finger size. The upper and lower cutoff wavenumbers in Table 5.2 and figure 5.2, for any θ , correspond to a lower and an upper limit on the widths of growing fingers, respectively; all fingers with widths outside this range will be eliminated. The relation between finger size (λ) and wavenumber (k) is ($k = 2\pi l_{sc}/\lambda$), where l_{sc} is the length scale. Using representative numbers for the various parameters (dispersion coefficient, injection velocity, mold thickness and fiber tow diameters), the following conclusions are arrived at (see figure 5.2).

- (a) In general, the diameter of the fiber tows is less than the lower limit on finger widths for growing fingers. This means that fingers of very small sizes, of the order of tow diameter are eliminated, while those of intermediate sizes grow.
- (b) When dispersion mechanism is more dominant, the mold thickness is lesser than the upper limit of growing finger widths; this means that all large fingers in this situation are unstable. As reaction becomes more significant in comparison to dispersion (larger values of θ), some of the large fingers are eliminated.

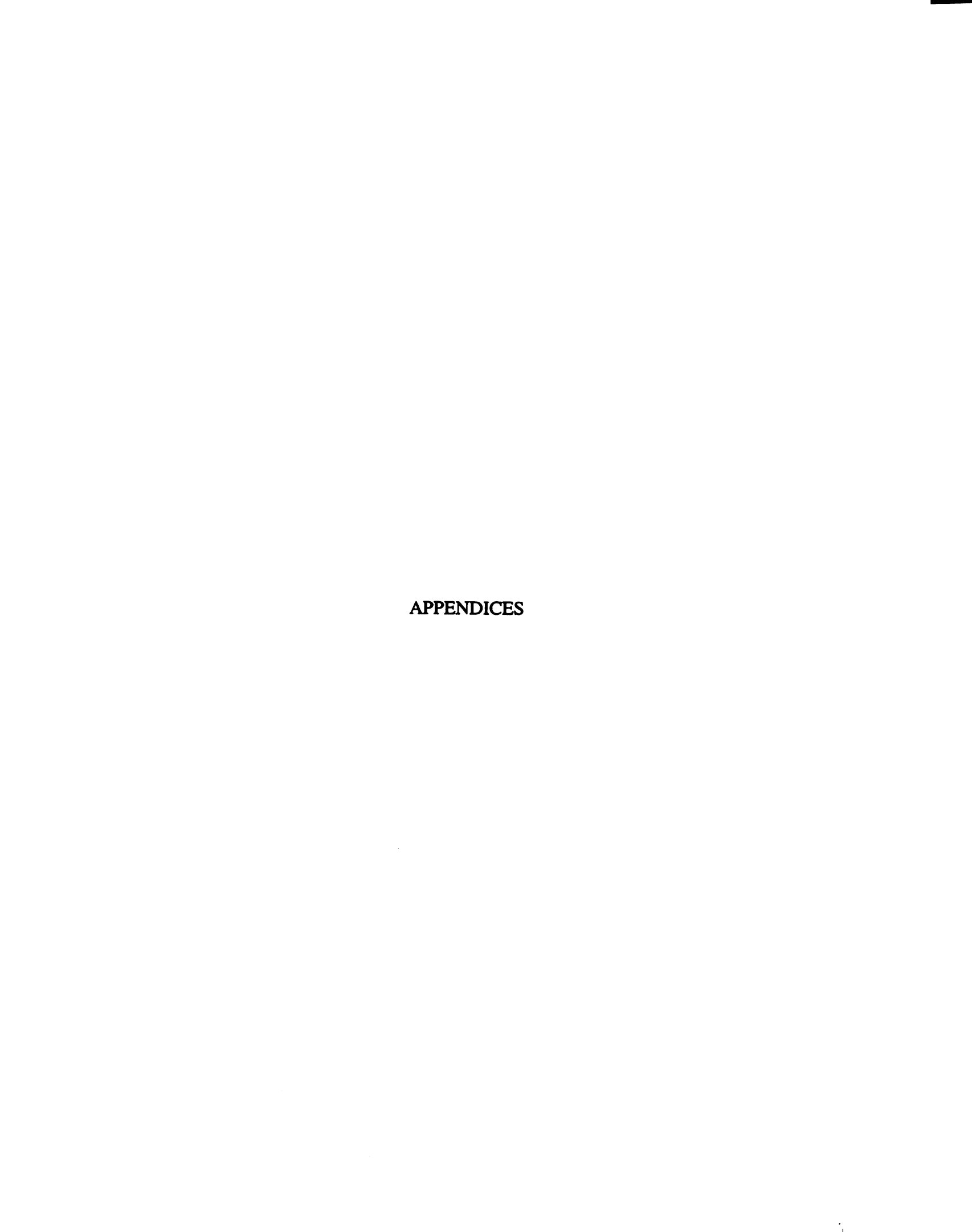
A mechanism has been suggested for the stabilization of large fingers by reactive

coupling. For resins with S < 0, small fingers grow at a faster rate than chemical reaction can act to stabilize them; in the case of large fingers, the rate of growth of the fingers is slow enough to enable the reactive coupling mechanism to damp them out.

6.2 RECOMMENDATIONS FOR FUTURE WORK

The main focus of this dissertation has been on the role of the polymerization reaction on the stability of the flow process. In the discussion of chapter 3, where the flow of resin past cylinder arrays was studied, the effects of viscoelastic properties of the resin have not been looked into (in the third regime). A more detailed investigation of the elastic effects would provide better understanding of the phenomenon.

Another area that deserves further attention is the combined effect of chemical reaction and dispersion. In chapter 5, only the initial growth rates were considered. A complete numerical computation of the eigen value problem, at all times, would be useful. Though the presence of dispersion and reaction terms in the model equations makes the numerical procedure more involved, the actual behavior of the disturbances at large times would be an interesting topic for further research.



APPENDIX A: EXCHANGE OF STABILITIES ANALYSIS FOR MOLD FILLING WITH CHEMICAL REACTION, WITHOUT DISPERSION

In the stability analysis of Chapter 4, all disturbances are expressed as Fourier type expansions. For example, disturbances in pressure are given by equations of the type:

$$p' = p(\xi) \cdot \exp([i\{k_x x + k_y y\}] \cdot \exp(\sigma t))$$
 (A-1)

where $p(\xi)$ is the amplitude of the disturbance, k_x and k_y are the wavenumbers in the respective directions and σ is the growth rate. This follows the resolution of the disturbances by the method of normal modes into various components, each satisfying the linear system (eigenvalue problem). In general, the growth rate σ is complex, described as

$$\sigma = \sigma_R + i\sigma_I \tag{A-2}$$

where σ_R is the real part and σ_I is the imaginary part. When the real part of the growth rate is positive, the disturbance in unstable; when it is negative, the disturbance attenuates with time and is termed stable; when it is zero, it is said to be neutrally stable. The imaginary part of the growth rate corresponds to an oscillatory variation in the disturbance.

The cutoff wavenumber is defined as the wavenumber of the disturbance at which the real part, σ_R , of its growth rate, σ , is zero. This means that, at the cutoff point, the disturbance neither grows nor decays. However, if the imaginary part, σ_I , of the growth rate is non-zero, the disturbance retains an oscillatory variation with time and is termed overstable. The principle of exchange of stabilities is said to be satisfied when both the

real and imaginary parts of the growth rate vanish at the cutoff point. In this case, at the onset of instability a stationary pattern of motions prevails, in contrast to the occurrence of oscillatory motions at the onset of instability in case of overstability.

For the general eigenvalue problem

$$Lu = \lambda u \tag{A-3}$$

exchange of stabilities is examined by performing the following mathematical operation:

$$\langle v, Lu \rangle = \langle L^{\Theta}v, u \rangle \tag{A-4}$$

where L is a linear operator, L^{Θ} is the complex conjugate of the operator L, λ is the eigenvalue and <...> is the inner product operator.

For the problem discussed in chapter 4, in the absence of dispersion, the eigenvalue problem was obtained as (equation 4-23)

$$\frac{\partial}{\partial \xi} \left[\bar{\lambda} \frac{dp}{d\xi} \left(\frac{\sigma - S}{\sigma - S + V} \right) \right] = bk^2 \bar{\lambda} p \tag{A-5}$$

In this eigenvalue problem, then, both sides of equation (A-5) are multiplied by the complex conjugate of "p" to give, taking $\{(\sigma-S)/(\sigma-S+V) \equiv h\}$,

$$p^* \frac{\partial}{\partial \xi} \left[\bar{\lambda} \frac{dp}{d\xi} \cdot h \right] = bk^2 \bar{\lambda} p p^* \tag{A-6}$$

This may be expanded to give

$$\frac{\partial}{\partial \xi} \left[\bar{\lambda} (p^* \frac{dp}{d\xi}) \cdot h \right] - \bar{\lambda} \left(\frac{dp}{d\xi} \right) \left(\frac{dp}{d\xi} \right)^* \cdot h = bk^2 \bar{\lambda} p p^*$$
(A-7)

In differential form, this becomes

$$d\left[\bar{\lambda}h(p^*\frac{dp}{d\xi})\right] - \bar{\lambda}h\left(\frac{dp}{d\xi}\right)\left(\frac{dp}{d\xi}\right)^*d\xi = bk^2\bar{\lambda}pp^*d\xi \tag{A-8}$$

This equation may now be integrated in the limits $(\xi = -z_f)$ to $(\xi = 0)$, yielding

$$\left[\bar{\lambda}h(p^*\frac{dp}{d\xi})\right]_{-z_f}^0 - \int_{-z_f}^0 (\bar{\lambda}h) \left(\frac{dp}{d\xi}\right) \left(\frac{dp}{d\xi}\right)^* d\xi = \int_{-z_f}^0 bk^2 \bar{\lambda}pp^* d\xi \tag{A-9}$$

The boundary conditions at $\xi = -z_f$ and $\xi = 0$ (equation 4-26) on the pressure disturbance and its first derivative lead to the first term on the left hand side of equation (A-9) being null. This results in

$$-\int_{-z_f}^{0} (\bar{\lambda}h) \left(\frac{dp}{d\xi}\right) \left(\frac{dp}{d\xi}\right)^* d\xi = \int_{-z_f}^{0} bk^2 \bar{\lambda}p p^* d\xi$$
 (A-10)

Both the products (pp^*) and $(dp/d\xi)(dp^*/d\xi)$ are positive. In addition, (bk^2) is positive. This means that $\{\overline{\lambda}pp^*\}$ and $\{\overline{\lambda}(dp/d\xi)(dp^*/d\xi)\}$ are both of the same sign. So "h" has to be negative in the domain of the problem, for the above equation to be satisfied. Also, since the right hand side of the equation is real, "h" has to be real, i.e. the imaginary part h_I is zero, in the equation

$$h = h_R + ih_I \tag{A-11}$$

Now, from this definition of "h", we obtain

$$h_R + ih_I = \frac{\sigma_R + i\sigma_I - S}{\sigma_R + i\sigma_I - S + V}$$
 (A-12)

which yields

$$h_I = \frac{\sigma_I V}{\left(\sigma_R - S + V\right)^2 + \sigma_I^2} \tag{A-13}$$

For h_I to be zero, we need V = 0 or $\sigma_I = 0$. A sufficient condition that arises for real growth rate, i.e. for $\sigma_I = 0$, is that V must not equal zero anywhere in the flow domain, i.e. V

should not change sign.

The schematic for the shell balance for one-dimensional flow past porous media is shown:

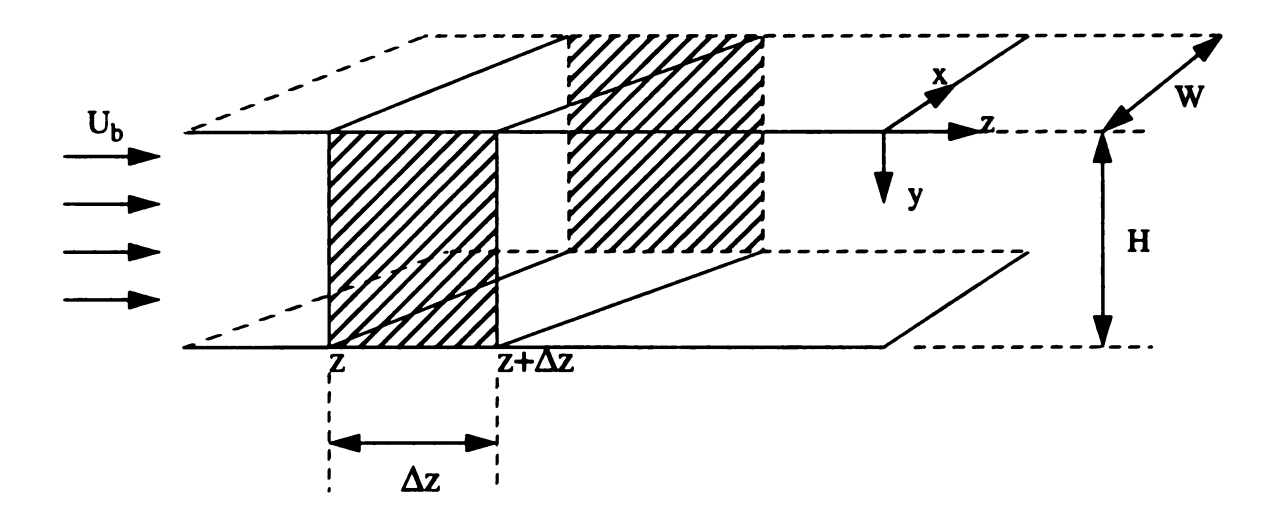


Figure A.1 Schematic for shell balance

Let the change in concentration of the reactant, between the planes at $\{z\}$ and $\{z+\Delta z\}$, be Δc .

The volume of the shell is [WH Δz]. U_o here is the interstitial velocity and ϵ is the porosity.

Net accumulation (A) of the reactant, in time Δt is = [WH Δz] $\epsilon \Delta c$.

Reactant entering the shell by FLOW (F_{in}) in time Δt is = $(\Delta t) [WH(U_bc)|_z]$

Reactant leaving the shell by FLOW (F_{out}) in time Δt is $= \Delta t \left[WH(U_b c) |_{z+\Delta z} \right]$

Reactant consumed by CHEMICAL REACTION (R_R) in time (Δt) is = R Δt [WH Δz] ϵ

Reactant entering the shell by DISPERSION (D_{in}) in time Δt is = (Δt) [WH] [-D(∂c /

$$(\partial z)]|_{z} \epsilon$$

Reactant leaving the shell by DISPERSION (D_{out}) in time Δt is = Δt [WH] [-D($\partial c/\partial z$)] $\Big|_{z+\Delta z} \varepsilon$

The overall shell balance is now written by combining the individual terms

$$A = F_{in} - F_{out} - R_R + D_{in} - D_{out}$$
 (B-1)

That is,

$$[WH\Delta z]\varepsilon(\Delta C) = (\Delta t) \left[WH \left[(U_b C) \Big|_z - (U_b C) \Big|_{z+\Delta z} \right] \right] - (\Delta t) [WH\Delta z]\varepsilon R$$

$$+ (\Delta t)\varepsilon WH \left[-D\frac{\partial C}{\partial z} \Big|_z + D\frac{\partial C}{\partial z} \Big|_{z+\Delta z} \right]$$
(B-2)

Dividing through by $[WH\Delta z] \Delta t$, we get:

$$\varepsilon \frac{\Delta C}{\Delta t} = \frac{U_b C|_z - U_b C|_{z + \Delta z}}{\Delta z} - \varepsilon R + \varepsilon \frac{-D \frac{\partial C}{\partial z}|_z + D \frac{\partial C}{\partial z}|_{z + \Delta z}}{\Delta z}$$
(B-3)

Now, dividing through by ε and taking limits as Δt , $\Delta z \rightarrow 0$, we get, using the definition of interstitial velocity $(U_b = U_o \varepsilon)$:

$$\frac{\partial C}{\partial t} = \frac{\partial}{\partial z} (-U_o C) - R + \frac{\partial}{\partial z} \left(D \frac{\partial C}{\partial z} \right)$$
 (B-4)

Eq. (B-4) may be rewritten for a three dimensional flow field as

$$\frac{\partial C}{\partial t} + \underline{u} \bullet \nabla \alpha - \nabla \bullet [D \bullet \nabla C] = -R \tag{B-5}$$

Using the equation of continuity (dU/dz = 0) and assuming D to be constant, we get, for a second order reaction,

$$-C_o \frac{\partial \alpha}{\partial t} = U_o C_o \frac{\partial \alpha}{\partial z} - R_o (1 - \alpha)^2 - D C_o \frac{\partial^2 \alpha}{\partial z^2}$$
 (B-6)

This yields:

$$\frac{\partial \alpha}{\partial t} + U_o \frac{\partial \alpha}{\partial z} - D \frac{\partial^2 \alpha}{\partial z^2} = \left(\frac{R_o}{C_o}\right) (1 - \alpha)^2$$
 (B-7)

This is the final, component balance equation, in DIMENSIONAL quantities.

Scaling:

Equation (B-7) may be rewritten in dimensionless terms using appropriate scaling factors. For the general scaling factors for time, length and velocity, given by t_0 , z_0 , $U_0(=z_0/t_0)$ respectively, the following dimensionless form of the component balance equation is obtained:

$$\frac{\partial \alpha}{\partial t} + \frac{\partial \alpha}{\partial z} - \frac{t_o}{t_D} \frac{\partial^2 \alpha}{\partial z} = \frac{t_o}{t_R} (1 - \alpha)^2$$
 (B-8)

where $t_D \equiv z_0^2/D$ is the dispersion time scale and $t_R \equiv c_0/R_0$ is the reaction time scale. Also, let the flow time scale be t_F . The time scale t_0 may now be selected from the three choices t_D , t_R , or t_F .

We now define dimensionless quantities as below:

Peclet Number, Pe = $t_D/t_F = (z_0U_0/D)$.

Damkohler number, Da = $t_F/t_R = (z_o/U_o) / (c_o/R_o)$.

$$\theta = (Pe) \times (Da) = t_D/t_R$$

CASE 1. The length and time units are scaled by the reaction time scale, c₀/R₀.

time -
$$t_0 = t_R = c_0/R_0$$
;

length -
$$z_0 = z_R = U_0 c_0/R_0$$
;

velocity -
$$v_0 = U_0$$
;

we obtain, in dimensionless quantities:

$$\frac{\partial \alpha}{\partial t} + \frac{\partial \alpha}{\partial z} - \frac{t_R}{t_D} \frac{\partial^2 \alpha}{\partial z^2} = (1 - \alpha)^2$$
 (B-9)

These scaling factors were used in chapter 4, where the problem of mold filling with chemical reaction in the absence of dispersion was studied. In that problem, due to the absence of dispersion, $t_D \rightarrow \infty$ and the third term on the l.h.s. of this equation vanishes.

CASE 2. The length and time units are scaled by the dispersion time scale, z_0^2/D .

time -
$$t_0 = t_D = z_0^2 / D$$
;

length - $z_0 = z_D$;

velocity - $v_o = U_o$;

Using these definitions, the time scale may also be expressed as D/U_0^2 ; the length scale as D/U_0 .

Applying these scales we obtain, in dimensionless quantities:

$$\frac{\partial \alpha}{\partial t} + \frac{\partial \alpha}{\partial z} - \frac{\partial^2 \alpha}{\partial z^2} = \frac{t_D}{t_R} (1 - \alpha)^2$$
 (B-10)

These scaling factors were used in the paper by Tan & Homsy (1986), where there was no chemical reaction. This means that $t_R \to \infty$ and the term on the r.h.s. of the equation vanishes. In chapter 5 however, where both dispersion and chemical reaction are present, this equation is rewritten using the definition $\theta = (Pe) \times (Da) = t_D/t_R$.

$$\frac{\partial \alpha}{\partial t} + \frac{\partial \alpha}{\partial z} - \frac{\partial^2 \alpha}{\partial z^2} = \theta (1 - \alpha)^2$$
 (B-11)

BIBLIOGRAPHY

Babbington, D.A., J.H. Enos and J.M. Cox, "High speed resin transfer molding of vinyl ester resins," AUTOCOM '87, Dearborn, Michigan, Paper no. EM87-351 (1987).

Bacri, J.C., Rakotomalala, N., Salin, D. and Woumeni, R., "Miscible viscous fingering: Experiments versus continuum approach", Phys. Fluids A 4(8), 1611(1992).

Bruschke, M.V. and S.G. Advani, "A finite element approach to mold filling in anisotropic porous media," Polymer Composites 11, 398 (1990).

Castro, J.M. and Macosko, C.W., "Studies of Mold Filling and Curing in the Reaction Injection Molding Process", AIChE J 28(2), 250(1982).

Chadam, J., D. Hoff, E. Merino, P. Ortoleva and A. Sen, "Reactive infiltration instabilities", IMA J. Appl. Math., 36, 207(1986).

Chadam, J., A. Pierce and P. Ortoleva, "Stability of reactive flows in porous media: Coupled porosity and viscosity changes:, SIAM J. Appl. Math., 51(3), 684(1991).

Chmielewski, C., C.A. Petty and K. Jayaraman, "Crossflow of elastic liquids through cylinder arrays" J. Non-Newtonian Fluid Mech. 35, 309 (1990).

Chuoke, R.L., van Meurs, P. and van der Poel, C., "The Instability of Slow, Immiscible Viscous Liquid-Liquid Displacements in Permeable Media", Trans. AIME 216, 188(1959).

R.E. Collins, "Flow of fluids through porous materials", Reinhold Publishing, (1961).

Coulter, J.P. and S.I. Guceri, "Resin transfer molding: process review, modeling and research opportunities," Proc. Manufacturing International '88, ed. T.G. Gutowski, ASME, NY, p. 79 (1988).

Finlayson, B.A., "Nonlinear Analysis in Chemical Engineering", McGraw-Hill Inc., p.73 and p.113 (1980).

Garcia, M.A., C.W. Macosko, S. Subbiah, and S. I. Guceri, "Modeling of reactive filling in complex cavities," Intern. Polymer Processing VI, p.73, (1991).

Gonzalez-Romero, V.M. & C.W.Macosko, J. Rheol., 29(3), 259(1985).

Gorell, S.B. and G.M. Homsy, "A theory for the most stable variable viscosity profile in graded mobility displacement processes", AIChE J., 31(9), 1498(1985).

Hickernell, F.J. and Yortsos, Y.C., "Linear Stability of Miscible Displacement Processes in Porous Media in the Absence of Dispersion", Studies in Appl. Math. 74, 93(1986).

Hill, S., "Channelling in Packed Columns", Chem. Eng. Sci. 1, 247(1952).

Homsy, G.M., "Viscous Fingering in Porous Media", Ann. Rev. Fluid Mech. 19, 271(1987).

Jayaraman, K. and C.N. Satyadev, "The Role of Fluid Rheology in Resin Transfer Molding", Advanced Composite Materials: New Developments and Applications Conference Proceedings, Detroit, Michigan, USA, pp. 225-232 (1991).

Kim, D.H. and Kim, S.C., "Engineering Analysis of Reaction Injection Molding of Epoxy

Resin", Poly. Comp., 8, 208(1987).

Kim, Y.R., S.P. McCarthy, J.R. Fanucci, S.C. Nolet and C. Koppernaes, "Resin flow through fiber reinforcements during composite processing," SAMPE Quarterly, p. 16, (1991).

Losure, N.S., "Viscous Fingering Flows in Reactive Resin Systems", Ph.D. Thesis, Michigan State University, 1994.

Macosko, Christopher W., "RIM, Fundamentals of Reaction Injection Molding", Hanser Publishers, New York, 1989.

Malkin, A.Y., Ivanova, S.L., Frolov, L.G., Ivanova, A.N. and Andrianova, Z.S., "Kinetics of Anionic Polymerization of Lactams. (Solution of non-isothermal kinetic problems by the inverse method)", Polymer, 23, 1791(1982).

Manickam, O. and G.M. Homsy, "Stability of miscible displacements in porous media with nonmonotonic viscosity profiles", Phys. Fluids A5(6), 1356(1993).

Osinski, J.S., "Characterization of Fast-Cure Resins for Reaction Injection Molding", Polym. Eng. Sci., 23, 756(1983).

Owen, M.J., V. Middleton, C.D. Rudd, and I.D. Revill, "Fiber wet-out in resin transfer molding" Proc. of Conference on Interfacial Phenomena in Composite Materials, University of Sheffield, p. 208 (1989).

Park, C.W. and G.M. Homsy, "The instability of long fingers in Hele-Shaw Flows", Phys.

Fluids, 28(6), 1583(1985).

Parnas, R.S. and F.R. Phelan, "The effect of heterogeneous porous media on mold filling in resin transfer molding," SAMPE Quarterly p. 53, (1991).

Paterson, L., "Fingering with miscible fluids in a Hele Shaw cell", Phys. Fluids 28(1), 26(1985).

Perkins, T.K. and O.C. Johnston, "Mechanics of viscous fingering in miscible systems", Soc. Pet. Eng. J., March 1962, pp. 70-84.

Perkins, T.K. and O.C. Johnston, "A review of diffusion and dispersion in porous media", Soc. Pet. Eng. J., December 1965, pp. 301-317.

Saffman, P.G. and Taylor, Sir G., "The penetration of a fluid into a porous medium or Hele-Shaw cell containing a more viscous liquid", Proc. Roy. Soc. (London), Series A, 245, 120(1958).

Satyadev, C.N. and K. Jayaraman, "Analysis of finger growth during the flow of reacting liquid through porous fiber preforms", Simulation of Materials Processing: Theory, Methods and Applications - NUMIFORM-95, pp. 333-338, Eds. Shan-Fu Shen and Paul Dawson (1995).

Schincariol, R.A., F.W. Schwartz and C.A. Mendoza, "On the generation of instabilities in variable density flow", Water. Resour. Res., 30(4), 913(1994).

Schowalter, W.R., "Stability Criteria for Miscible Displacement of Fluids from a Porous

Medium", A.I.Ch.E. J. 11(1), 99(1965).

Slobod, R.L. and Thomas, R.A., "Effect of Transverse Diffusion on Fingering in Miscible-Phase Displacement", Soc. Pet. Eng. J. 3, 9(1963).

Tan, C.T. and Homsy, G.M., "Stability of miscible displacements in porous media: Rectilinear flow", Phys. Fluids 29(11), 3549(1986).

Tan, C.T. and G.M. Homsy, "Simulation of nonlinear viscous fingering in miscible displacement", Phys. Fluids 31, 1330(1988).

Tan, C.T. and Homsy, G.M., "Viscous fingering with permeability heterogeneity", Phys. Fluids, A4(6), 1099(1992).

Wang, K.K. and C.A. Hieber, "Injection Molding Simulation," Proc. Manufacturing International '88, ed. T.G. Gutowski, ASME, p.87 (1988).

Yortsos, Y.C. and M. Zeybek, "Dispersion driven instability in miscible displacement in porous media", Phys. Fluids 31(12), 3511(1988).

Zimmerman, W.B. and G.M. Homsy, "Nonlinear viscous fingering in miscible displacement with anisotropic dispersion", Phys. Fluids A3, 1859(1991).

Zimmerman, W.B. and G.M. Homsy, "Three dimensional viscous fingering: A numerical study", Phys. Fluids A4(9), 1901(1992).